UNCLASSIFIED

AD. 292 180

Reproduced
by the

ARMED SERVICES TECHNICAL INFORMATION AGENCY
ARLINGTON HALL STATION
ARLINGTON 12, VIRGINIA

UNCLASSIFIED

NOTICE: When government or other drawings, specifications or other data are used for any purpose other than in connection with a definitely related government procurement operation, the U. S. Government thereby incurs no responsibility, nor any obligation whatsoever; and the fact that the Government may have formulated, furnished, or in any way supplied the said drawings, specifications, or other data is not to be regarded by implication or otherwise as in any manner licensing the holder or any other person or corporation, or conveying any rights or permission to manufacture, use or sell any patented invention that may in any way be related thereto.

63-2-1

CATALOGED BY ASTIA
AS AD No. 292180

AIR FORCE INSTITUTE OF TECHNOLOGY

AIR UNIVERSITY
UNITED STATES AIR FORCE

292180

SCHOOL OF ENGINEERING

WRIGHT-PATTERSON AIR FORCE BASE, OHIO

ASTIA
RECEIVED
JAN 2 1963
TISIA C

AF-WP-O-MAY 62 3,500

THE DESIGN AND PERFORMANCE OF A CONVERGENT-DIVERGENT NOZZLE FOR THE MECHANICAL ENGINEERING LABORATORY SHOCK TUBE

Carroll Clifford Rands, B.S.
Captain USAF

GAE/ME/62-3

AF-WP-O-SEP 62 25

THE DESIGN AND PERFORMANCE OF A CONVERGENT-DIVERGENT NOZZLE FOR THE MECHANICAL ENGINEERING LABORATORY SHOCK TUBE

THESIS

Presented to the Faculty of the School of Engineering of
the Air Force Institute of Technology
Air University
in Partial Fulfillment of the
Requirements for the Degree of
Master of Science

By
Carroll Clifford Rands, B.S. M.E.
Captain USAF
Graduate Aeronautical Engineering

August 1962

Preface

This study originated as a desire to improve the performance of the Mechanical Engineering Laboratory shock tube. The basic shock tube was capable of flows up to a Mach number of approximately 1.4 for 1.4 milliseconds. As a result of this project, the modified shock tube is now capable of Mach 2.6 - 2.8 flows over a variety of Reynolds numbers for up to 18 milliseconds.

I would like to express my appreciation to the following individuals, whose assistance, guidance, and advice was invaluable to the successful completion of this study: Dr. A.J. Shine, Prof. M.E. Franke, and Lt. P.F. Meyfarth, Head and members of the faculty of the Mechanical Engineering Department; Mr. John Parks, M. E. Laboratory Technician; Mr. M.W. Wolfe, School Shops Supervisor; and Mr. Clif Howell, ASD Technical Photographer. The individual effort that each of these people provided cannot be measured, but it was most certainly appreciated.

My special thanks to my wife and children for their patience and understanding during the accomplishment of the project and the preparation of this report.

Carroll C. Rands

Contents

List of Figures

Figure | Page

List of Tables

List of Symbols

c : Velocity of sound in feet per second

cm : Centimeters

cps : Cycles per second

fps : Feet per second

H : Horizontal oscilloscope trace setting in milliseconds per centimeter

k : Ratio of specific heats

M : Mach number

msec : Milliseconds

p : Pressure

psi : Pounds per square inch

P : Pressure ratio

t : Time

T : Temperature in degrees Rankine, also Temperature ratio

v : Volts

V : Vertical deflection scale of the oscilloscope trace in volts per centimeter

W : Velocity relative to the shock tube

x : Distance along the shock tube

ρ : Density ratio

Subscripts

1 : Low pressure region ahead of the incident shock - initial channel pressure

2 : Region between incident shock and contact surface

3 : Region between contact surface and expansion waves

4 : High pressure region ahead of expansion waves - initial chamber pressure

5 : Region between reflected shock wave and the nozzle entrance

6 : Nozzle test section during operation

21, 41, 52, etc.: A ratio, e.g., $P_{21} = \frac{p_2}{p_1}$

s : Conditions referring to the incident shock wave

Abstract

This study concerns the installation and test of a two-dimensional, sharp-edge-throat, Mach 3 nozzle in the Mechanical Engineering Laboratory shock tube.

Preliminary tests on an abrupt area reduction resulted in the selection of a 1-inch nozzle throat height. Wooden nozzle blocks were installed and test runs were conducted with a constant chamber pressure and varied channel pressure to produce incident shock waves of increasing strength. Analysis of high-speed motion pictures indicates that the nozzle test section Mach number is independent of incident shock strength; however, available and usable test times increase with increasing incident shock strength.

A plenum chamber attached to the low-pressure channel helped produce Mach 2.6 - 2.8 flows for up to 18 milliseconds.

GAE/ME/62-3

THE DESIGN AND PERFORMANCE OF A CONVERGENT - DIVERGENT NOZZLE FOR THE MECHANICAL ENGINEERING LABORATORY SHOCK TUBE

I. Introduction

Purpose

The original objective of this study was: ". . . to design and test a section which will increase the Mach number capabilities of the Mechanical Engineering Department shock tube. Basically the objective requires that a convergent-divergent section, a second diaphragm, and a low-pressure chamber be added to the present tube."

Early in the study, it became apparent that material would not be available to build a new test section. After a search of the literature, it was decided that a second diaphragm might not be necessary (Ref 6). The study was then re-defined as, "The Design and Performance of a Convergent-Divergent Nozzle for the Mechanical Engineering Laboratory Shock Tube."

Background Information

Early in the age of hypersonic flight, the need for a method to simulate high-temperature, high-Mach number flows

became apparent. The shock tube has been used for several years for various studies in high-temperature, high-speed flows and its limitations are well known to its users.

The characteristics and operating principles of the shock tube are adequately described by Glass, Martin, and Patterson (Ref 4, 5, 7). In general, the shock tube is a long metal tube consisting of a high-pressure chamber separated from a low-pressure channel by a frangible diaphragm. When the diaphragm is ruptured, a series of expansion waves propagates into the high-pressure chamber and a series of compression waves propagates into the low-pressure channel. The compression waves rapidly coalesce into a normal shock wave which continues to travel into the low-pressure channel. At this time, there are four distinct regions of flow in the shock tube (Fig 1).

Regions 1 and 4 are at rest and have not been disturbed by either the shock wave or the expansion waves.

The fluid in region 2 has been heated and accelerated by the incident shock wave. The flow in this region is uniform and steady, but of short duration. For a given diaphragm pressure ratio, the flow Mach number is a function of the ratio of specific heats of the fluid in the low pressure channel. Considering air as the fluid, M_2 reaches a maximum value of 1.89 with an infinite diaphragm pressure ratio.

The fluid in region 3 has been accelerated and cooled by

the expansion waves. A temperature discontinuity or contact surface separates region 3 and region 2. Region 3 is not generally used for test purposes because it is "cold" flow.

Researchers pondered the idea of attaching a nozzle to the end of the shock tube and expanding the flow in region 2 to a higher Mach number. Hertzberg investigated the problem and concluded it would be possible to achieve hypersonic flow simulating free-flight conditions using this method (Ref 8). He also investigated the advantages and disadvantages of three possible nozzle arrangements: "non-reflected" shock method, "reflected" shock method, and the non-steady expansion method (Ref 10). Further studies were conducted concerning flow starting phenomena and real gas effects in the hypersonic shock tunnel (Ref 6, 15).

Progress was made very rapidly in the development of hypersonic shock tubes and today, they are being operated in the range from Mach 8 to 35 with Reynolds numbers from 40 million per foot to 100 per foot.

With this advance in shock tube technology, the members of the Mechanical Engineering Department expressed a desire to improve the performance of the M. E. Laboratory shock tube. They realized that this shock tube did not possess the potential for hypersonic flow, but it certainly could be modified to produce a higher supersonic flow. It was their desire that originated this study.

Scope of Study

This study concerns the design and performance of a supersonic nozzle installed in the Air Force Institute of Technology Mechanical Engineering Laboratory shock tube.

A preliminary investigation was conducted to determine the action of a shock wave when it impinges on an abrupt area change. The strength of the shock wave transmitted through the reduced area section was compared with the strength of the incident shock wave and Schlieren photographs were taken of the flow field. The results of this investigation were applied to the selection of a nozzle throat size.

A two-dimensional, sharp-edge-throat nozzle was constructed with a design exit Mach number of 3 and a throat height of 1 inch. A series of runs was conducted to:

1. Record the Schlieren image of the flow field in and through the nozzle.

2. Determine the test section Mach number as a function of incident shock strength.

3. Determine the total test time available, the test flow duration, and the time loss due to the starting shock in the nozzle as a function of incident shock strength.

4. Determine the necessity for a second diaphragm in front of the nozzle.

5. Determine how the nozzle throat height might be varied from 1 inch.

Air was used as the working fluid in both the chamber and the channel for all runs.

The following chapters briefly discuss the theory of operation, describe the equipment and apparatus, and present the results. Conclusions were based on an evaluation of the Schlieren photographs of the flow field taken during each run.

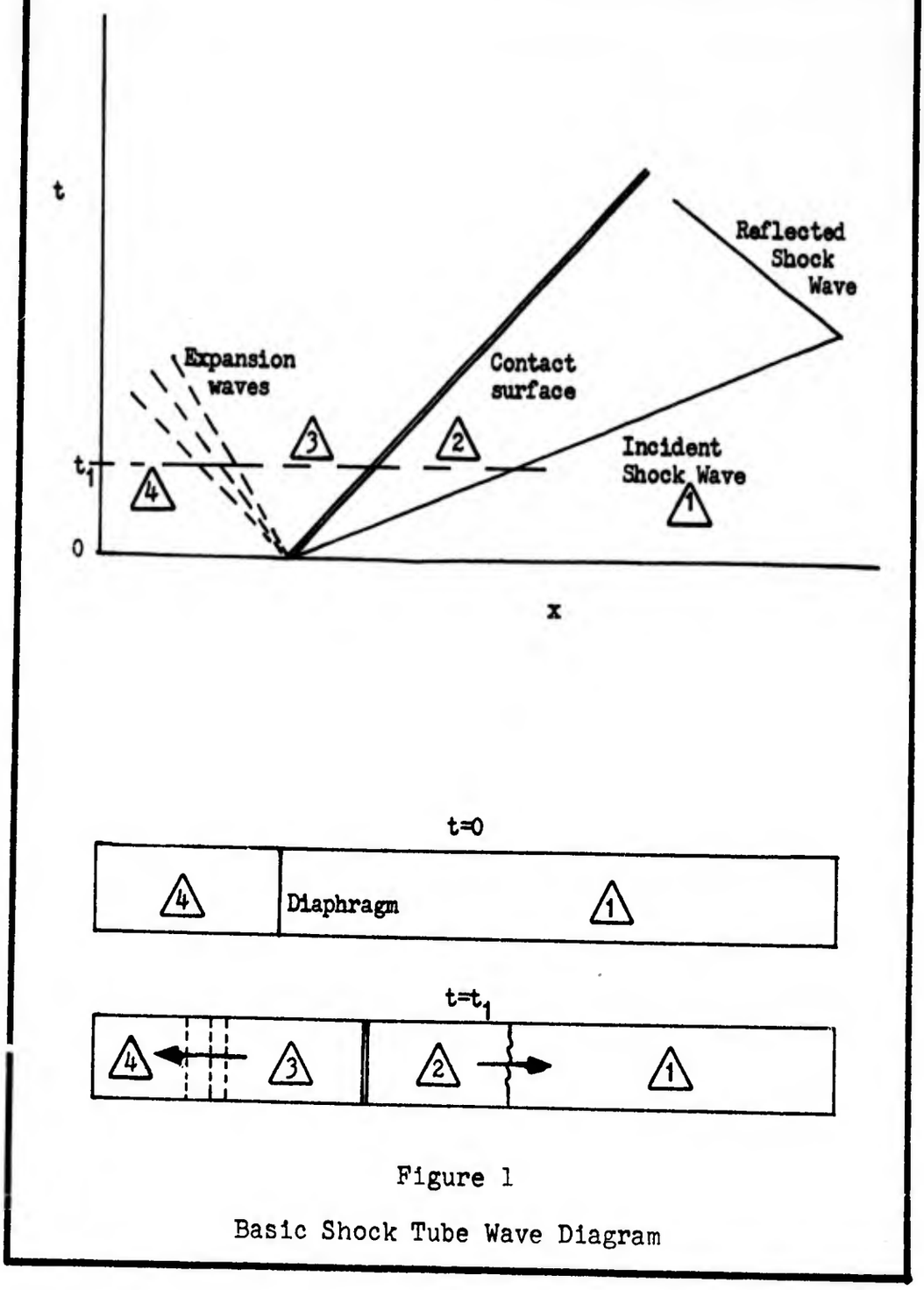

Figure 1

Basic Shock Tube Wave Diagram

II. Theory

A detailed analysis of the process in a "reflected" shock type shock tunnel is quite complex and is beyond the scope of this study. However, an idealized, simplified explanation is readily understandable (Ref 6, 7, 10). A wave diagram of the process is shown in Figure 2.

The incident shock wave accelerates, compresses, and heats the air behind it as it travels down the tube. It strikes the nozzle face and is almost completely reflected since the nozzle entrance is small compared to the area of the shock tube. The reflected shock further compresses the air and leaves a slug of hot, compressed, nearly stagnant air at the entrance to the nozzle. This slug of air is then expanded through the nozzle to the desired test section conditions.

The test time available is considered to be the time interval between the arrival at the nozzle entrance of the incident shock and the shock reflected from the contact surface. This interval is shown in Figure 2. The time available is reduced by the flow starting phenomena in the nozzle (Ref 6).

As the incident shock strikes the nozzle face, another shock wave and contact surface are formed at the nozzle entrance. As this system proceeds through the nozzle, a disturbance is created which rapidly forms into an upstream-facing shock wave. This starting shock tends to remain in the

nozzle and must be swept downstream before a useful flow can be established. The flow will continue undisturbed until a disturbance from upstream disrupts it, or until the pressure ratio across the nozzle drops below the critical value required for sonic velocity at the nozzle throat.

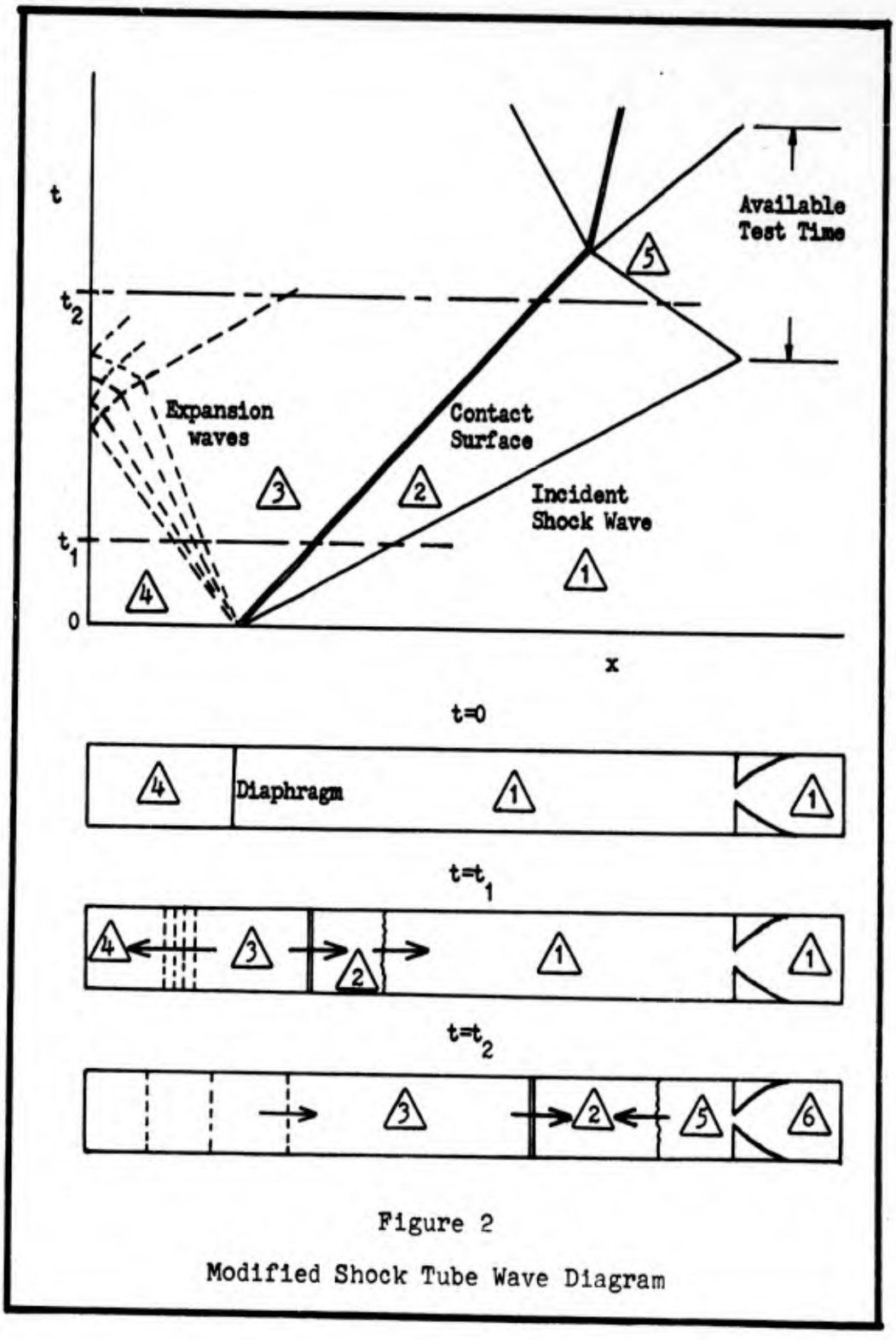

Figure 2

Modified Shock Tube Wave Diagram

III. Equipment

Basic Shock Tube

General. The Mechanical Engineering Laboratory shock tube is pictured in Figure 3. It was designed and built by Davis and French as an independent study in 1955 (Ref 2). Egan and Foster completed the project and tested it as their study in 1956 (Ref 3). Details of construction and operation are presented in their reports.

Description. In general, the shock tube is made of aluminum jig-plate in 5 four-foot sections. When assembled, it is a closed rectangular tube, 20 feet long, with a constant internal cross-section 4 inches wide by 8 inches high.

Section 1 is the high-pressure chamber. The remaining four sections are bolted together to form the low-pressure channel. Sheets of Mylar film are used as the diaphragm which separates the high and low pressure sections. Section 1 is held in place against the low-pressure channel by a hydraulic clamping arrangement.

Transducer Mounts. Transducer mounting plugs are located on the top of the shock tube at 100", 128". 140", 148", and 174" downstream of the diaphragm, and in the end plate. In this report, these positions are designated for transducers 1, 2, 3, 4, 5, and 6 as shown in Figure 8.

Test Section. Section 5 contains the test section. A 6-1/4 inch diameter optically flat viewing window is located on each side of the section. The center-line of the windows is 168 inches from the diaphragm. Sixty threaded brass plugs are located at various positions in the top, bottom, and sides of the section. These plugs may be removed and their holes used for mounting test equipment or models between the viewing windows.

Air Supply. Dry, oil-free air is supplied to the high-pressure chamber from the laboratory's compressed air system. Pressures up to 100 psi are available. A 150 inch mercury manometer, a 100 psi Bourdon gauge, and a 200 inch Wallace & Tiernan gauge are provided for pressure measurement.

Vacuum System. The low-pressure channel can be evacuated to 0.25 inches of mercury, or lower, with two Cenco vacuum pumps. Pressure in the low-pressure channel is determined with a 36 inch U-tube mercury manometer.

Temperature Measurement. Thermocouples are provided for temperature measurement in both the high and low pressure sections. A bulb-type thermometer is also available at the operator's table.

Diaphragm Rupturer. A manually-operated plunger device mounted in section 1 was used to rupture the diaphragm for runs during the initial part of the study. This device was unsatisfactory when the high-speed motion picture camera was

used to record the Schlieren images. For these runs, an electrically heated wire, actuated through the camera control, was used in place of the manual plunger. This apparatus is described in Appendix A.

Plenum Chamber

A plenum chamber at the end of the shock tube was necessary for the runs with the nozzle in the test section. This chamber provides additional downstream volume and is equivalent to adding several more sections to the shock tube. Shock waves and starting disturbances do not reflect from the plenum chamber entrance as they would from a closed end. Instead, they are dissipated by the large increase in area as they enter the chamber.

To serve as the plenum chamber, a small air tank was modified with an adapter section, mounted on casters, and attached to the end of section 5. Another Cenco vacuum pump was connected to the tank to reduce the time necessary to evacuate the entire low-pressure section. A switch to control this pump was installed at the operator's table. Two views of the plenum chamber and pump are given in Figure 4.

Instrumentation

Transducers. Endevco Corporation, Model 2501-500, piezoelectric transducers were used as shock wave indicators.

These transducers are sensitive to a pressure change and produce a voltage proportional to the impressed pressure step. The transducers are mounted at known locations in the mounts provided along the top of the tube. Appendix E contains a discussion regarding the use of these transducers for measuring a pressure step.

Oscilloscopes. The two oscilloscopes used in the study are shown in Figure 5.

The Tektronic Type 531 has a horizontal sweep rate that is variable from 0.02 microseconds per cm. to 12 seconds per cm. It has been modified with a single sweep circuit which prevents re-triggering of the sweep. A Tektronic Type 123 preamplifier is used to amplify the voltage pulse from the transducer to trigger the sweep.

The Hickok Type 1805 is basically the same as the Type 531 but has a sweep delay circuit. This circuit allows a preselected time delay to be applied to its sweep.

The Tektronic Type 53B and Type 53/54D vertical amplifiers are interchangable. The Type 53B provides for input of one channel only and presents this information over a vertical range from 0.05 to 20 volts per cm. The Type 53/54D presents two input channels of information over a range from 1 millivolt per cm. to 50 volts per cm.

Oscilloscope Cameras. A modified Polaroid camera using either Type 42 or 44 film was attached to each oscilloscope

to record the trace for later evaluation. The picture of the trace was used to determine the shock wave velocity (Appendix B).

Flow Visualization

Schlieren System. A folded Schlieren system with the knife edge vertical was used for flow visualization. Both still and motion pictures were used to record the flow images. Figure 6 is a schematic diagram of the arrangement.

Still Photography. For the still pictures, a Polaroid film pack containing either Type 42 or 44 film was mounted on a bellows arrangement as shown in Figure 7.

The light source for this arrangement was a General Electric FT-230 spark lamp. A power supply for the lamp was constructed by the laboratory technicians for earlier studies. Figure 8 shows a schematic of the circuit and the sequence is as follows. The incident shock wave causes a voltage pulse from transducer 1. This pulse is amplified by the Type 123 preamplifier and triggers the Type 531 oscilloscope which passes the signal to the delayed sweep of the Type 1805 oscilloscope. After a pre-determined delay time, calculated to catch the desired phenomena in the test section, the Type 1805 triggers the spark lamp power unit with a 150 volt, saw-tooth pulse. The spark lamp is fired and the desired results are recorded on film.

This system records the flow field image at one particular

instant during the run.

Motion Picture Photography. A Wollensak "Fastax", Model WF 3-16mm, high-speed framing camera was used to record the flow field image for an entire run. This camera is capable of film speeds up to 7,000 frames per second. When set for maximum speed, a 100-foot roll of film provides a camera run-time of approximately 0.6 seconds. The camera was operated through a Wollensak "Goose" Control Unit, Model J-515. The camera and control unit are shown in Figure 9.

A 24 volt battery was connected to the diaphragm rupturer through an "Event" time delay relay in the "Goose" and a safety switch at the operator's table. An initiator switch started the camera immediately and 400 milliseconds later the shock tube was fired. The electrical circuit is diagrammed in Figure 10.

A 1000 cps pulse generator printed 1 millisecond timing marks on the edge of the film. These marks were used during later evaluation of the film to provide an accurate time reference.

The steady light source required for this system, was provided by a Sylvania Type 300 AC, concentrated-arc lamp in place of the spark lamp.

The motion picture photography and services were provided by the Technical Photography Division of ASD.

Downstream View

Upstream View

Figure 3

The Mechanical Engineering Lab Shock Tube

Figure 4

Modified Shock Tube with Plenum Chamber

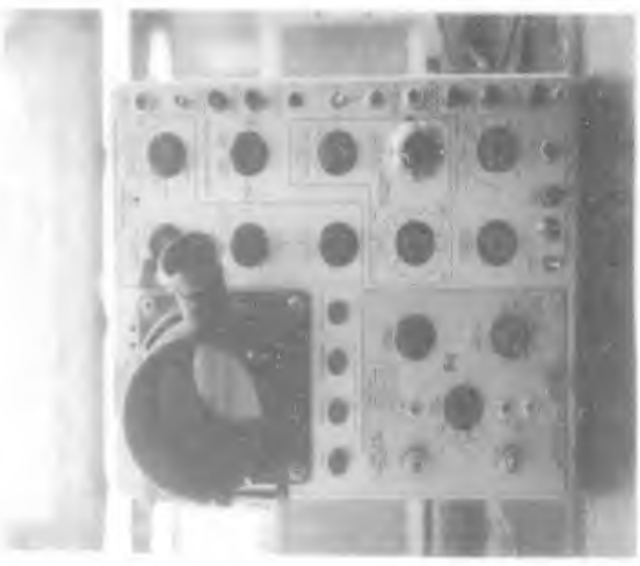

Type 1805

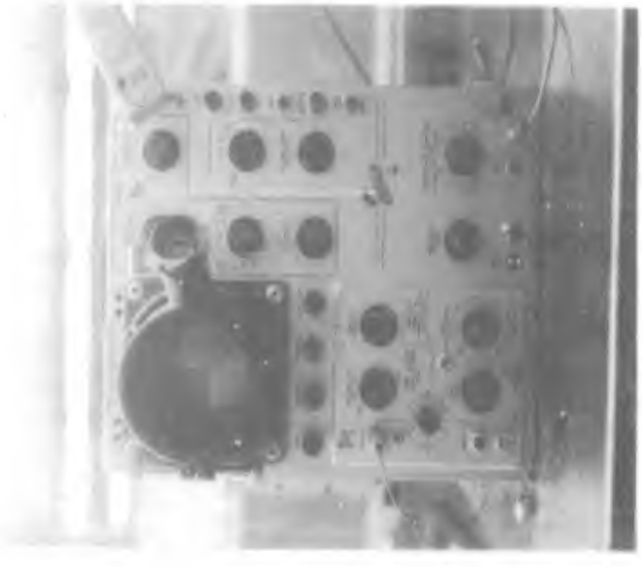

Type 531

Figure 5

The Tektronic and Hickok Oscilloscopes

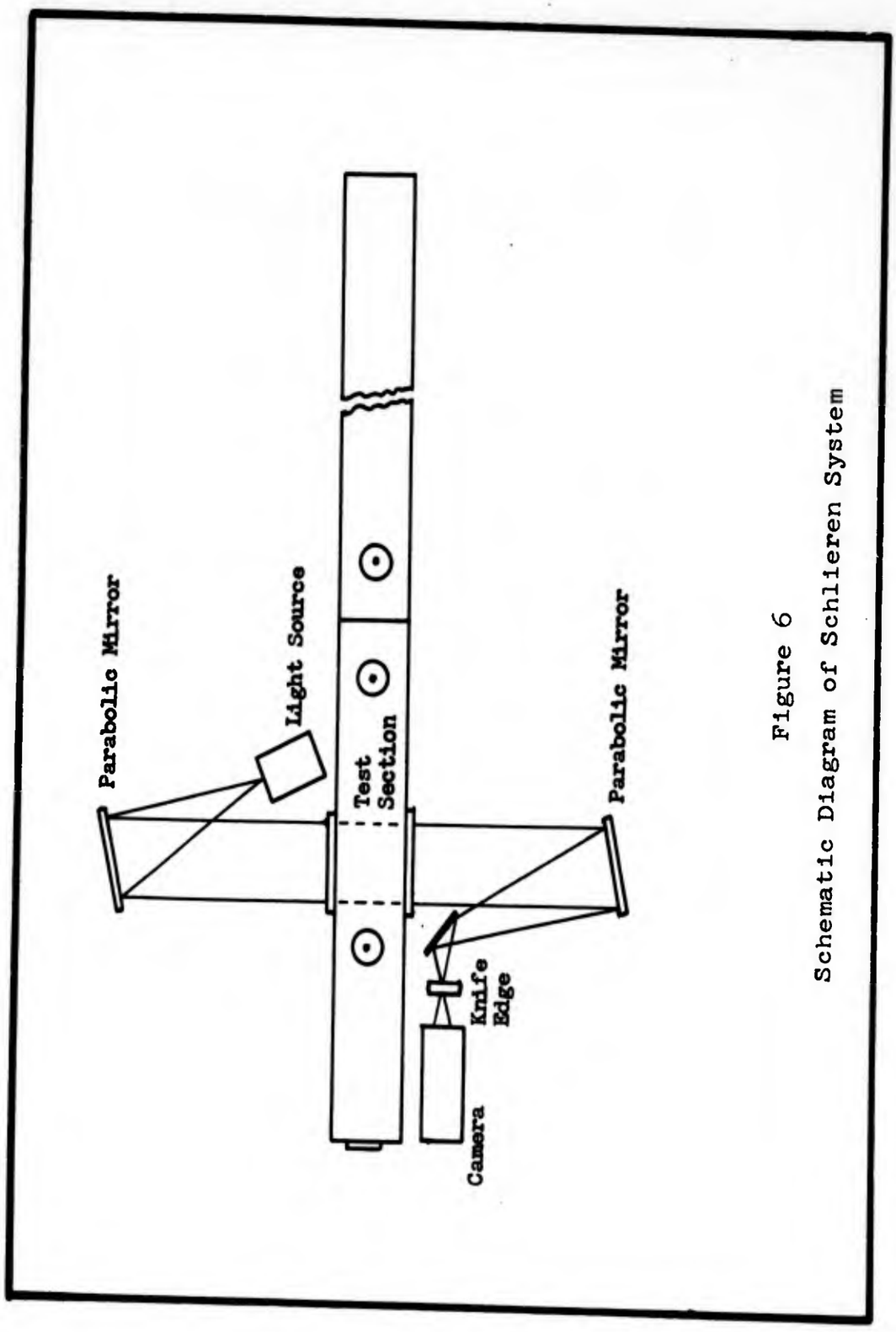

Figure 6
Schematic Diagram of Schlieren System

Figure 7

Still Camera Arrangement

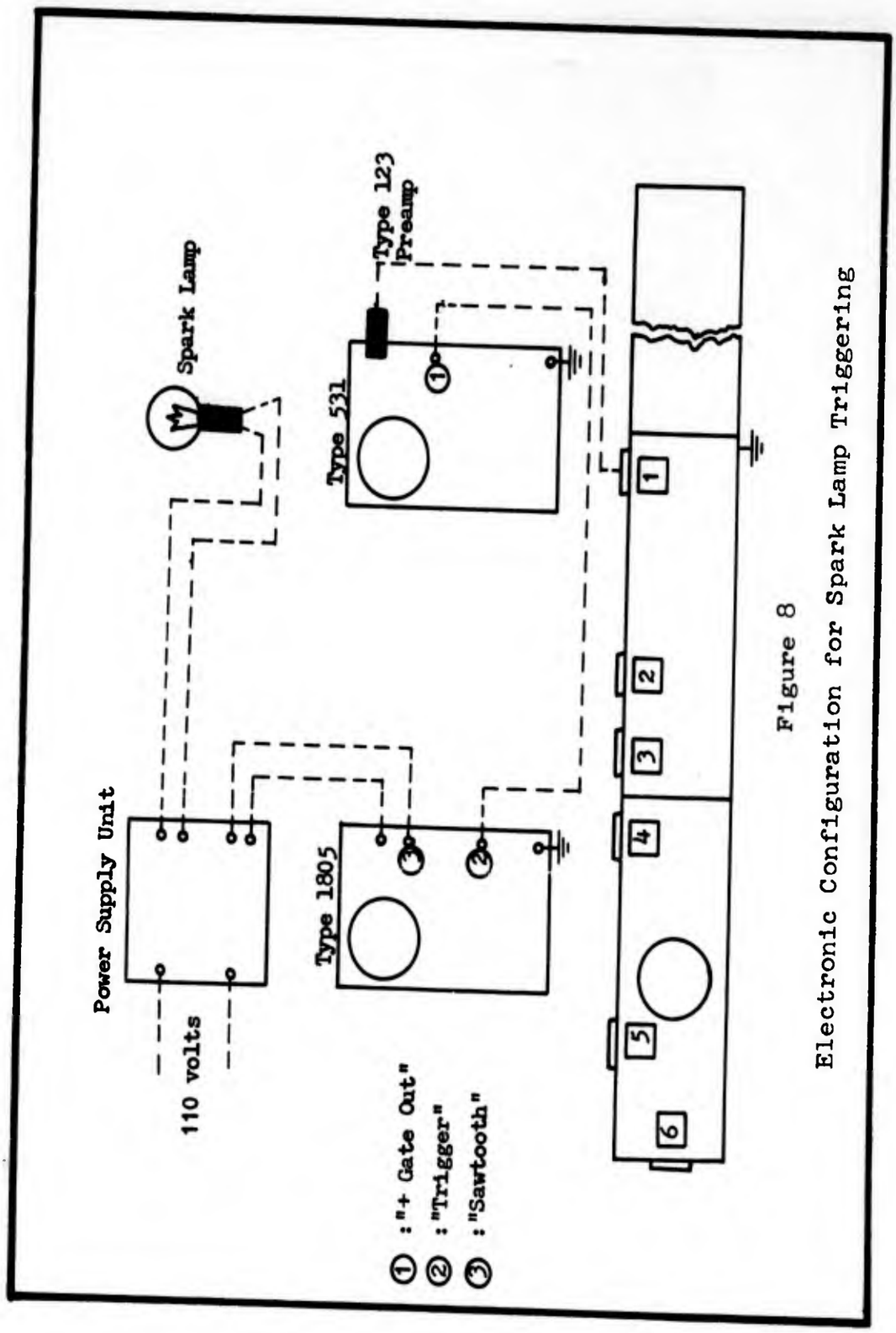

Figure 8

Electronic Configuration for Spark Lamp Triggering

Figure 9

The "Fastax" Camera and "Goose" Control Unit

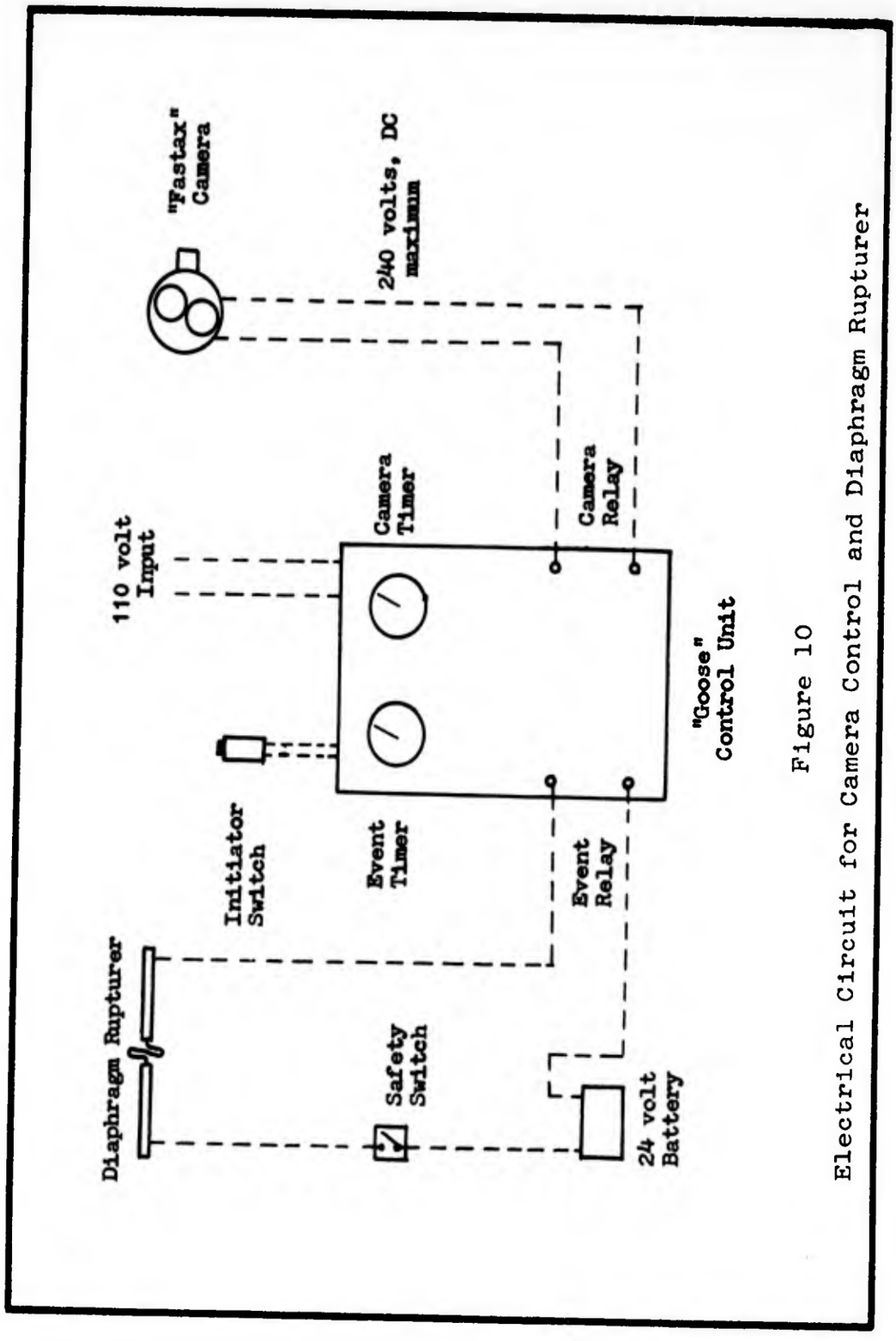

Figure 10

Electrical Circuit for Camera Control and Diaphragm Rupturer

IV. Preliminary Investigation

General

When a shock wave strikes an abrupt area change, it is broken into a reflected shock which travels back upstream, and a transmitted shock which travels through the reduced area section. The literature indicates that the shock transmitted through the reduced area section is stronger than the incident shock. Shock strength is defined in Appendix B. Hall discusses the theory and gives the following data (Ref 7:157).

For an area reduction of 50%, the ratio of the transmitted shock strength to the incident shock strength, $\frac{P_{51}}{P_{21}}$, varies from 1.19 at an incident shock strength, P_{21}, of 3, to 1.25 at a P_{21} of 50. For an area reduction of 80%, the ratio varies from 1.42 at a P_{21} of 6, to 1.48 at a P_{21} of 50. For an area reduction approaching 100%, the ratio varies from 1.60 at a P_{21} of 6, to 1.69 at a P_{21} of 50.

It was desirable to apply this information to the selection of nozzle throat area.

An experimental program was set up to determine the validity of this data applied to the M. E. Laboratory shock tube. The study was conducted in two phases using a device inserted in the shock tube to reduce the area. Phase I was conducted to compare the strength of the transmitted shock to the incident shock for differing incident shock strengths and

three different area reductions. Phase II was conducted using the Schlieren system to observe the flow field. The Schlieren image was recorded with still photography in one series and motion picture photography in another series.

The results of these tests were then applied intuitively to the selection of a nozzle throat area.

Area Reducers

The area reducers are shown in Figure 11. They were constructed of 3/4 inch aluminum plate, with aluminum face blocks and wood spacer blocks attached with bolts. The blocks were made in three different size sets to provide area reductions of 50.8%, 76.6%, and 89%. The height of the reduced area was 3-15/16 inches, 1-7/8 inches, and 7/8 inch, respectively. The top plate was drilled and tapped for transducer installation.

The assembly was mounted with lugs through the model mounting holes in the shock tube. The face blocks were aligned vertically even with the center-line of the test section windows as shown in Figure 12.

Phase I: Shock Strength Comparison

Test Program. A series of 10 runs with incident shock strengths from 1.2 to 7.0 was made with area reductions of 50.8%, 76.6%, and 89%.

Instrumentation. The incident shock velocity and the transmitted shock velocity were determined for each run using the electronic configuration shown in Figure 14.

As the incident shock passed transducer 1, the transducer generated a voltage pulse which started the trace on the Type 531 oscilloscope. A lead connected from the "Gate Out" of the Type 531 to the "Trigger or Ext Sweep In" of the Type 1805 oscilloscope conducted the starting pulse to start the trace on the Type 1805. As the incident shock passed transducer 3, the trace was deflected upward. The length of the trace from start to the deflection represents the time for the incident shock to travel between transducers 1 and 3.

The transmitted shock caused an upward deflection of the trace on the Type 1805 as the shock passed transducer 5, mounted in the top of the area reducer. When the transmitted shock struck transducer 6, the trace was deflected downward. The length of the trace between the two deflections represents the time for the transmitted shock to travel between transducers 5 and 6.

The incident and reflected shock strengths were determined from their respective velocities using the method discussed in Appendix B.

Results. In general, the results of this phase indicated that over the range of incident shock strengths used:

1. The ratio $\frac{P_{51}}{P_{21}}$ is less than 1 for an area reduction of 50.8%.

2. The ratio $\frac{P_{51}}{P_{21}}$ is greater than 1 and approximately the same for area reductions of 76.6% and 89%.

Thus, with a nozzle throat area equal to 20% or less of the shock tube area, the shock transmitted through the throat will be stronger than the incident shock.

In order to get more quantitative results, a study with many more runs would be required.

Phase II: Flow Visualization

This phase of the investigation was conducted using the still camera and spark lamp arrangement in one series, and the "Fastax" camera and associated equipment in the second series.

Still Photography. Using the same initial conditions to produce the same strength incident shock for each run, the time delay was varied to get still pictures of the shock wave at various positions in the test section. The incident shock wave had the following characteristics: W_s = 1450 fps, M_s = 1.25, P_{21} = 1.66 . The incident shock impinged on an area reduction of 50.8%.

The results of this series are presented in Figure 14. The line at the entrance to the area reducer is a vertical reference line. The incident shock is visible as a dark

reference line.

For runs 1 and 2, neither the incident shock nor the transmitted shock were strong enough to generate supersonic flow behind them, yet supersonic flow exists in the reduced area section, as confirmed by the presence of the standing shock waves. These shock waves remain until the transmitted shock reflects from the end of the shock tube, travels upstream and wipes them out. Flow continues into the reduced section for a short time after the standing shocks have dissipated.

Figure 17 is comparable to Figure 16 except that the camera speed was 650 frames per second faster for run 2.

Figure 18 shows that for strong incident shocks, with a low channel pressure, the flow starts very rapidly and ends abruptly.

Conclusions

It was concluded from this preliminary investigation that a nozzle throat height of 1 inch would be large enough to provide good flow starting characteristics and yet be small enough to maintain the critical pressure ratio across the nozzle such that sonic conditions exist at the throat for an appreciable length of time over a range of incident shock strengths.

Table I

Preliminary Test Data*

Run No.	p_4 in Hg abs	p_1 in Hg abs	P_{41}	W_s fps (a,b)	M_s (a,b)	P_{21} (a,c)
1	177.4	28.75	6.17	1620	1.42	2.19
2	212.2	28.91	7.34	1670	1.47	2.34
3	212.2	3.16	67.2	2490	2.19	5.41
4	218.5	1.53	143	2800	2.44	6.79

* - See Appendix B
a - Nominal Values
b - Maximum Error, ± 4.5%
c.- Maximum Error, ± 9.0%

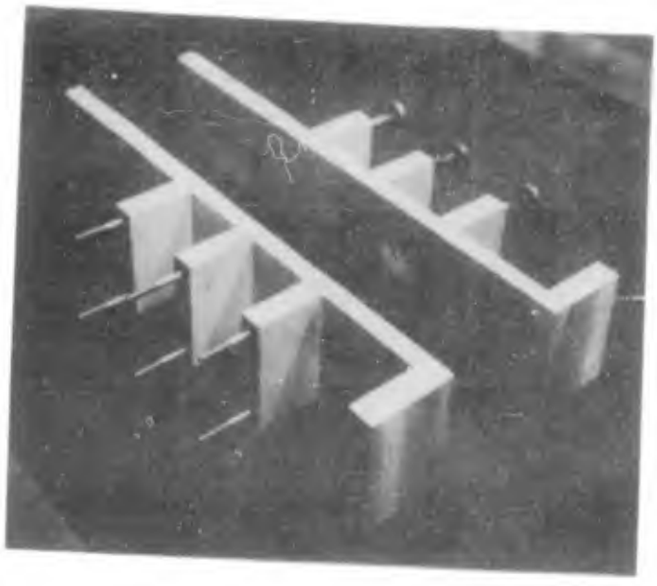

Figure 11

Area Reducers

Flow

Figure 12

Test Section with Area Reducers in Position

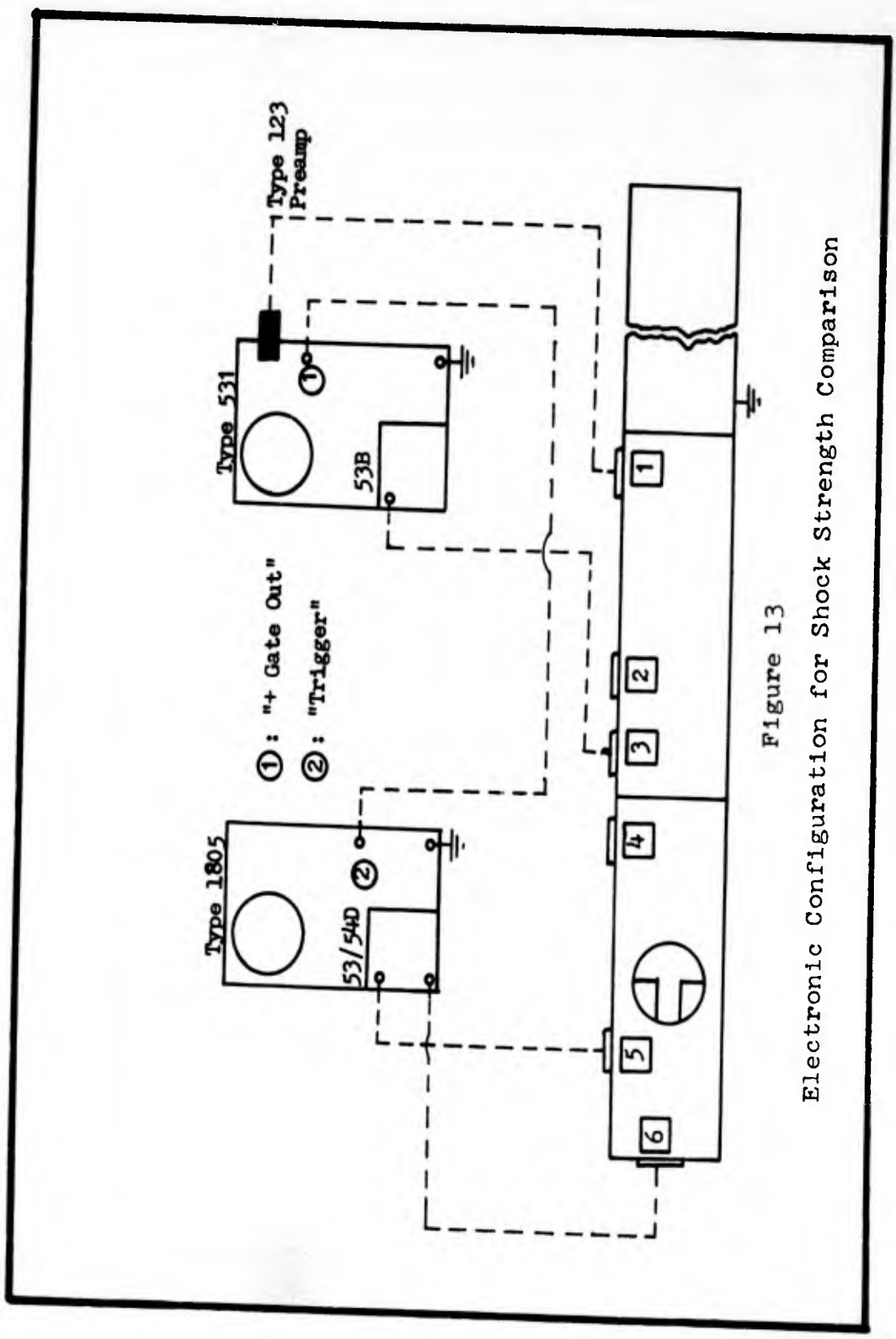

Figure 13

Electronic Configuration for Shock Strength Comparison

Figure 14a

Still Photo Sequence of Shock Wave Impinging on a 50.8% Area Reduction

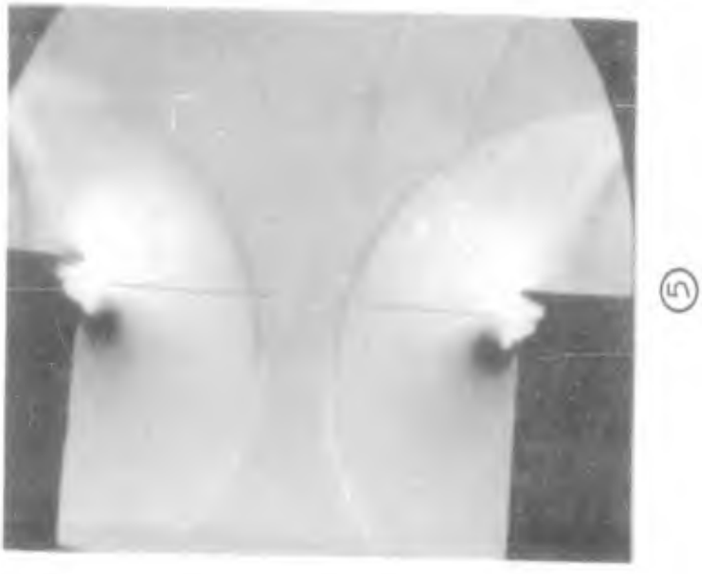

⑤

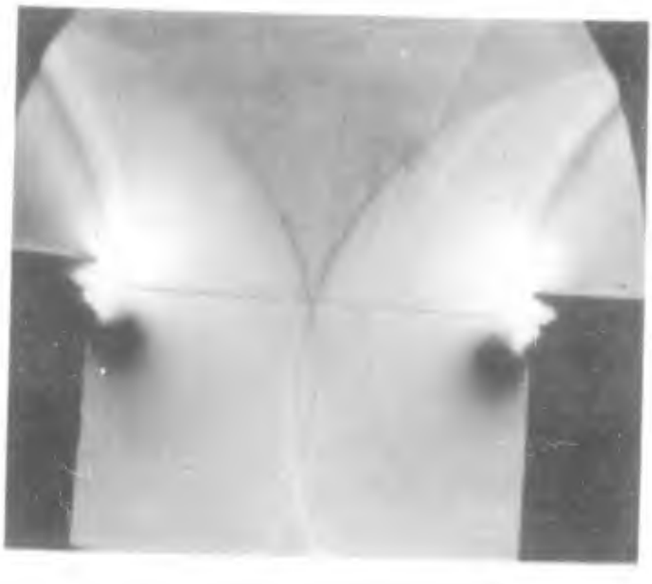

⑥

Figure 14b
Still Photo Sequence (cont.)

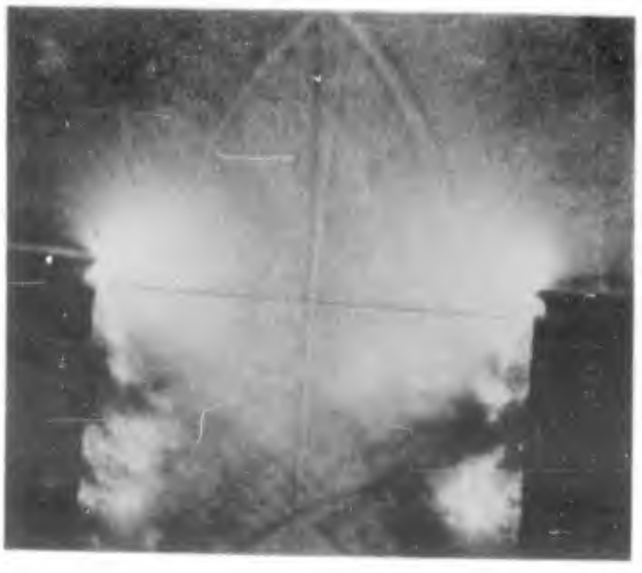

⑦

⑧

Figure 14c

Still Photo Sequence (concluded)

Figure 15

"Fastax" Camera Arrangement

with 89% Area Reducers in Test Section

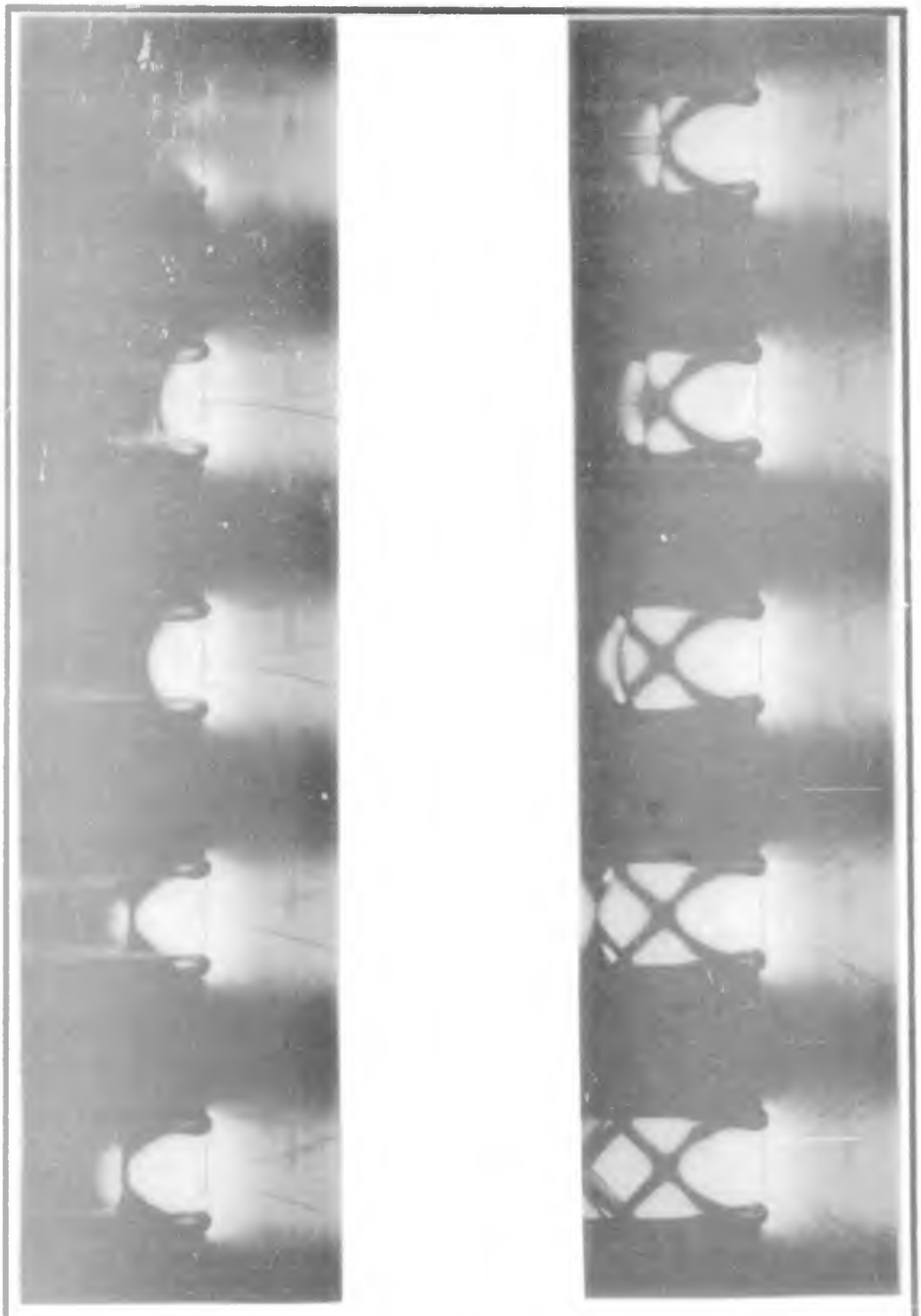

Figure 16a

Preliminary Investigation - Run 1 - Start
(3600 frames per second)

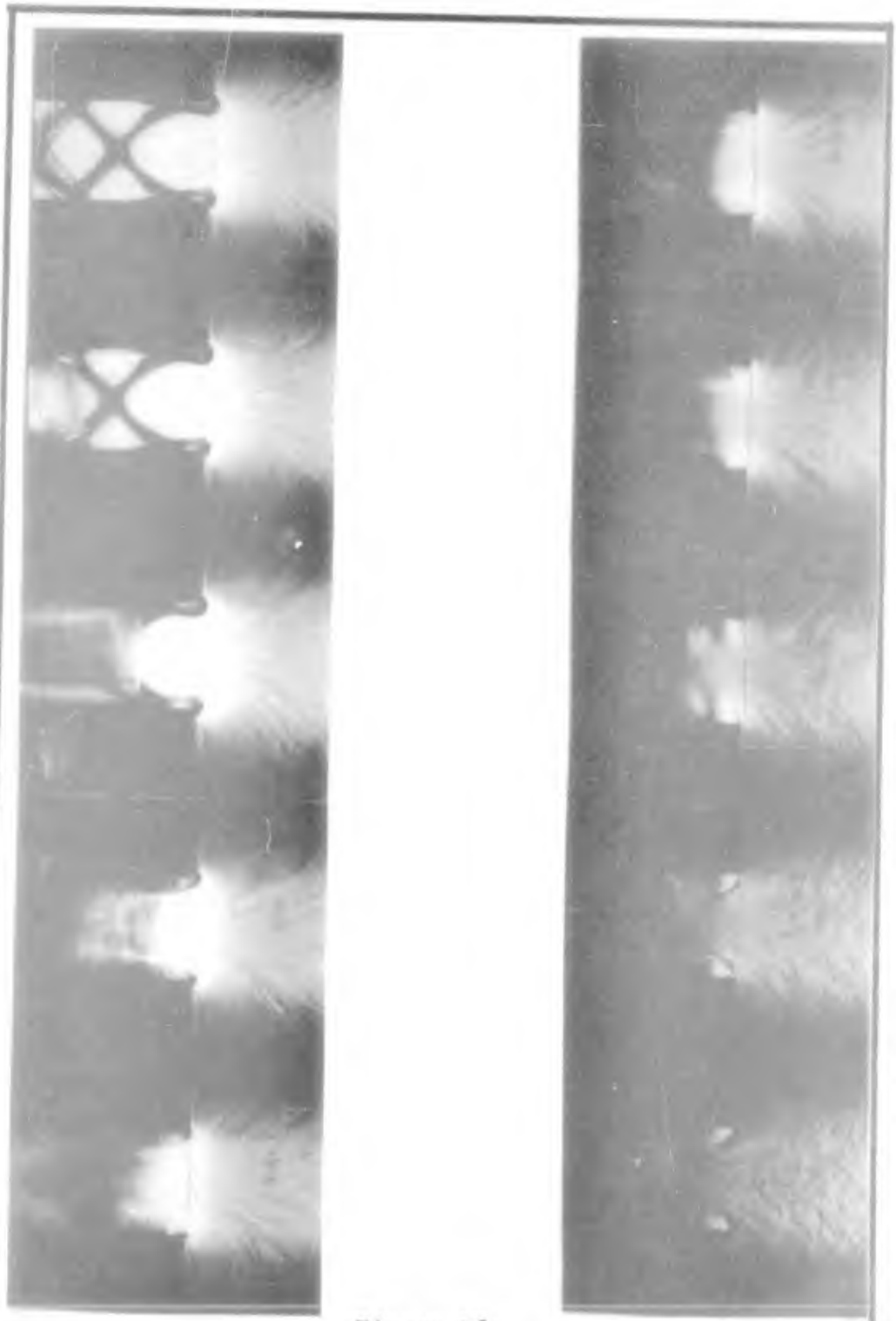

Figure 16b

Preliminary Investigation - Run 1 - End
(3600 frames per second)

Figure 16c

Preliminary Investigation - Run 1 - End
(3600 frames per second)

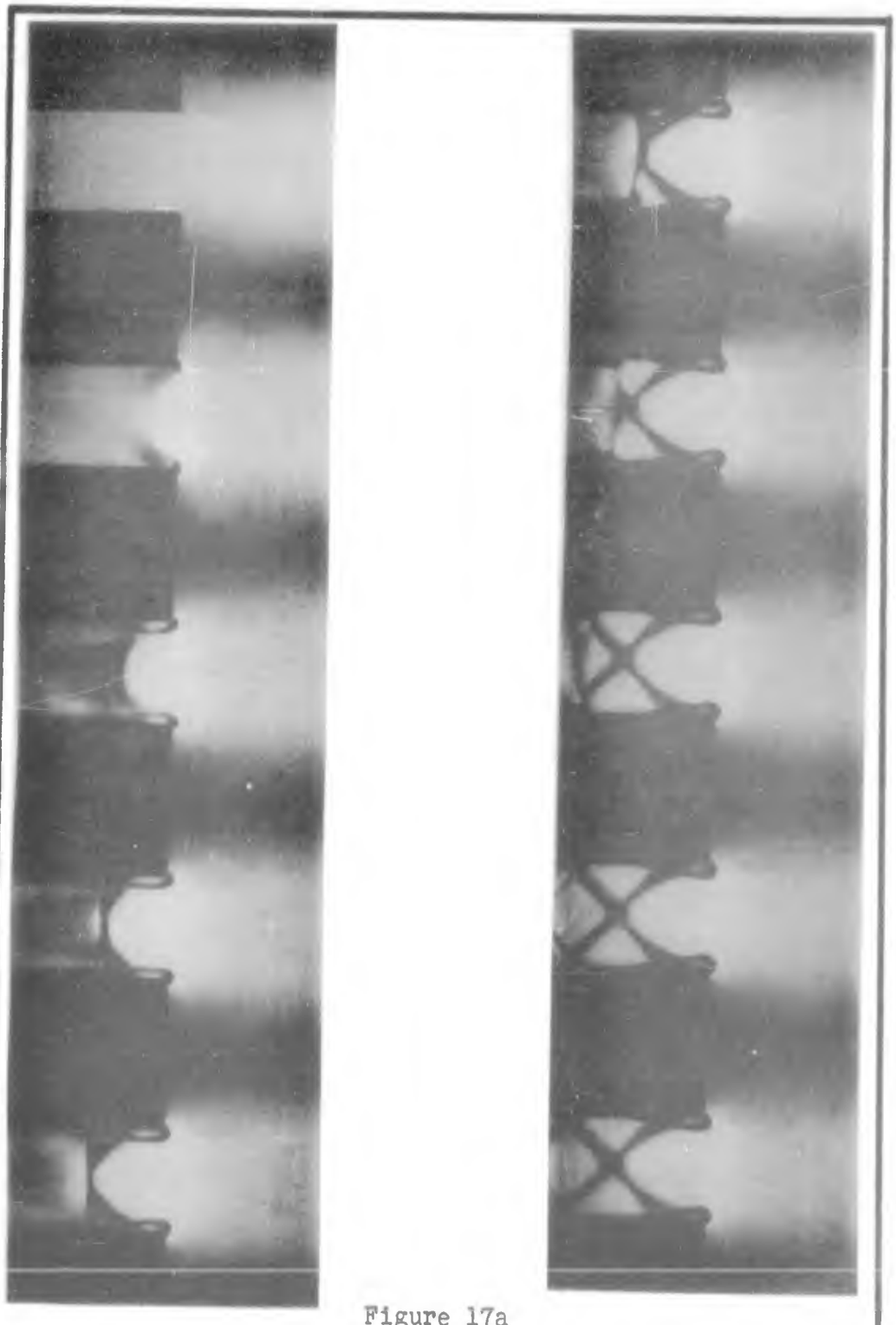

Figure 17a

Preliminary Investigation - Run 2 - Start
(4250 frames per second)

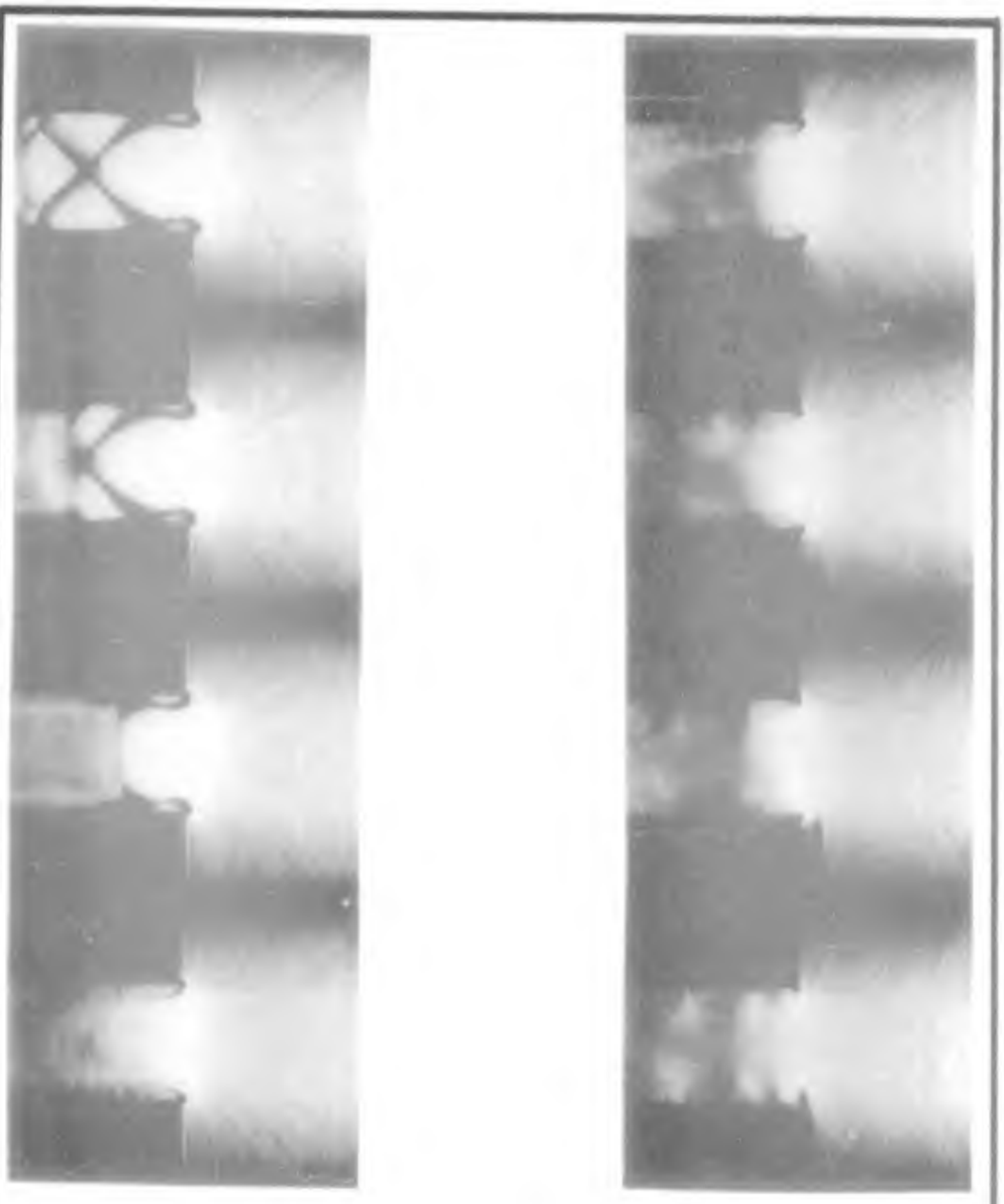

Figure 17b

Preliminary Investigation - Run 2 - End
(4250 frames per second)

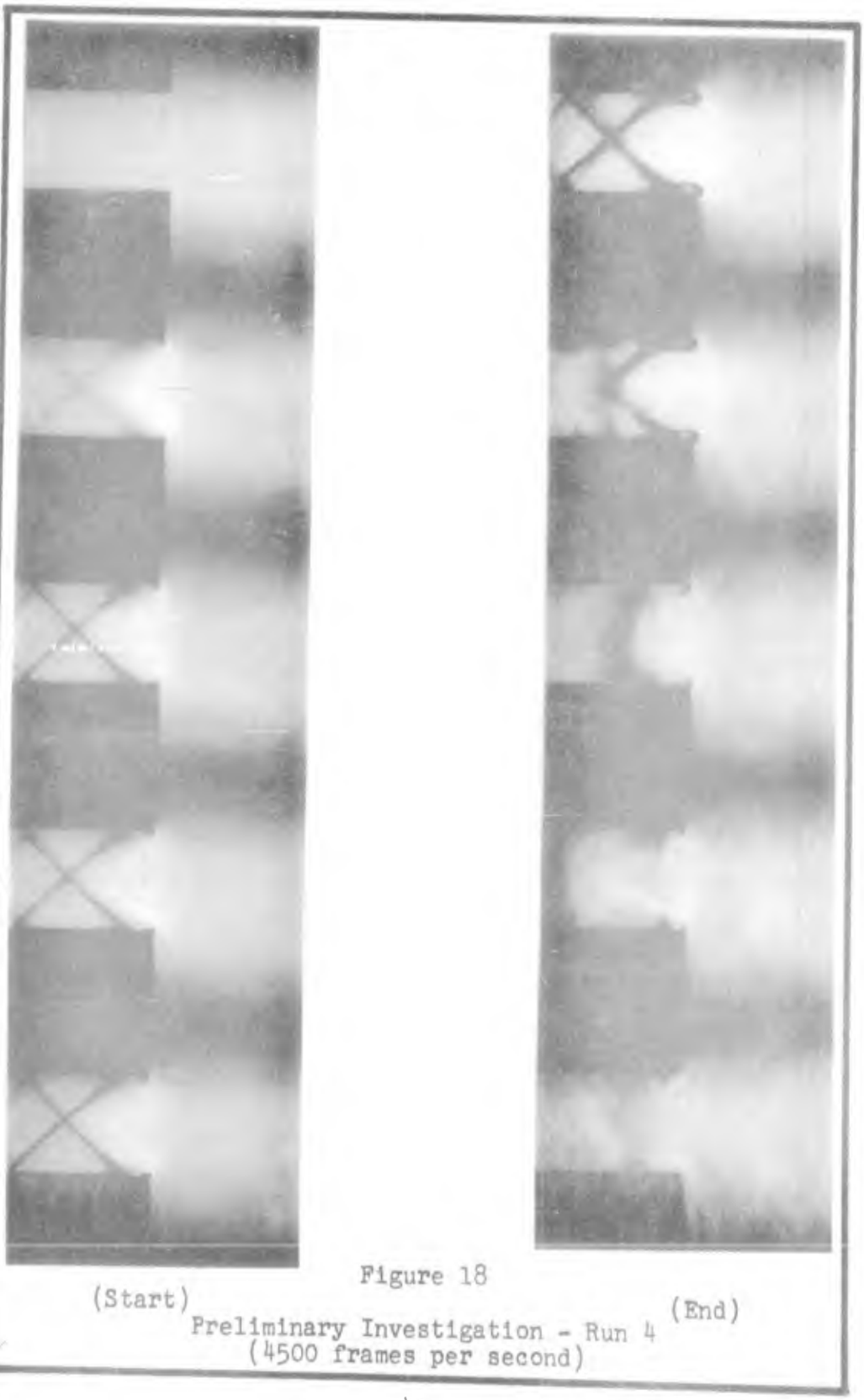

Figure 18

(Start) (End)

Preliminary Investigation - Run 4
(4500 frames per second)

V. Nozzle Design

A sharp-edge-throat type of supersonic nozzle was selected for this project because of its short length.

Using the method of characteristics as applied by Shames and Seashore (Ref 12), nozzle contours were graphically constructed for a nozzle with a throat height of 1 inch and Mach 3 at the exit. The graphical construction was laid out on 10 x 10 to the cm. graph paper with 10 cm. of scale equal to 1 inch. The coordinates were read directly from the graph paper with accuracy to three decimal places.

The calculated nozzle length and exit height was 8.48 and 4.235 inches, respectively. However, with accumulating errors in the graphical construction, the actual length and height were 8.88 and 4.50 inches. A check of the calculations and construction revealed no gross errors so the accumulated excess was permitted as a compensation for boundary layer.

The contours, as constructed, extend only from the throat to x = 11.00 (Fig 19). A 2-inch radius was selected for the entrance to provide parallel, uniform flow at the throat. A 3-inch straight section was added to the exit to provide a test section free from the interference of expansion waves at the exit lip.

Nozzle dimensions and contour coordinates are given in Figure 19.

The nozzle was cut out of two blocks of laminated birch hardwood. Each half of the nozzle had holes drilled and tapped into it so that it could be mounted securely at three different positions in the test section. Hole clearance provided for final alignment after the blocks were in the test section.

The surfaces of the nozzle exposed to the flow were sealed with several coats of varnish and finished with six coats of paste wax. The surface was very smooth and free of irregularities.

The nozzle blocks are shown in Figure 20.

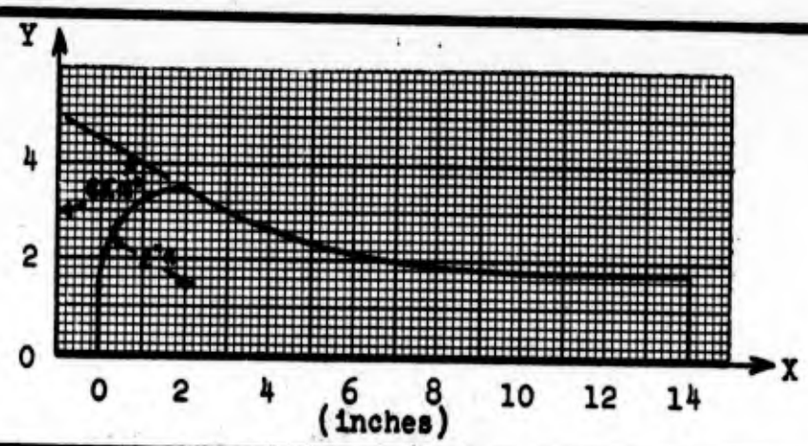

X	Y	X	Y
2.000	3.500	5.250	2.322
2.350	3.340	5.500	2.270
2.500	3.270	5.750	2.221
2.750	3.154	6.000	2.177
3.000	3.043	6.500	2.095
3.250	2.938	7.000	2.023
3.500	2.838	7.500	1.964
3.750	2.746	8.000	1.911
4.000	2.660	8.500	1.879
4.250	2.583	9.000	1.828
4.500	2.510	10.000	1.778
4.750	2.443	11.000	1.750
5.000	2.380	14.000	1.750

Figure 19

Nozzle Coordinates

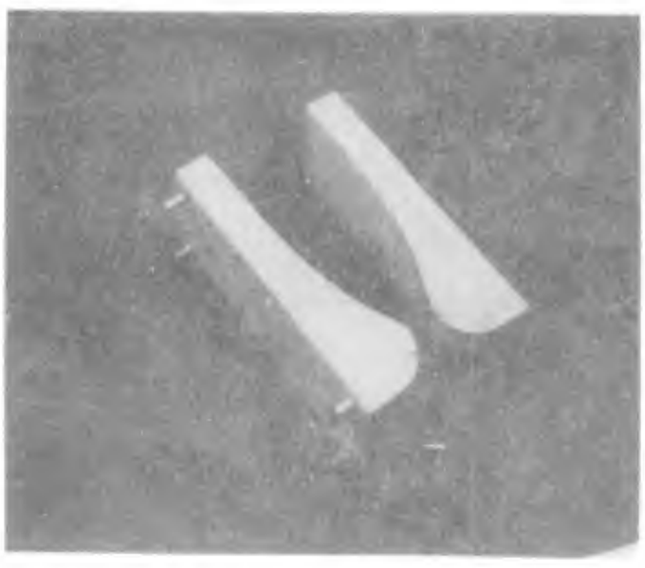

Figure 20

The Nozzle Blocks

VI. Nozzle Test Program

Objectives

A nozzle test program was conducted to determine:

1. The actual test section Mach number as a function of incident shock strength.

2. The available test time as a function of incident shock strength.

3. The usable test flow duration as a function of incident shock strength.

4. The test time lost because of the starting shock in the nozzle.

5. The extent of flow separation at the nozzle throat.

Test Program

The test program consisted of five series of runs with the plenum chamber attached to the shock tube and the nozzle blocks in the test section. The incident shock data is presented in Table II. Series A and B were preliminary in nature and were not used to obtain quantitative results. Series C, D, and E were evaluated and the results are presented in Chapter VII.

Series A and B. Series A and B consisted of three runs each, with varied pressure ratios to produce a weak shock wave ($P_{21} < 2$), a medium strength shock wave ($P_{21} \simeq 5$), and the strongest shock wave obtainable ($P_{21} > 10$).

Table II

Incident Shock Data#

Series	Run No.	p_4 in Hg abs	p_1 in Hg abs	P_{41}	W_s fps (a,b)	M_s (a,b)	P_{21} (a,c)
A	1	146.0	28.95	5.04	1460	1.27	1.72
	2	221.0	4.41	50.1	2340	2.04	4.67
	3	220.9	0.29	767	3470	3.02	10.45
B	1	144.8	28.80	5.03	1430	1.25	1.66
	2	220.8	4.40	50.2	2350*	2.1*	4.9*
	3	225.8	0.32	706	3430	3.00	10.34
C	1	224.0	28.95	7.74	1710	1.49	2.43
	2	224.0	19.96	11.2	1840	1.61	2.85
	3	224.5	14.16	15.9	1950	1.71	3.23
	4	225.7	9.97	22.6	2100	1.83	3.76
	5	225.2	5.00	45.0	2350	2.05	4.74
	6	223.0	0.35	637	3450	3.01	10.40
D	1	225.0	29.05	7.75	1710	1.49	2.43
	2	225.0	19.99	11.3	1850	1.62	2.88
	3	225.0	14.70	15.3	1990	1.74	3.36
	4	225.0	10.11	22.3	2090	1.82	3.71
	5	225.0	5.06	44.5	2360	2.06	4.78
	6	225.0	0.37	608	3410	2.96	10.08
E	1	225.0	29.04	7.75	1670	1.45	2.29
	2	225.0	19.86	11.3	1820	1.59	2.77
	3	225.0	15.13	14.9	2010	1.74	3.38
	4	225.0	10.11	22.3	2160	1.88	3.94
	5	225.0	5.10	44.1	2450	2.13	5.14
	6	225.0	0.42	536	3560	3.10	11.02

\# - See Appendix B
* - Estimated
a - Nominal Values
b - Maximum Error, ±4.5%
c - Maximum Error, ±9.0%

In Series A, the nozzle was located in the test section with the throat 1 inch downstream of the center-line of the test section windows.

In Series B, the exit plane of the nozzle was even with the center-line of the test section windows. An 18° wedge was mounted in the test section in the region of parallel, uniform flow. The wedge, mount, and mounting plugs are shown in Figure 21. Figure 22 shows the test section with the wedge in place.

Series C, D, and E. Series C, D, and E consisted of six runs each. In each series, a constant chamber pressure was maintained and the channel pressure was varied in six steps from atmospheric pressure to the lowest vacuum obtainable. Runs 1, 2, 3, and 4 were set up to have subsonic flow in region 2. Run 5 and 6 were to have supersonic flow. Since the initial conditions were held similar, corresponding runs are comparable between each series; i.e., Run C-1 compares with Run D-1 and E-1.

The configuration for Series C was the same as for Series B. This is referred to as the Model Test Position (Fig 23). Series D was conducted with the nozzle throat located 1 inch upstream from the center-line of the test section windows. This is referred to as the Throat Test Position (Fig 24). Series E was conducted with the nozzle throat 5 inches upstream from the center-line of the windows. This is referred

to as the Intermediate Test Position (Fig 25).

Data Collection

Incident Shock. Data concerning the incident shock was calculated from velocity measurements taken with the Type 531 oscilloscope and the Type 53/54D plug-in unit combination. The velocity was determined between transducers 1 and 3. Appendix B gives a detailed example.

Flow Field. The Schlieren image of the flow field was recorded by the same "Fastax" camera arrangement as used for the runs with the area reducers (Fig 10, 12). Timing marks were printed at 1 millisecond intervals along the film. The film was processed, viewed and edited. Selected portions of the film from each run were enlarged and printed for closer observation.

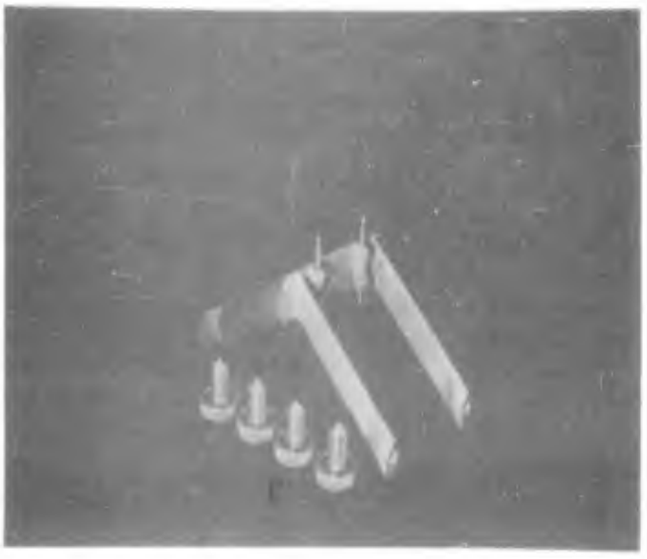

Figure 21

The 18° Wedge, Mount, and Mounting Plugs

Figure 22

"Fastax" Camera Arrangement

with Nozzle and Wedge in the Test Section

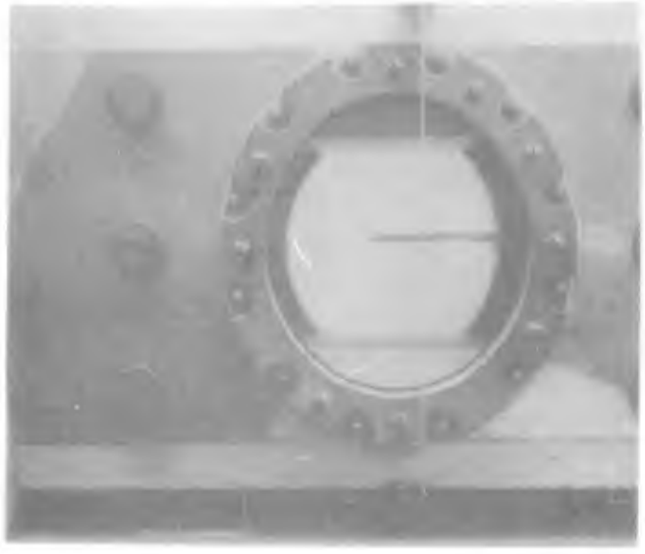

Flow

Figure 23

Test Section with Nozzle in the Model Test Position

(Exit plane of nozzle @ centerline of window)

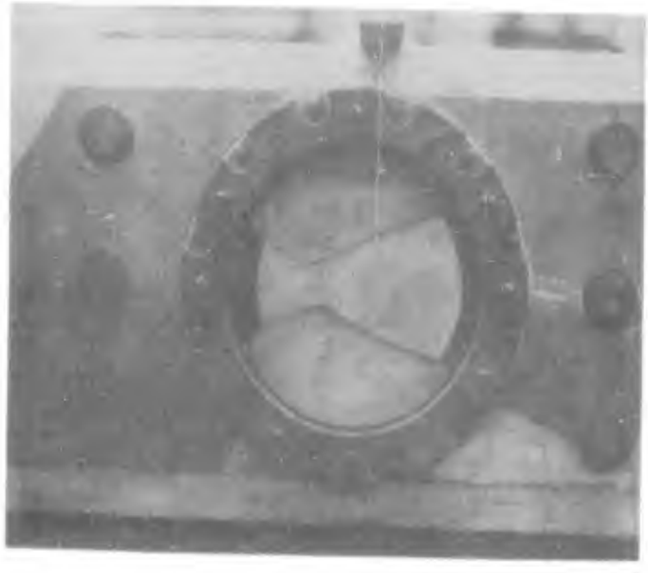

Flow

Figure 24

Test Section with Nozzle in the Throat Test Position

(Throat 1" upstream from centerline of window)

Flow

Figure 25

Test Section with Nozzle
in the Intermediate Test Position

(Throat 5" upstream from centerline of window)

VII. Nozzle Test Results

General

This chapter consists of a summary of test results and includes selected flow field pictures from Series C, D, and E. These pictures are included to provide the reader with a visual grasp for the process that takes place in the nozzle.

In each of the series of runs, the transmitted shock is visible as a rather oblique-looking figure as in Figure 38a. Its odd appearance is caused by the fact that it has been distorted and is no longer one-dimensional.

After the transmitted shock passes through the throat, flow begins and the starting shock is formed. This process is shown in Figures 33 through 37. The region between the transmitted shock and the starting shock is characterized by very turbulent flow.

By the time the starting shock reaches the test section, it has been weakened considerably and is not well defined (Fig 27 - 32). Uniform, steady flow is established after the starting shock has passed through the test section and an oblique shock is formed at the leading edge of the wedge.

As flow continues, the pressure ratio across the nozzle drops and the starting shock moves back into the test section, disrupting the oblique shock attached to the wedge. The starting shock continues upstream to the throat and then dissipates.

A short time thereafter, another transmitted shock is observed passing through the nozzle as shown in Figure 39. This transmitted shock is caused by the reflected incident shock which has been re-reflected by the contact surface (See Fig 2). Usable flow is not established behind this shock because the pressure ratio is too low. It is this shock that should have disrupted the test flow rather than the starting shock moving back upstream.

Test Section Mach Number

The test section Mach number was determined by measuring the oblique shock wave angle and using the method discussed in Appendix C.

The Mach number ranged from 2.6 to 2.8 during each run. This variation is probably caused by the unsteady nature of the pressure generating process. For the runs analyzed, the range of fluctuation was independent of incident shock strength.

Available Test Time

The available test time was determined by counting the timing marks on the film between the incident shock and the first disturbance from upstream. This time increased from 28 to 39 milliseconds as the incident shock strength increased. Table III summarizes the values for each run.

Usable Test Flow Duration

The usable test time was considered as that time during which the oblique shock wave attached to the wedge was well established and there were no transient disturbances in the steady flow through the test section. The usable duration varied from zero for Run C-1 to 18.4 milliseconds for Run C-6.

Although flow was nearly established for Run C-1, it was not long enough for testing purposes (Fig 27d).

Lost Test Time

Due to Nozzle Starting Shock. This time interval is that interval from the arrival of the incident shock until the oblique shock is formed on the wedge. The time loss decreased from 7.6 milliseconds for Run C-2 to 0.9 milliseconds for Run C-6.

This decrease could be caused by the increased transmitted shock strength and flow velocity since both increase with increasing incident shock strength.

Although not specifically proven in this study, it is believed that a possible primary cause is the lower pressure in the nozzle and plenum chamber. If this is true, the addition of a weak diaphragm in front of the nozzle would permit evacuation of the nozzle and plenum chamber to a lower pressure for all runs. This diaphragm would rupture when struck by the incident shock. The conditions in the middle section of the

of the shock tube, between the two diaphragms, could then be adjusted to produce the desired test section conditions.

Due to Pressure Drop. This loss is the difference between the test time available, and the sum of the usable test time and the time lost due to the nozzle starting shock. It varied from 23.5 milliseconds for Run C-2 up to 25 milliseconds for Run C-4 and then down to 18.7 milliseconds for Run C-6.

No specific tests were made to determine this loss; however, it was observed in each of the runs that the usable test flow dissipated before a disturbance from upstream arrived to disrupt it. This observation indicates that the mass flow rate through the nozzle is too large, thus allowing the pressure ratio to drop below the critical value required for sonic velocity at the throat, before the disrupting disturbance arrives at the nozzle. This condition could be corrected by designing the nozzle with a smaller throat.

Flow Separation

There was no detectable flow separation at the nozzle throat during steady operation.

Table III

Time Data*

Run No.	Available Test Time			Nozzle Starting Shock Time Loss	Pressure Drop Time Loss	Usable Test Time
	Series			Series	Series	Series
	C	D	E	C	C	C
1	28	28	28	#	#	#
2	33	34	34	7.6	23.5	1.9
3	34	35	35	5.8	24.3	3.9
4	35	35	35	4.0	25.0	6.0
5	36	36	36	2.6	22.8	10.6
6	38	37	39	0.9	18.7	18.4

* - Time in milliseconds
# - Flow did not start

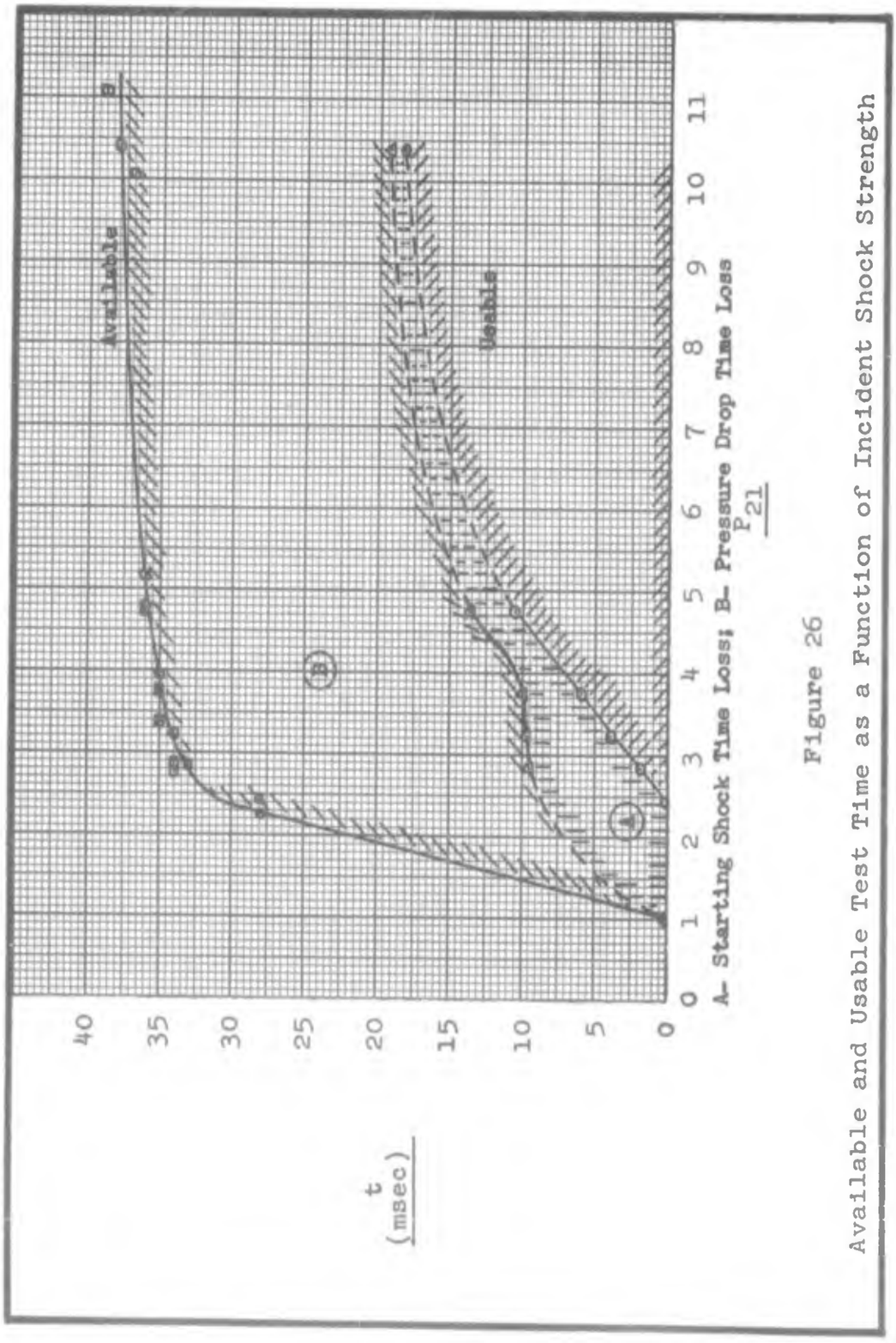

Figure 26

Available and Usable Test Time as a Function of Incident Shock Strength

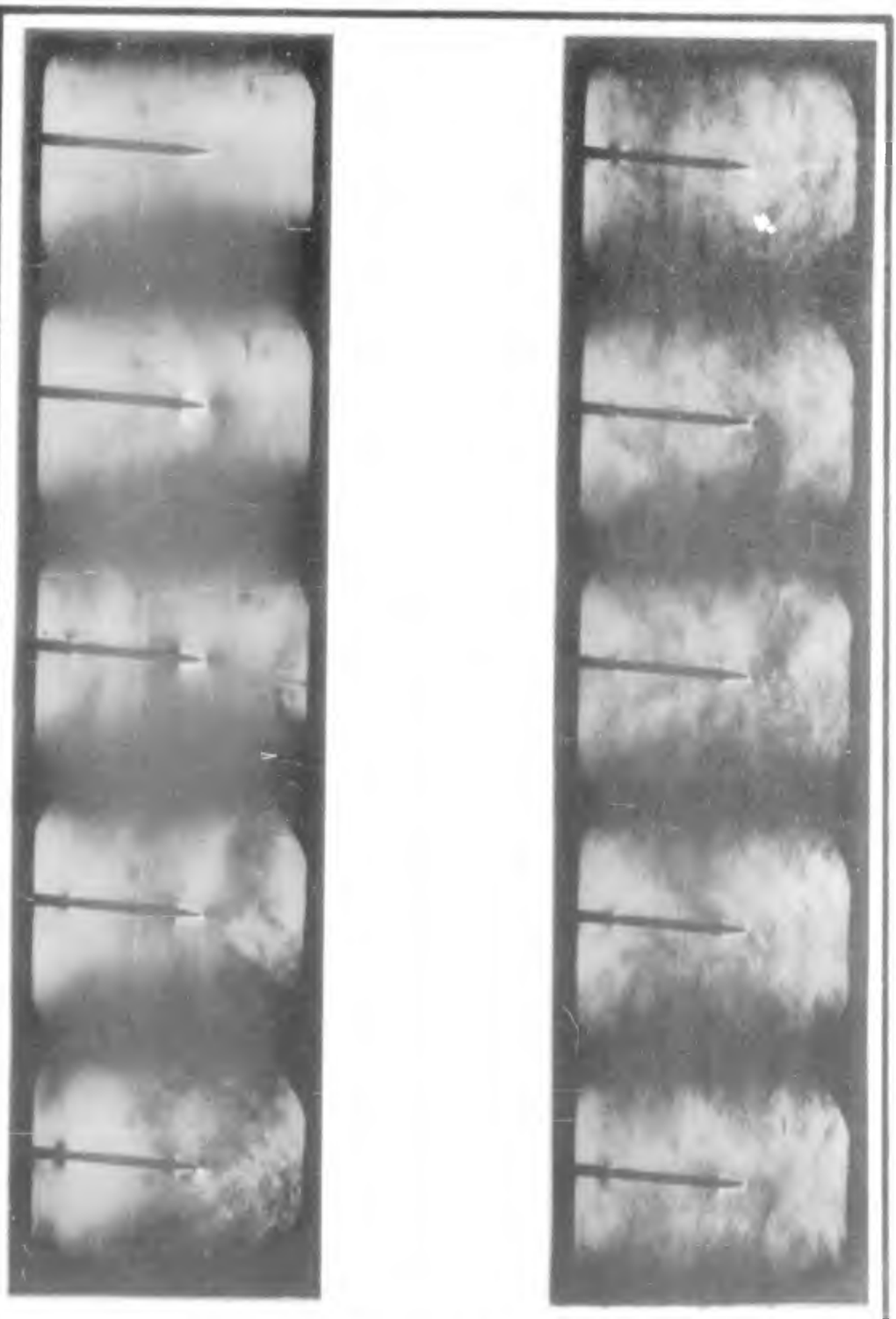

Figure 27a

Run C-1, Frames 1-10
(4725 frames per second)

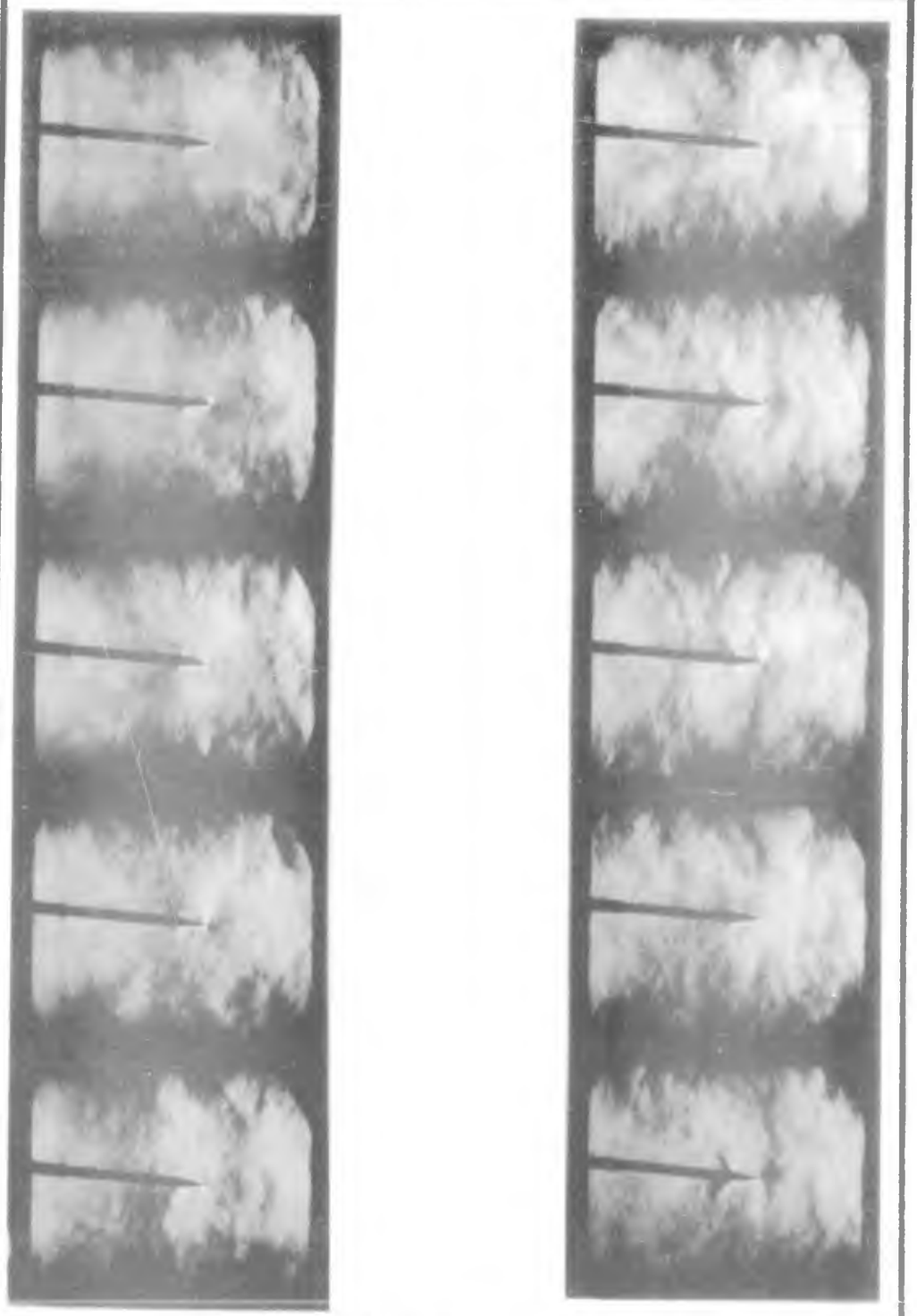

Figure 27b

Run C-1, Frames 11-20

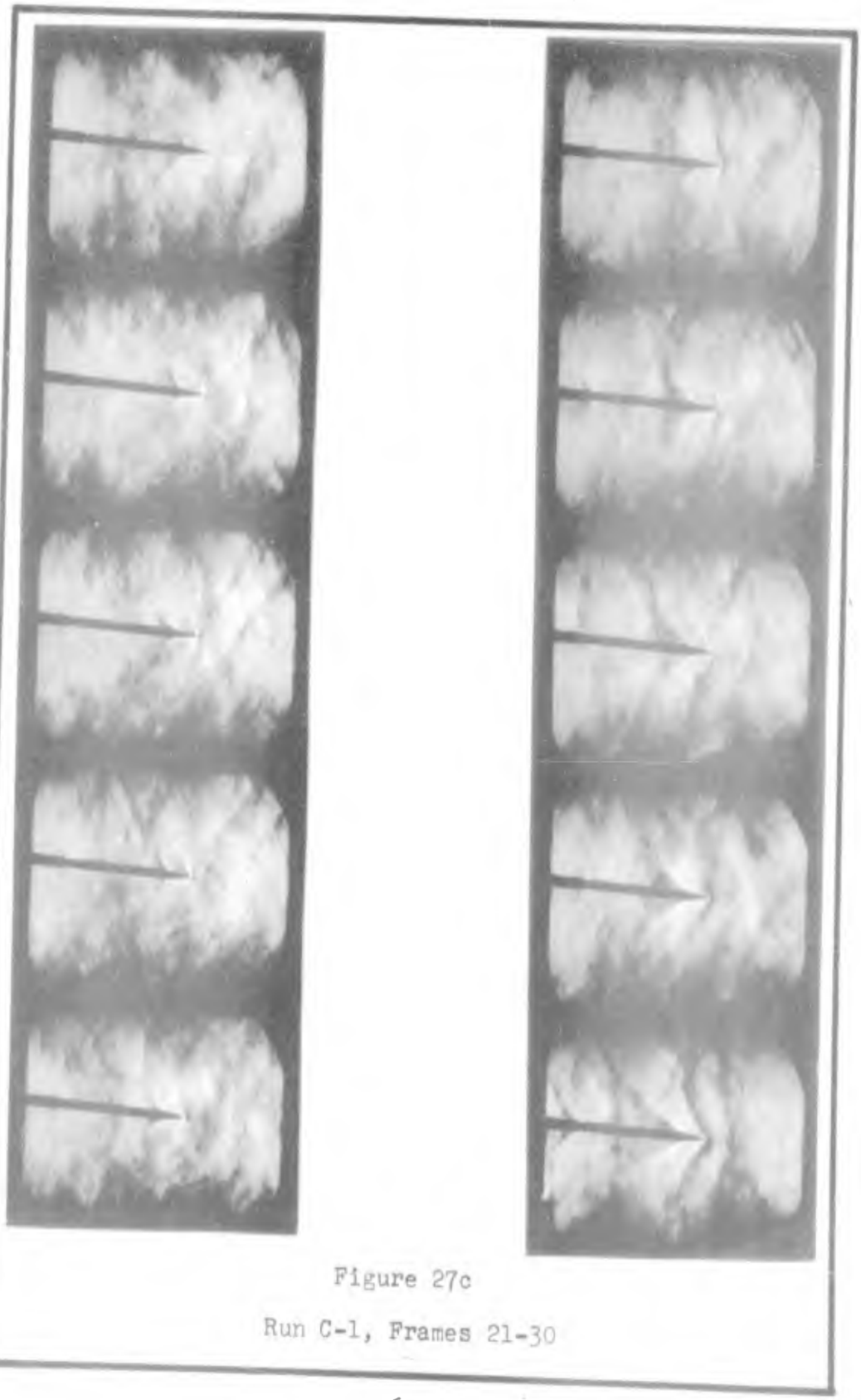

Figure 27c

Run C-1, Frames 21-30

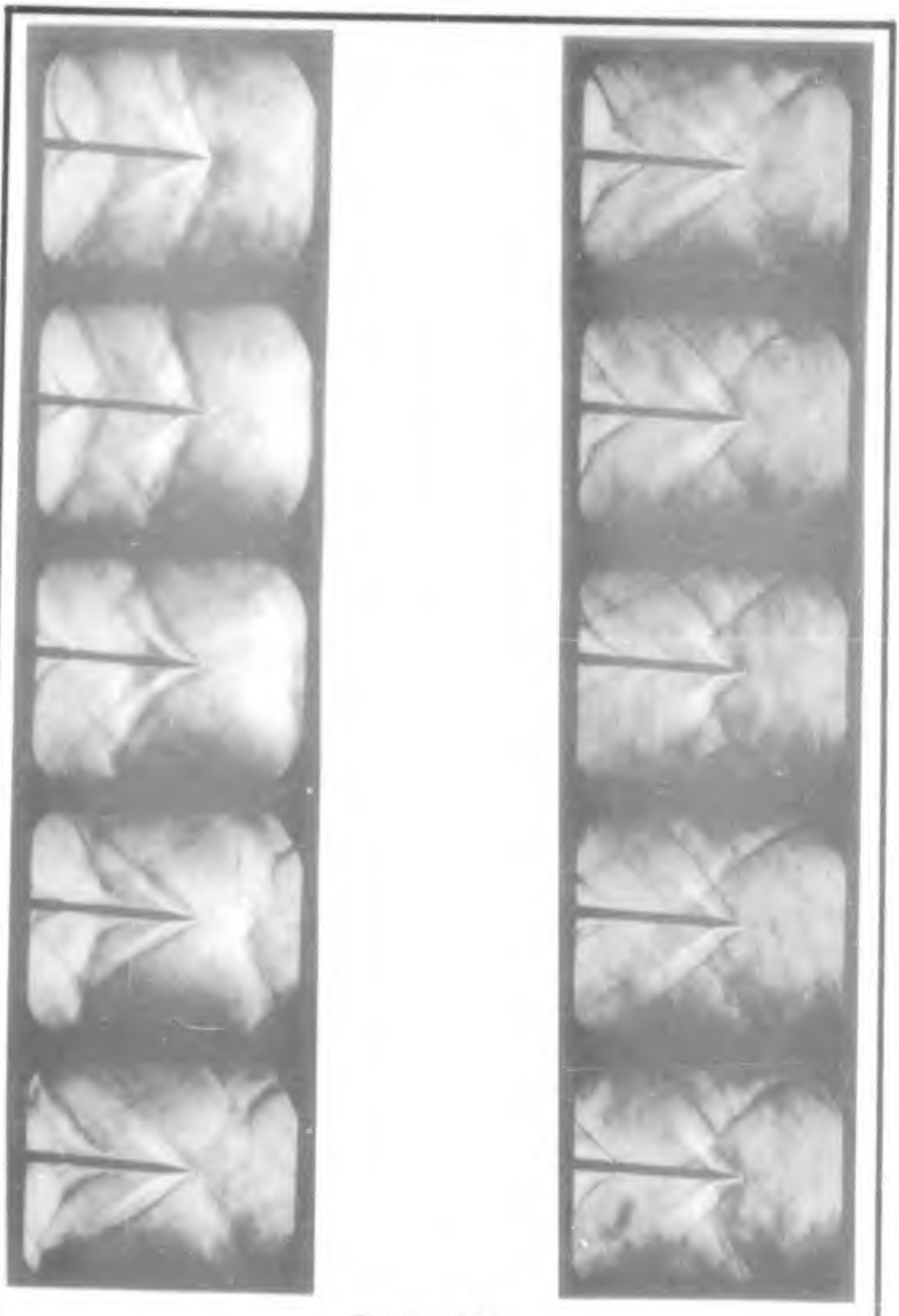

Figure 27d

Run C-1, Frames 31-40

Figure 27e

Run C-1, Frames 41-50

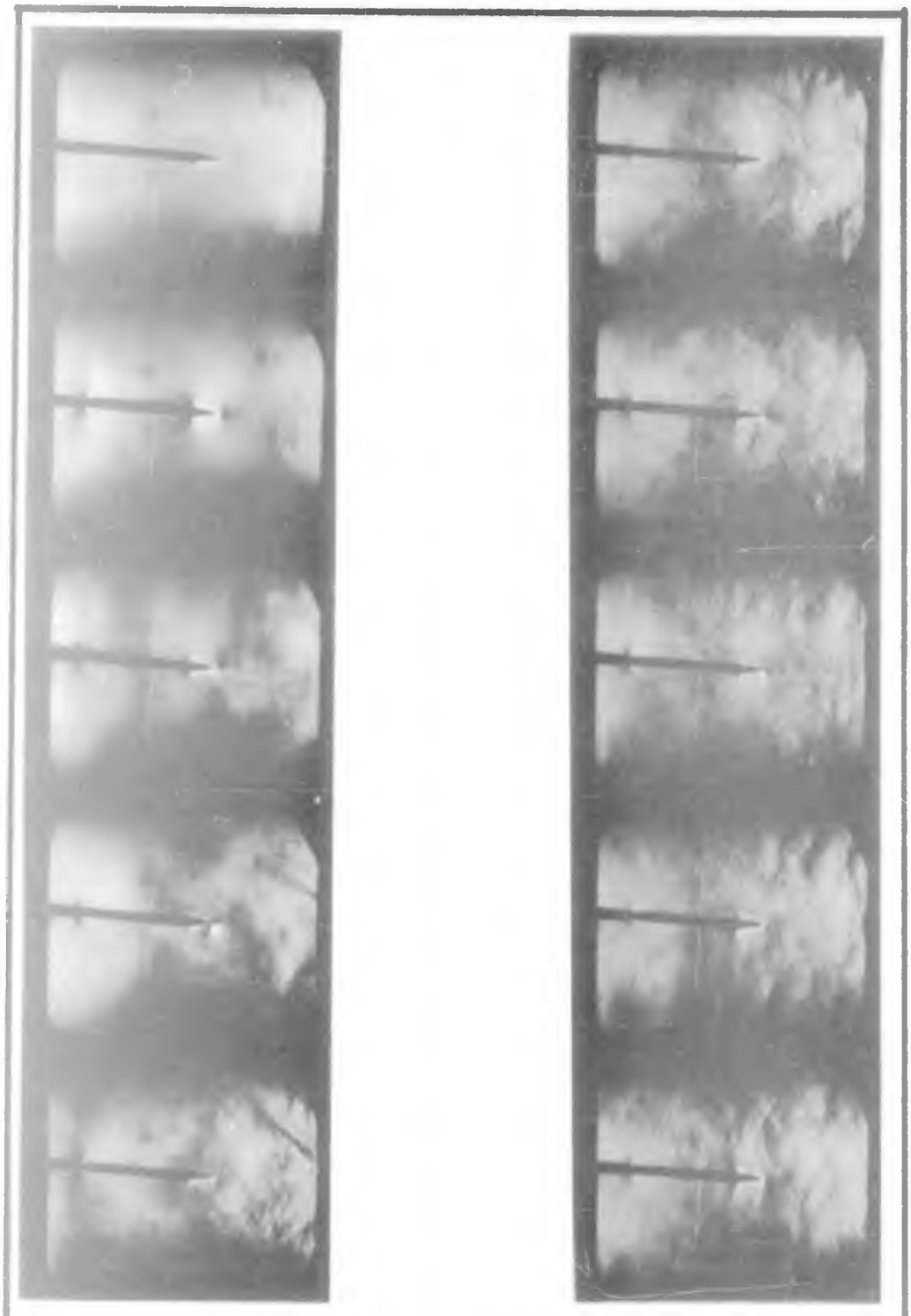

Figure 28a

Run C-2, Frames 1-10
(4850 frames per second)

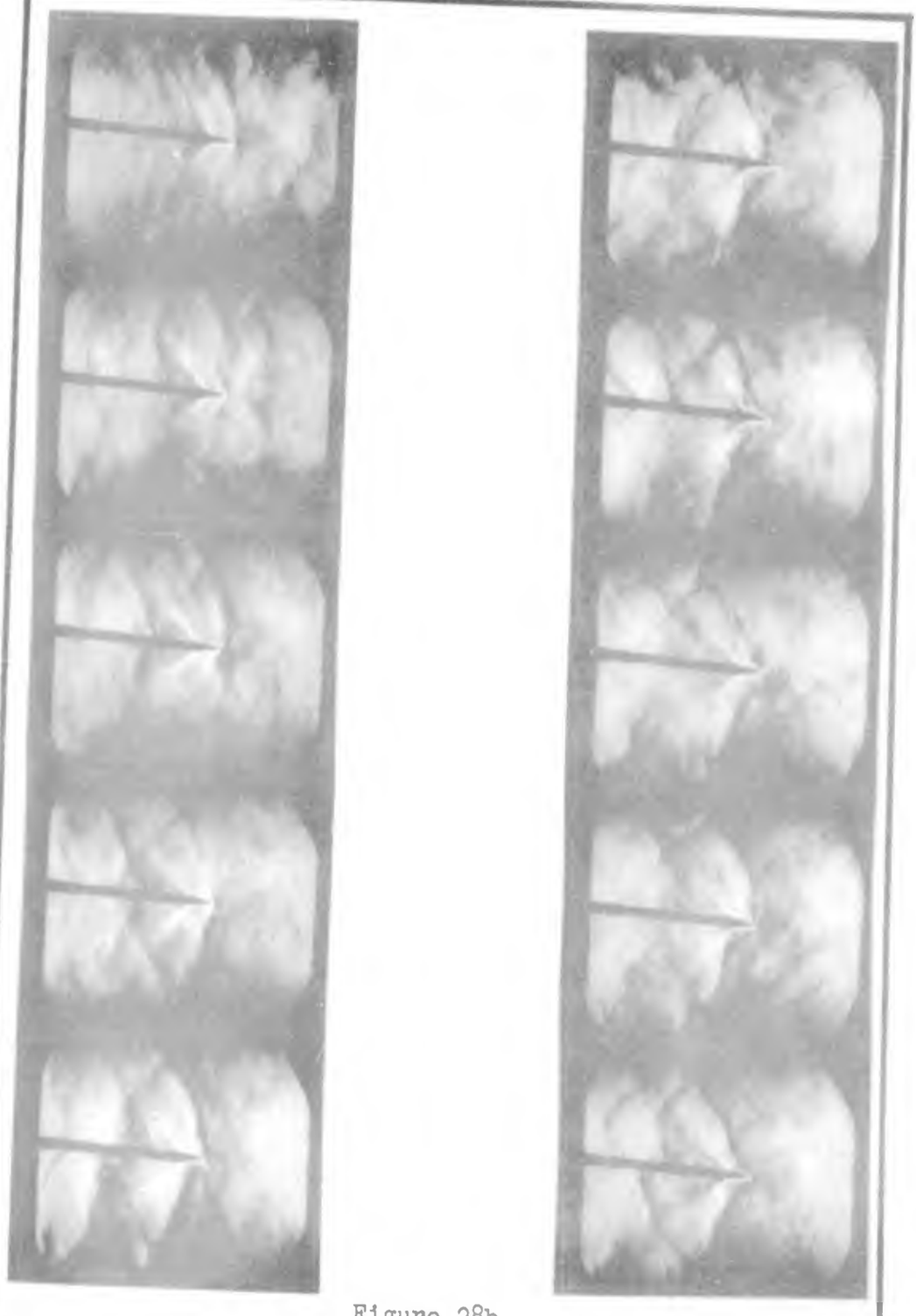

Figure 28b

Run C-2, Frames 11-20

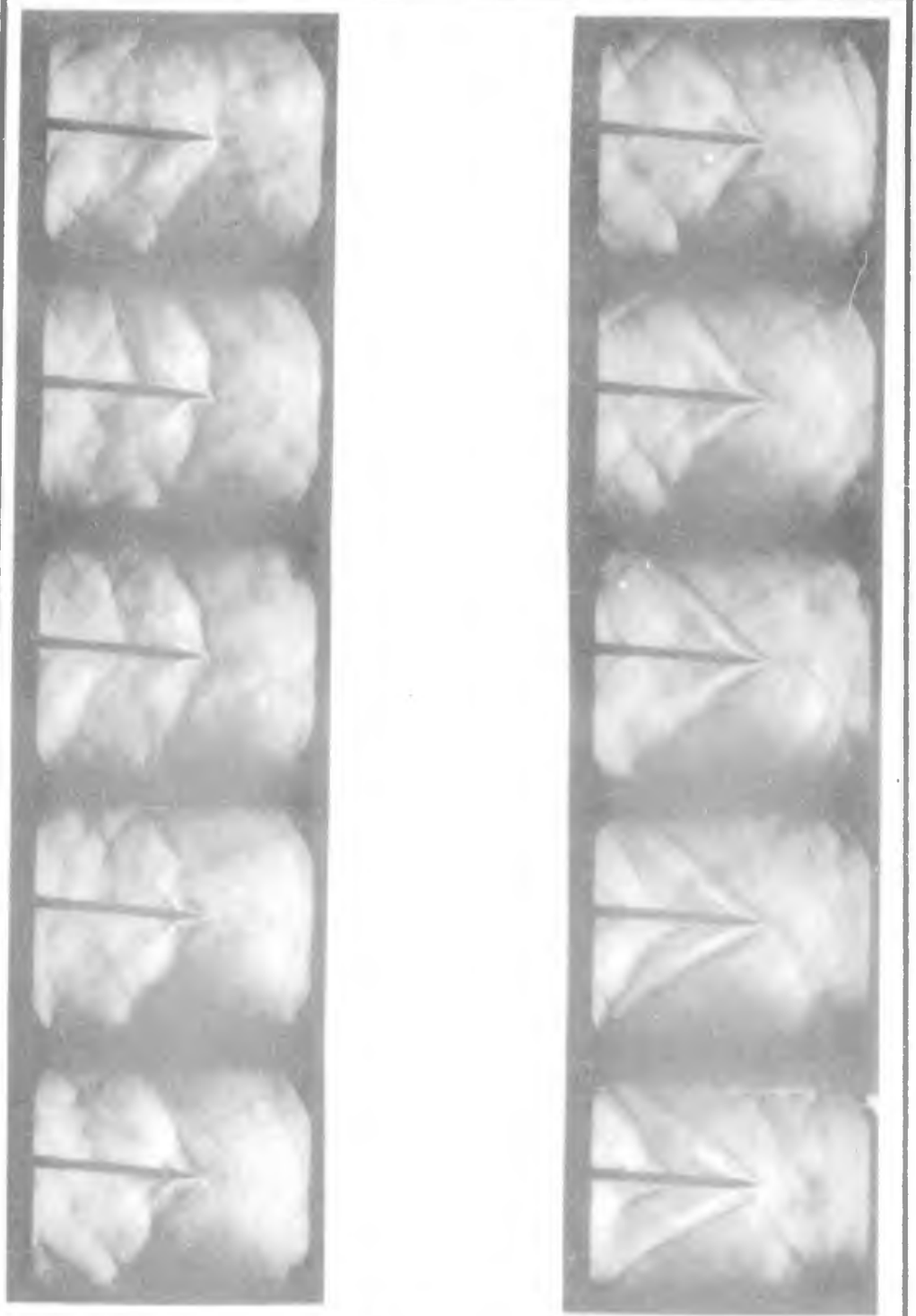

Figure 28c

Run C-2, Frames 21-30

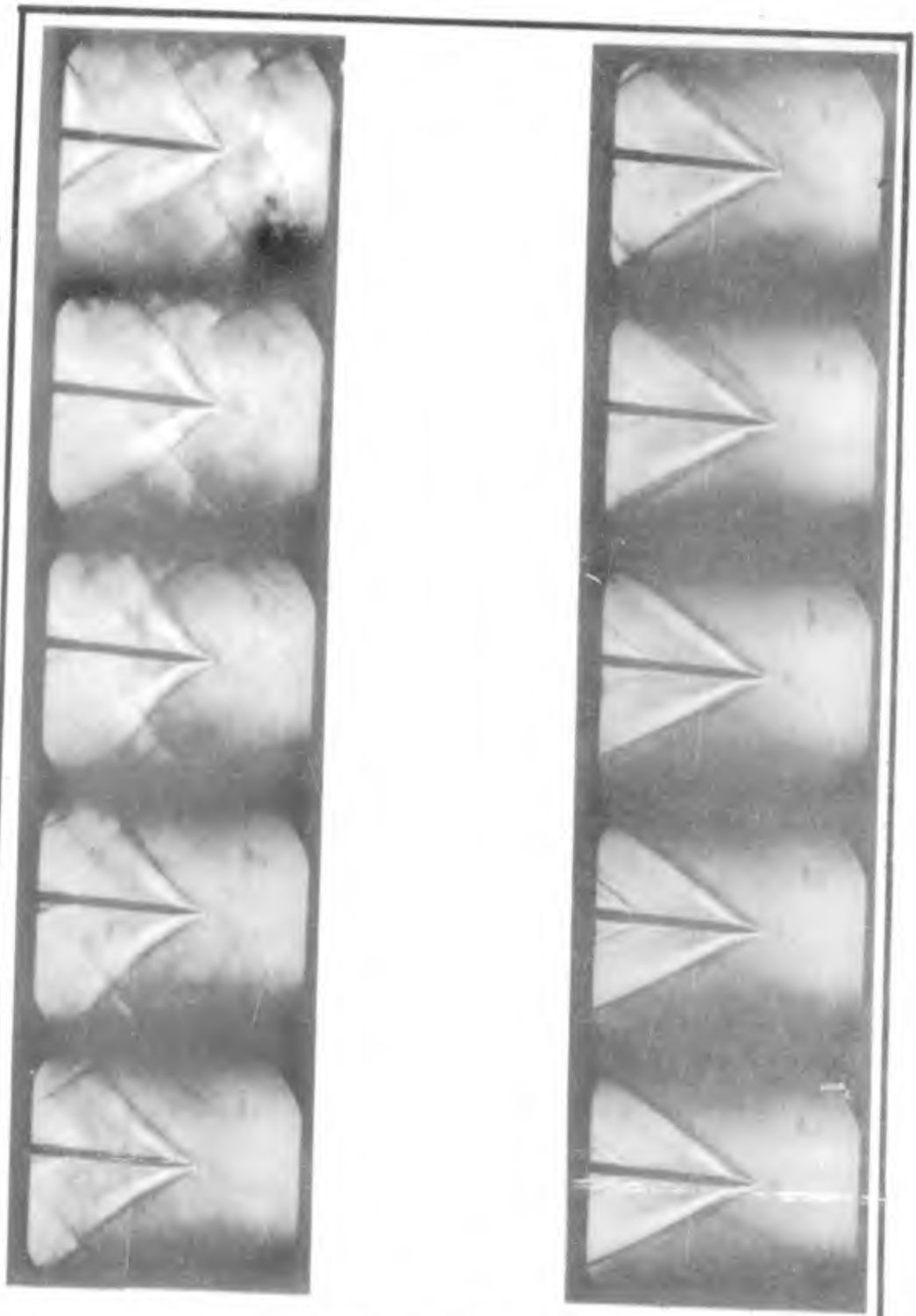

Figure 28d

Run C-2, Frames 31-40
(Frames 41-45 same as 40)

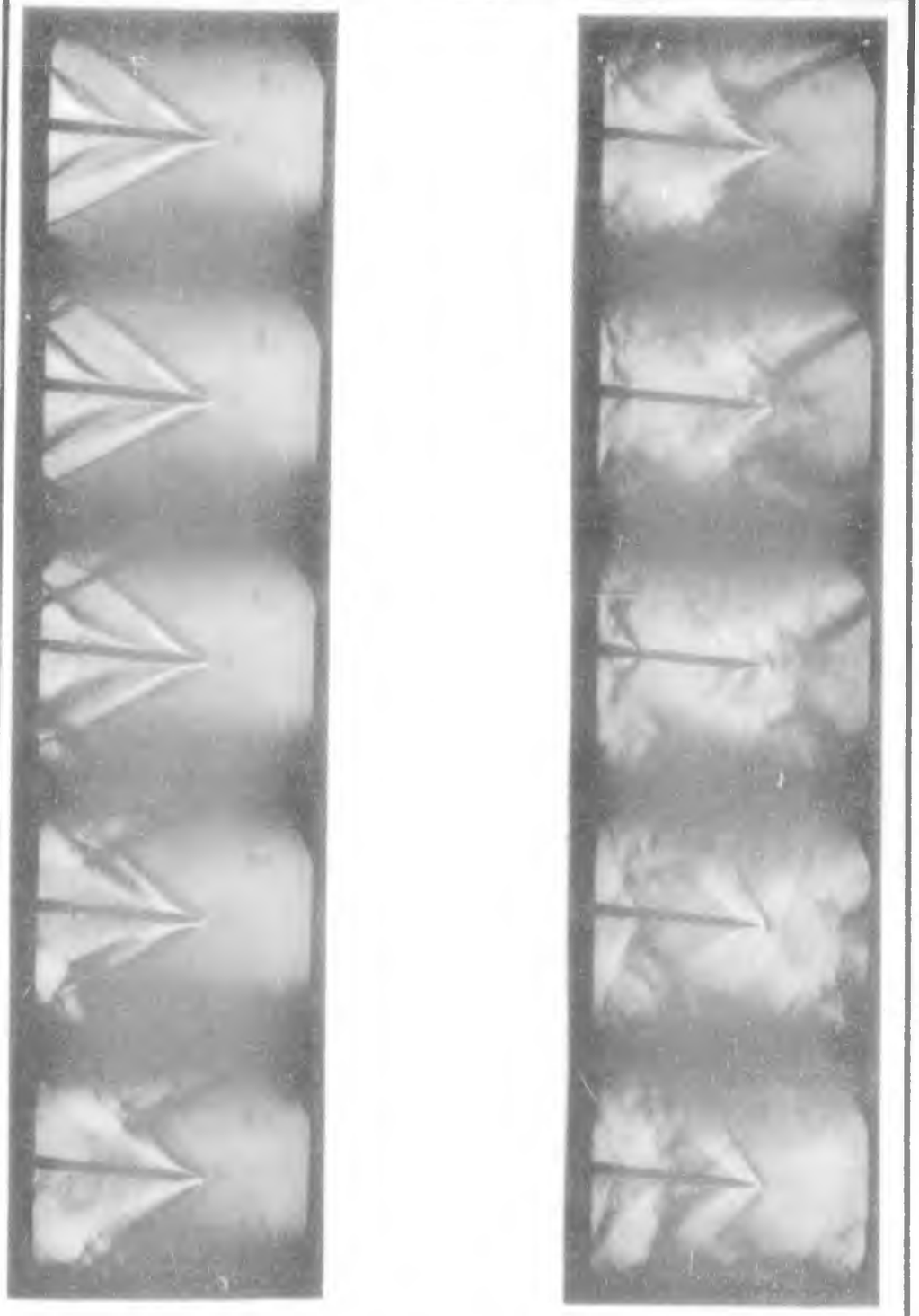

Figure 28e

Run C-2, Frames 46-55

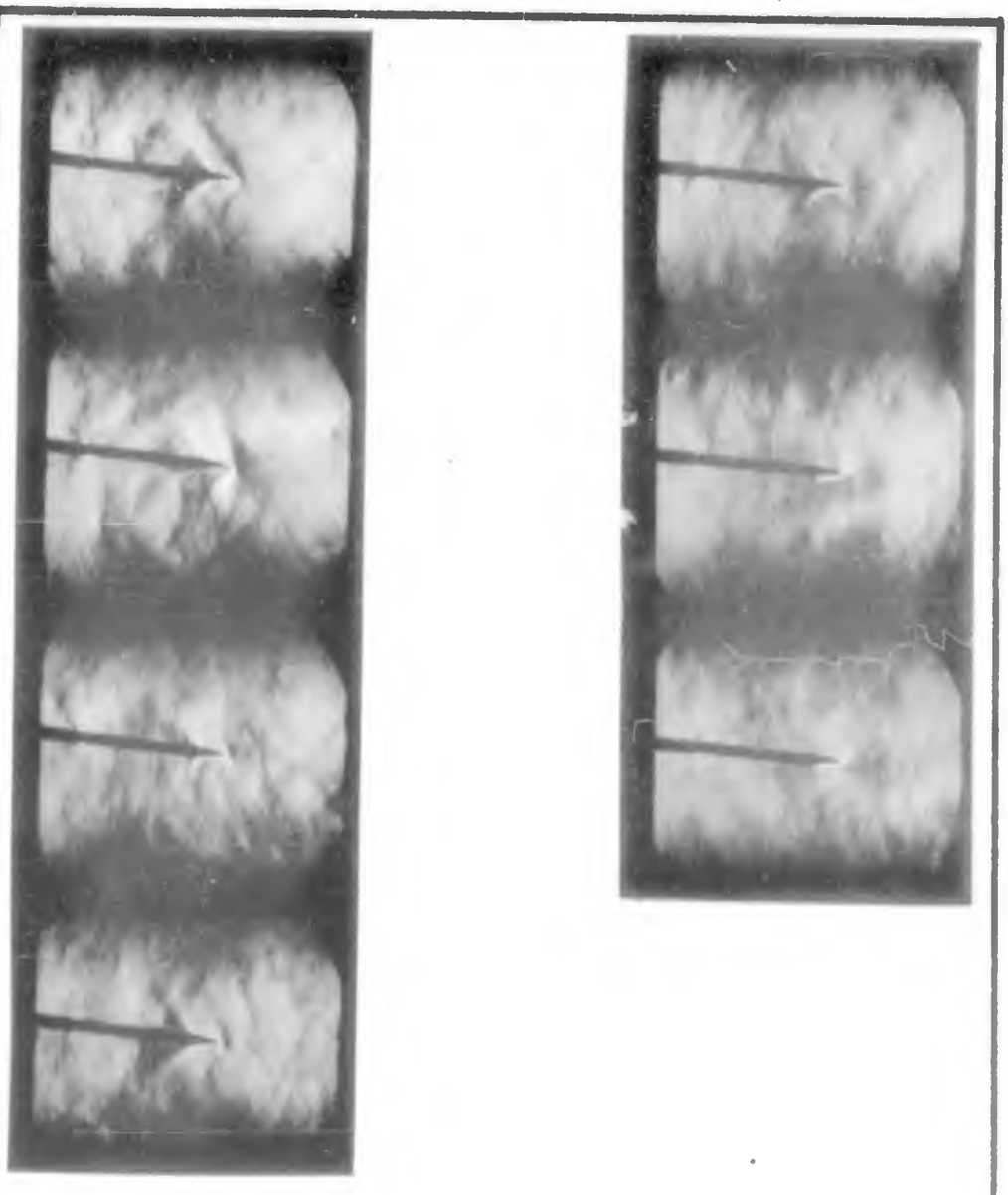

Figure 28f

Run C-2, Frames 56-62

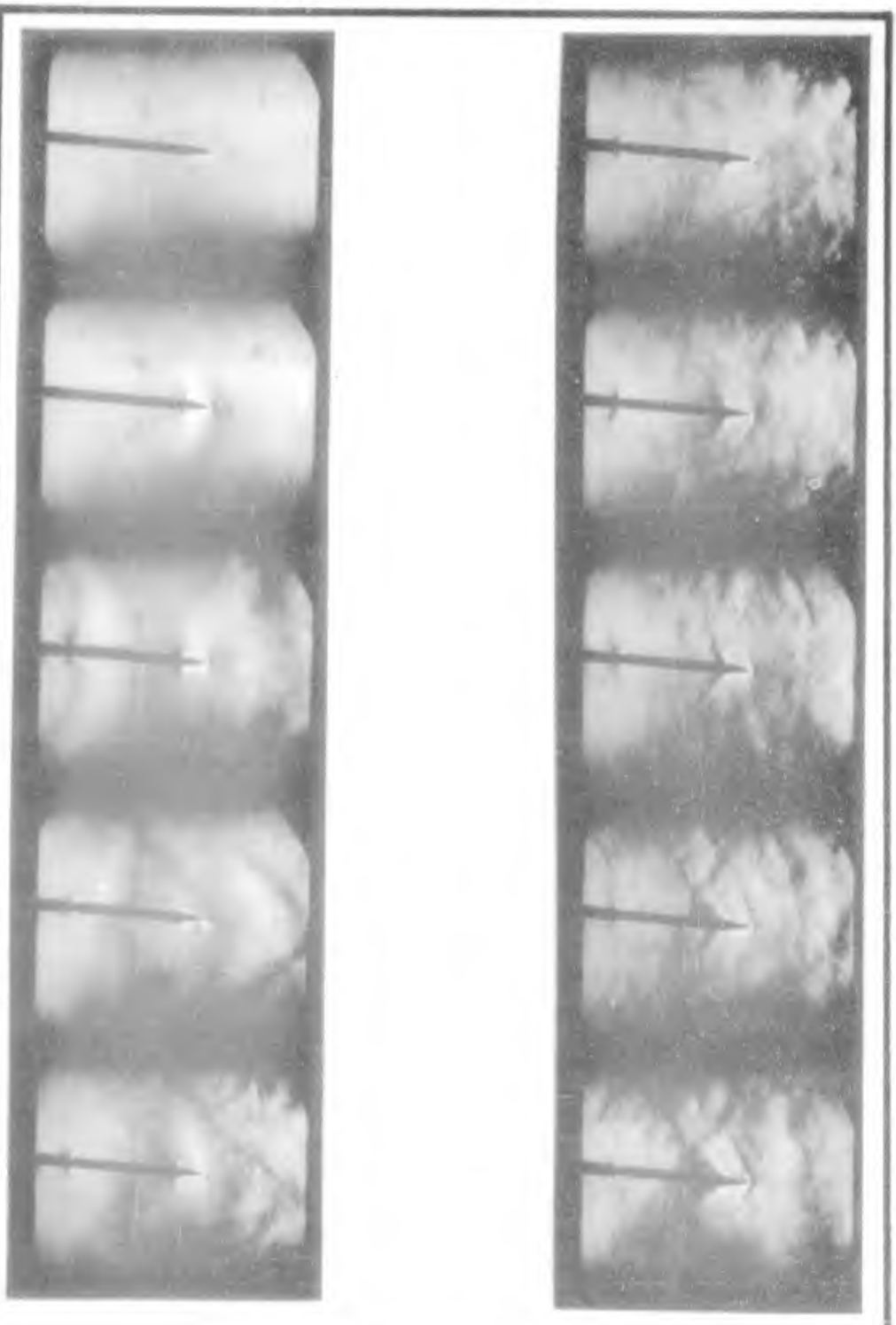

Figure 29a

Run C-3, Frames 1-10
(4815 frames per second)

Figure 29b

Run C-3, Frames 11-20

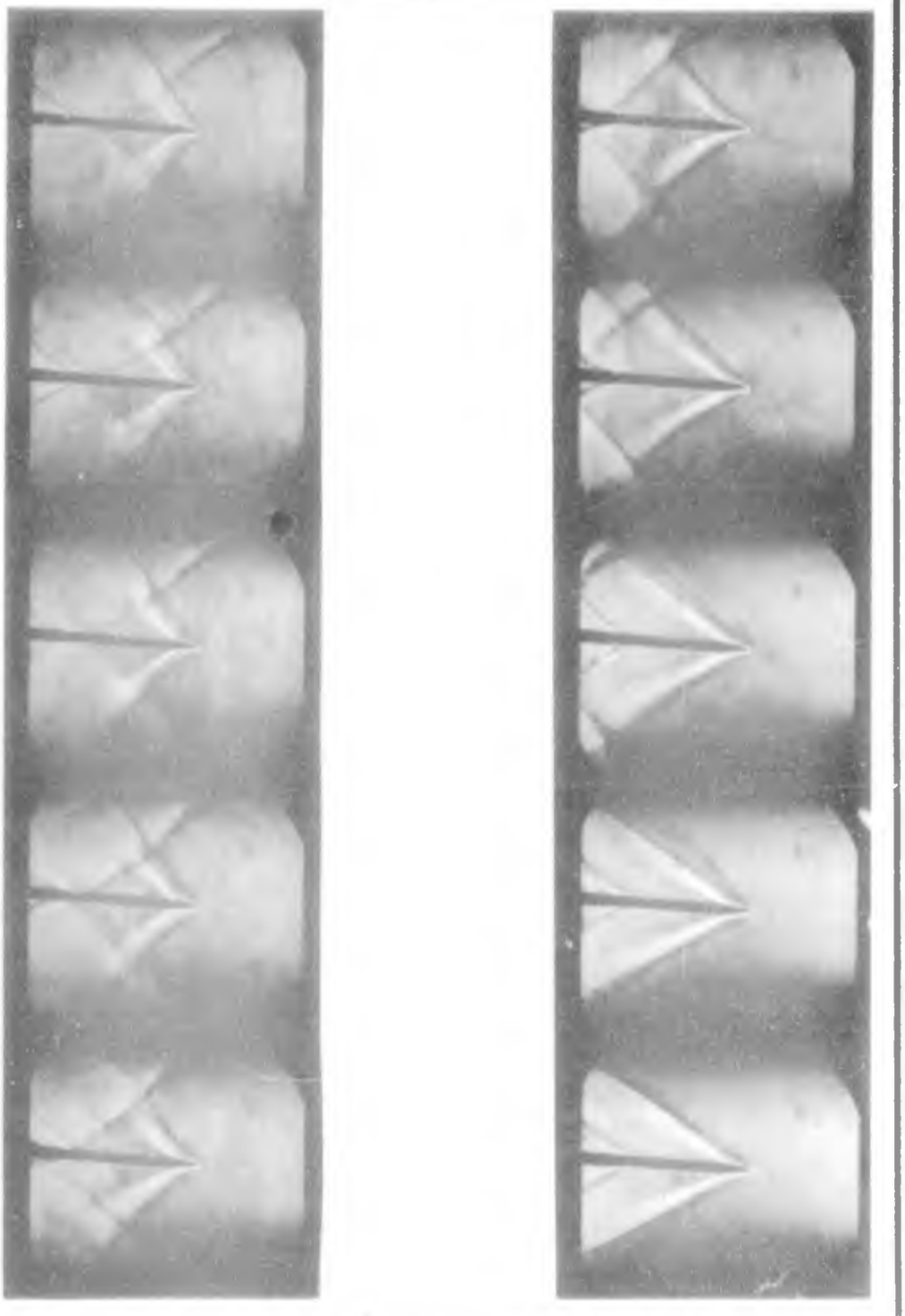

Figure 29c

Run C-3, Frames 21-30
(Frames 31-45 same as 30)

Figure 29d

Run C-3, Frames 46-55

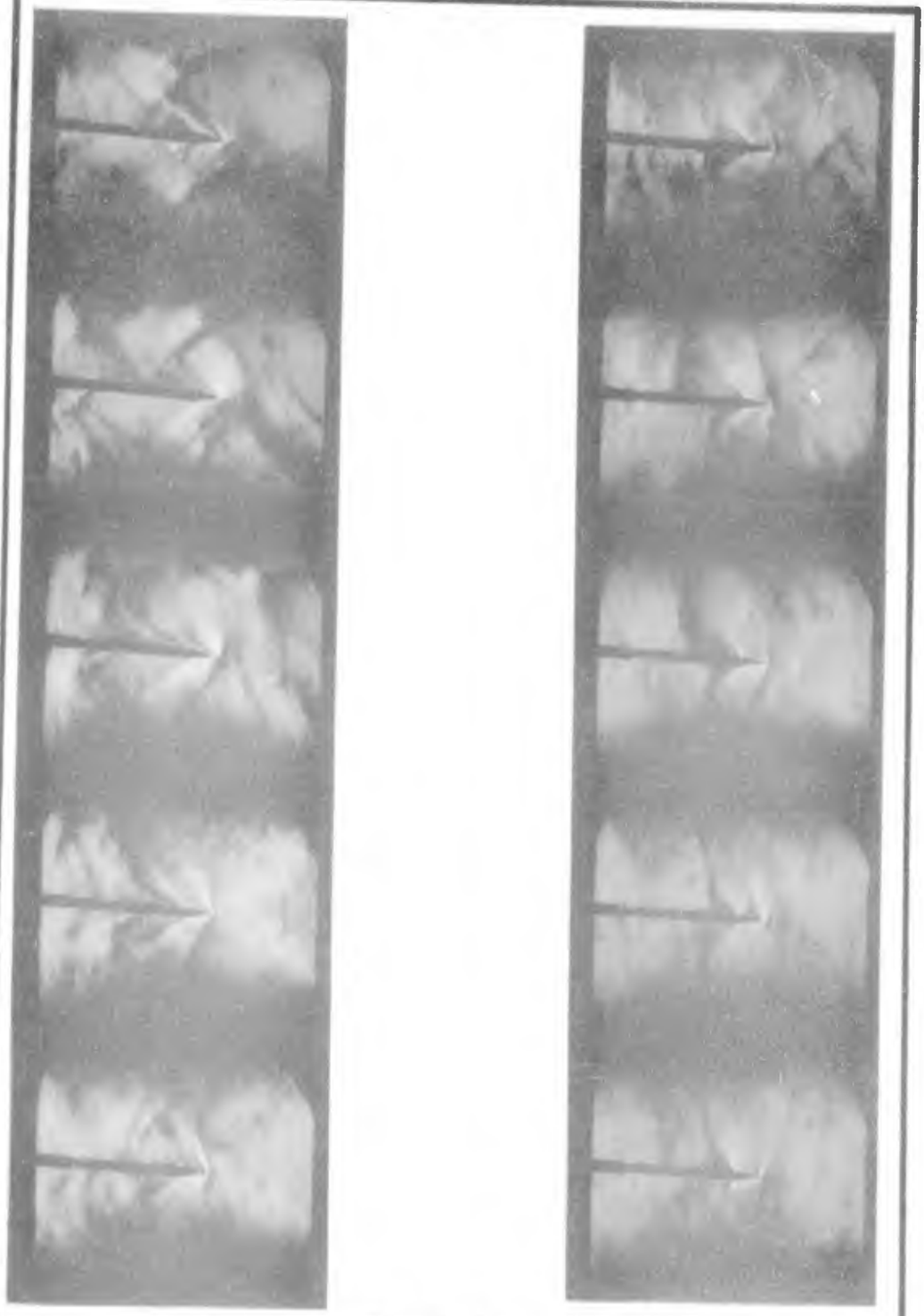

Figure 29e

Run C-3, Frames 56-65

Figure 29f

Run C-3, Frames 66-70

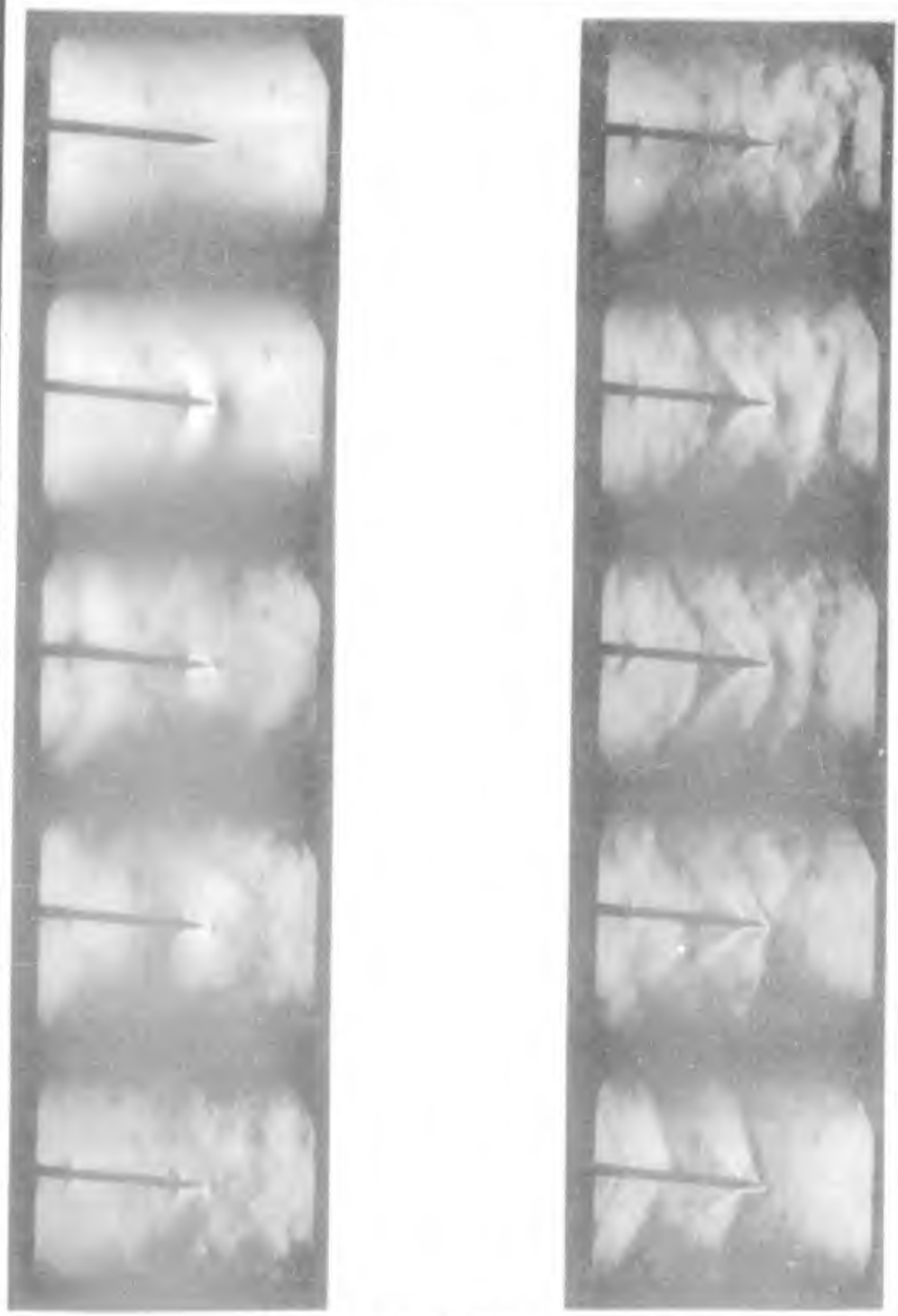

Figure 30a

Run C-4, Frames 1-10
(5000 frames per second)

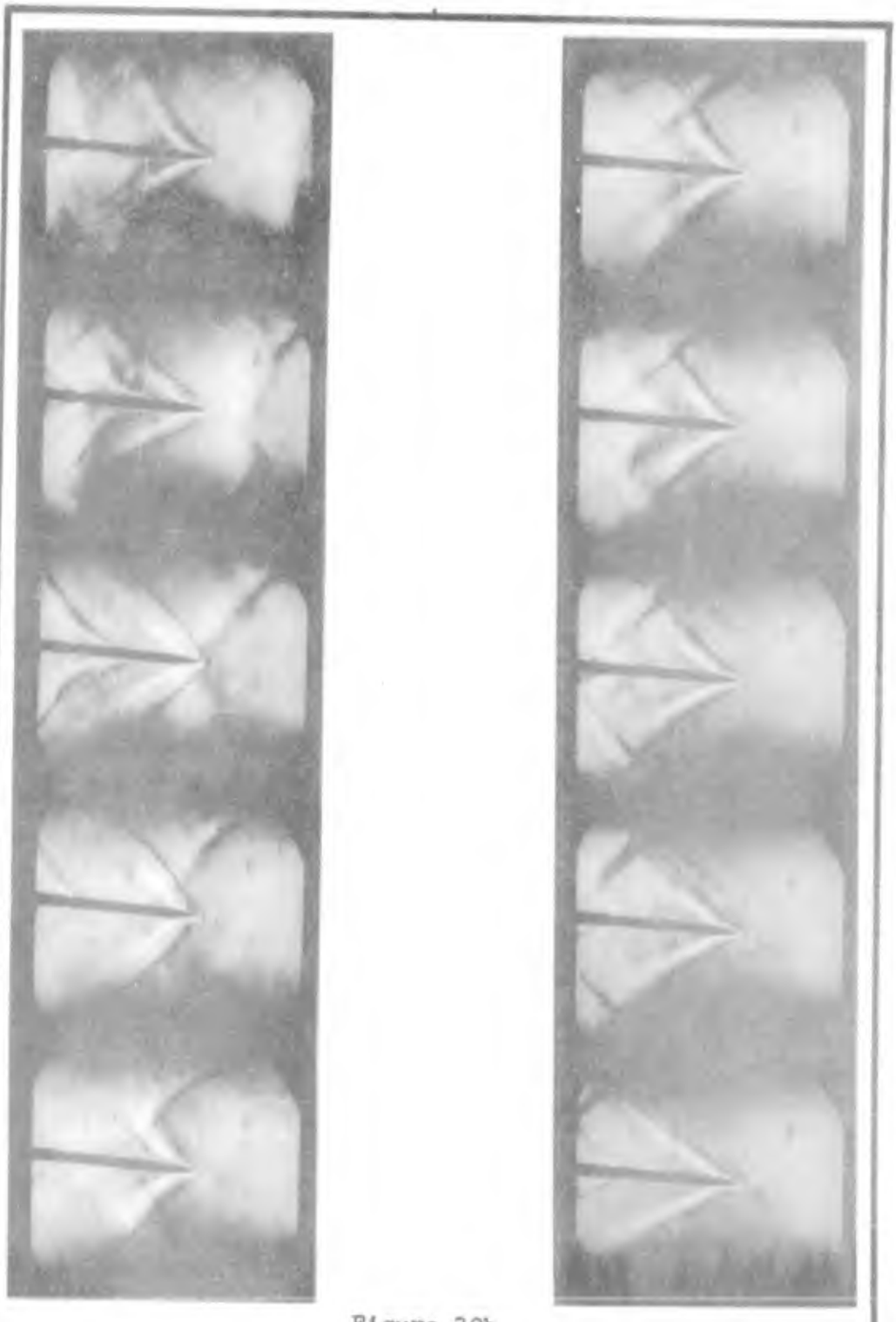

Figure 30b

Run C-4, Frames 11-20

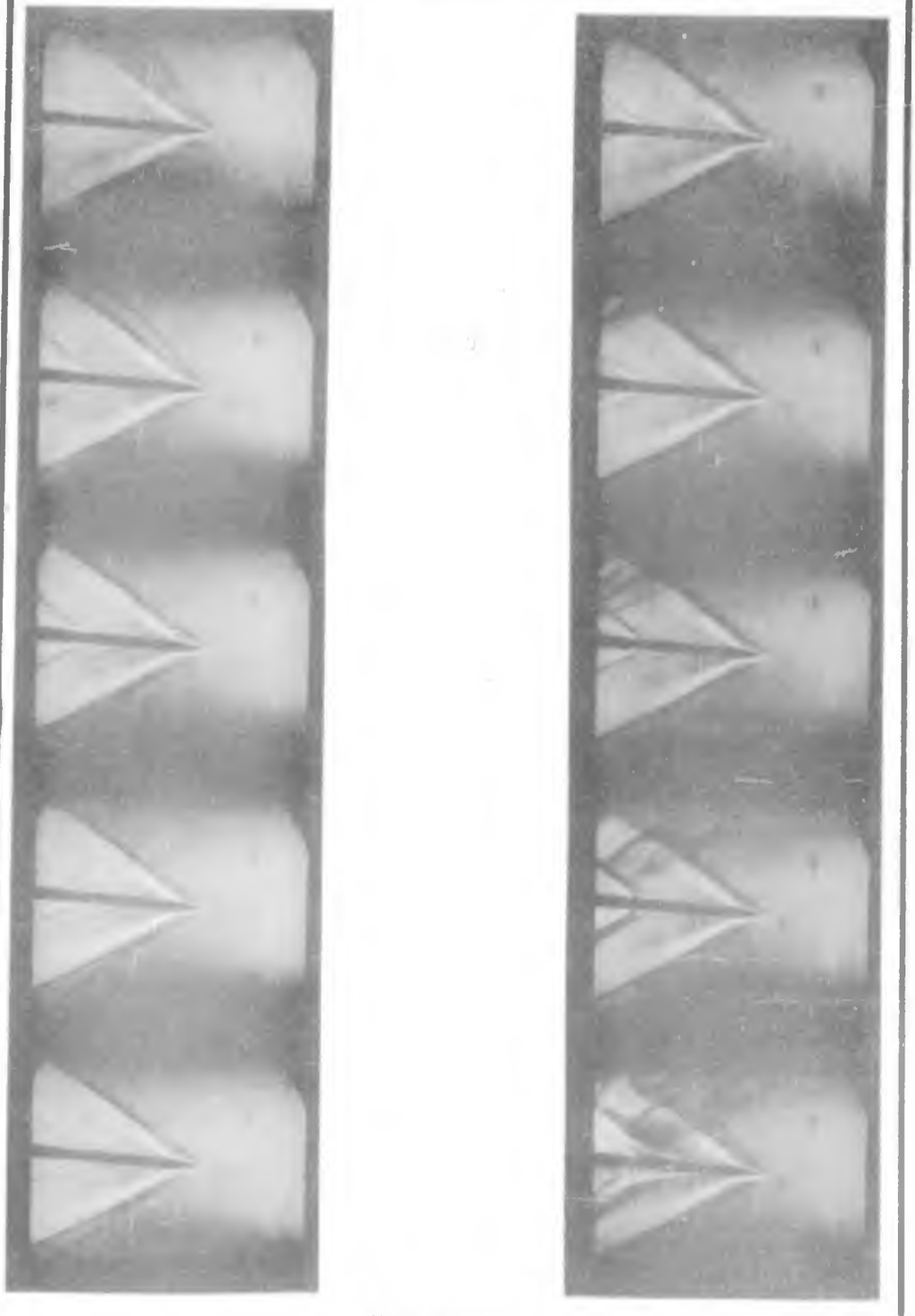

Figure 30c

Run C-4, Frames 21-25 and 51-55
(Frames 26-50 same as 25)

Figure 30d

Run C-4, Frames 56-65

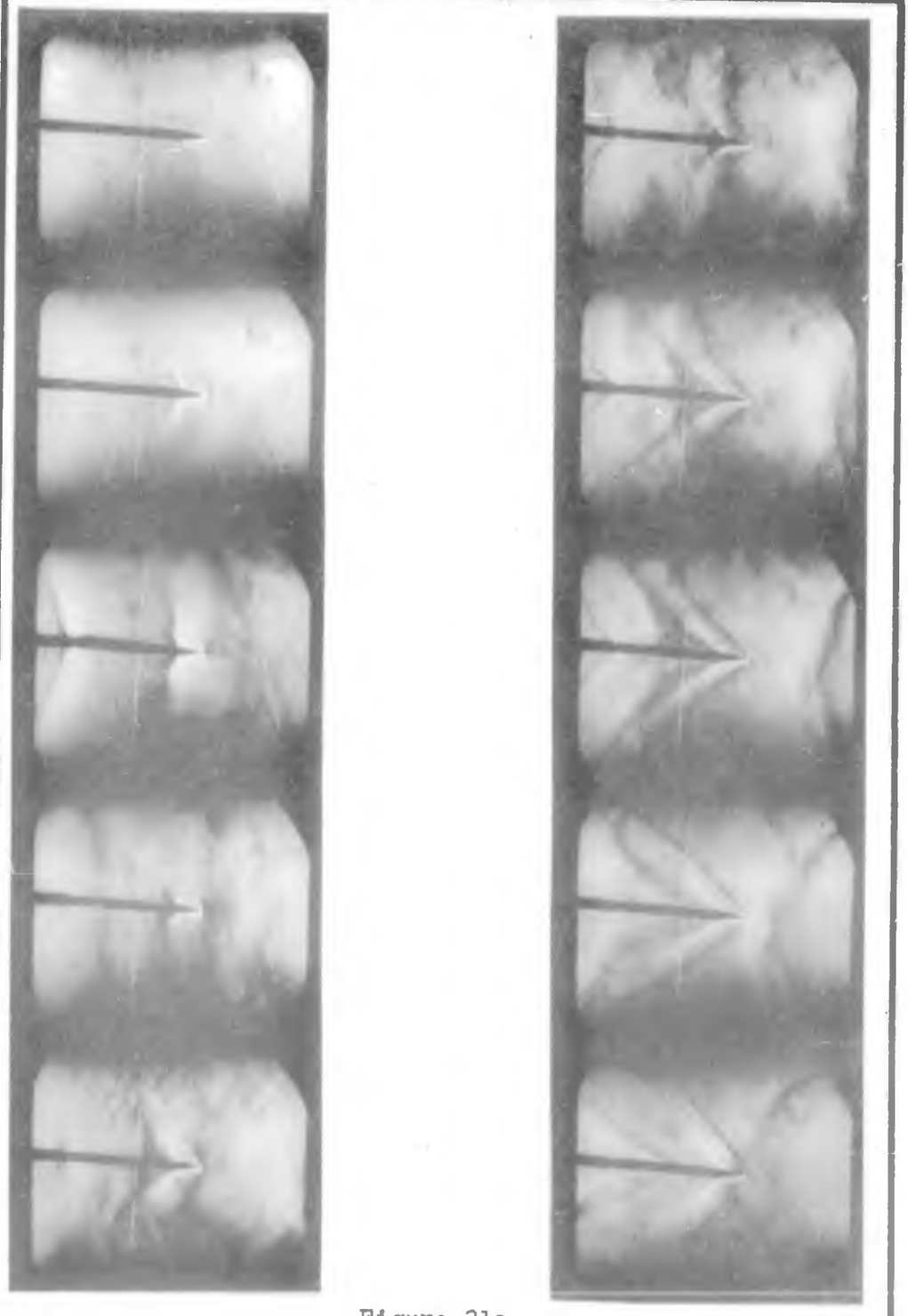

Figure 31a

Run C-5, Frames 1-10
(5000 frames per second)

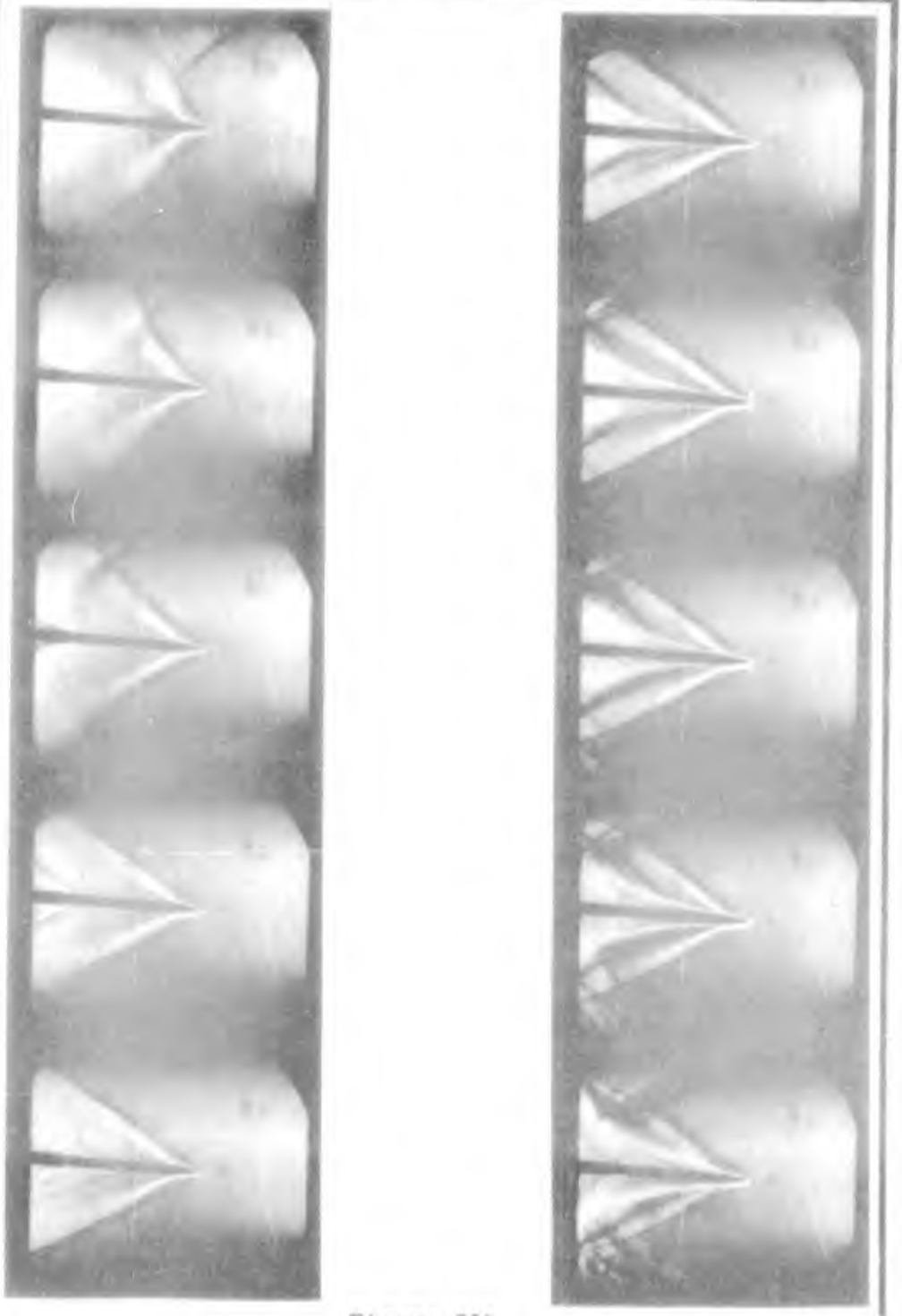

Figure 31b

Run C-5, Frames 11-15 and 71-75
(Frames 16-70 same as 15)

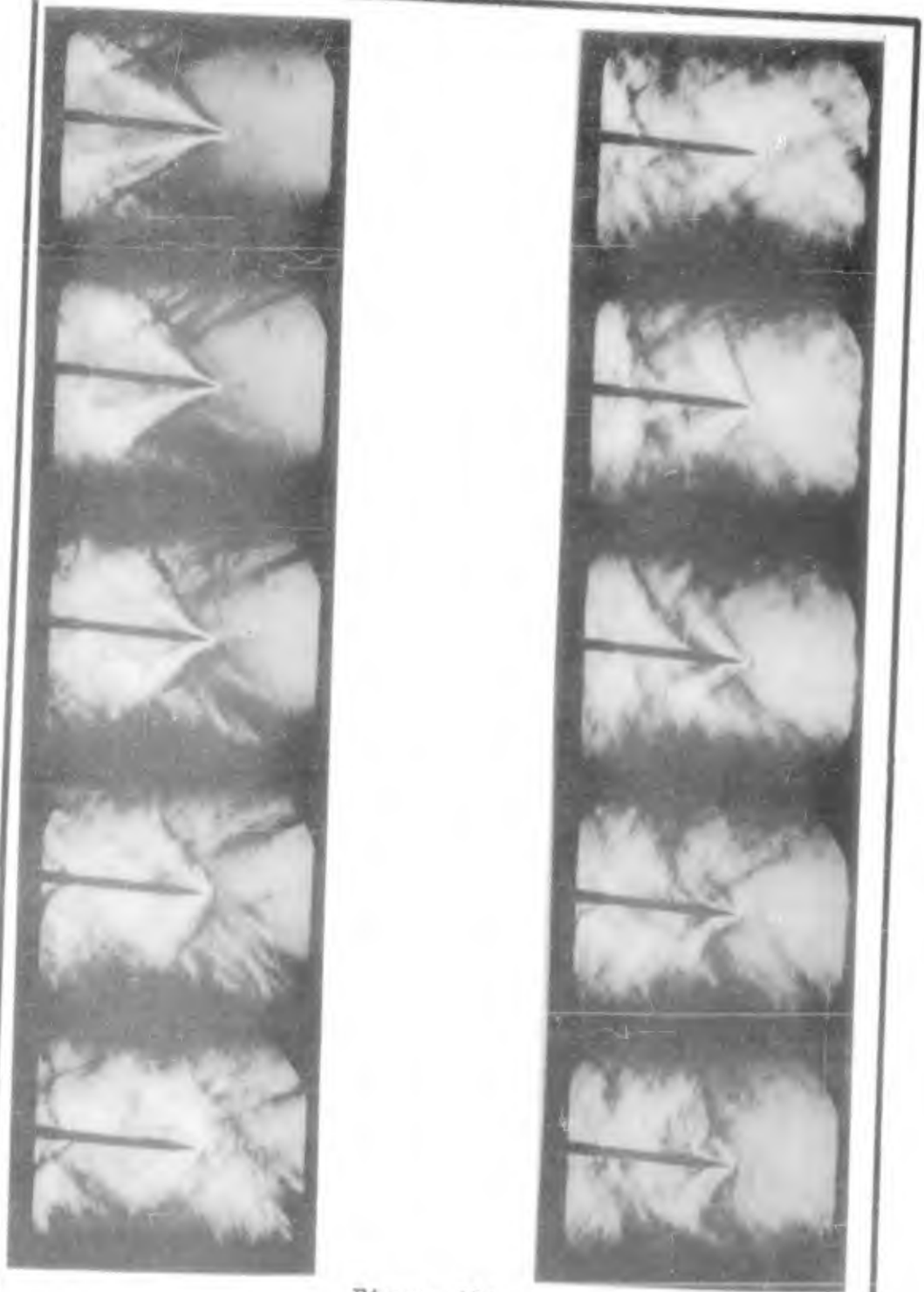

Figure 31c

Run C-5, Frames 76-85

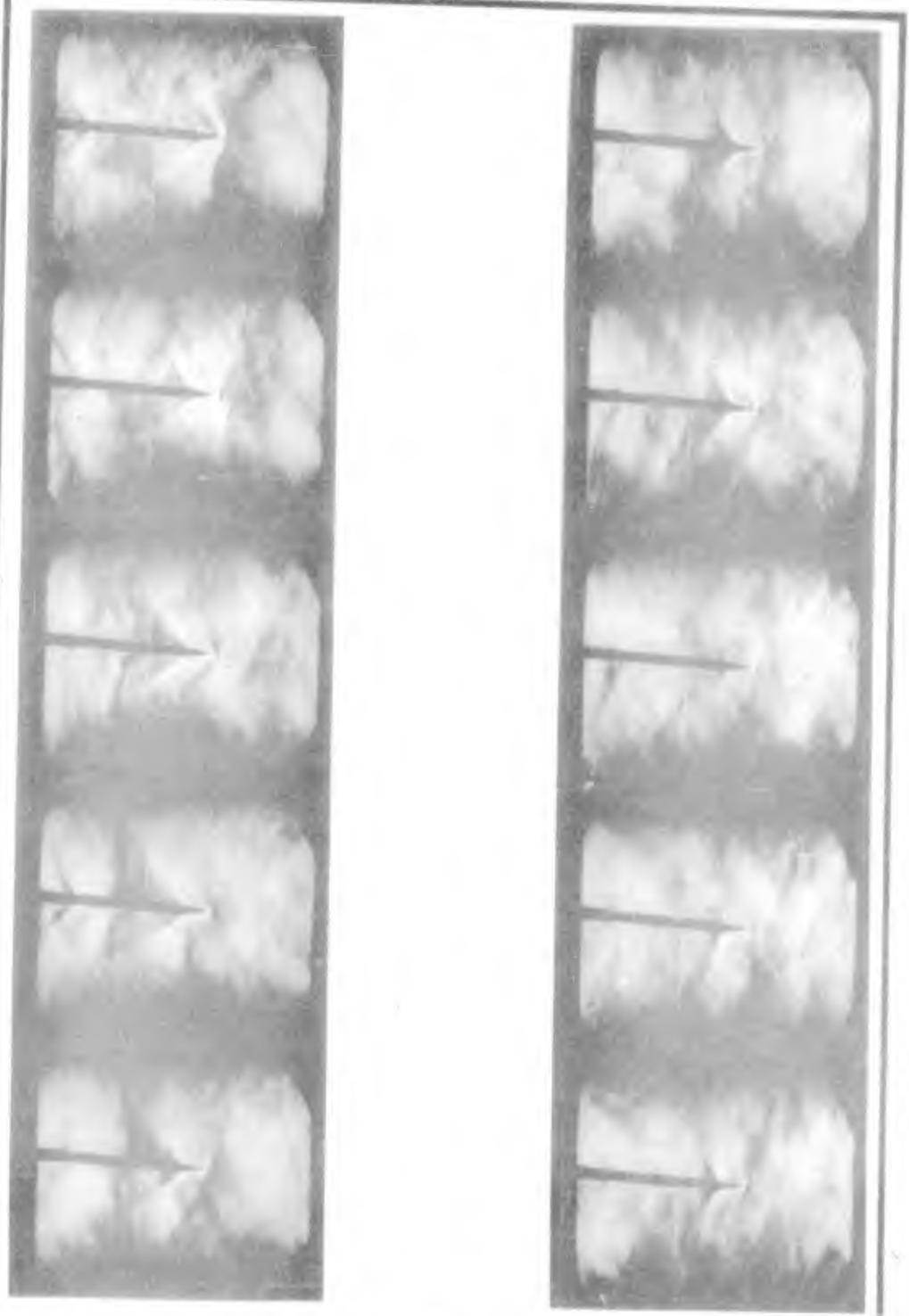

Figure 31d

Run C-5, Frames 86-95

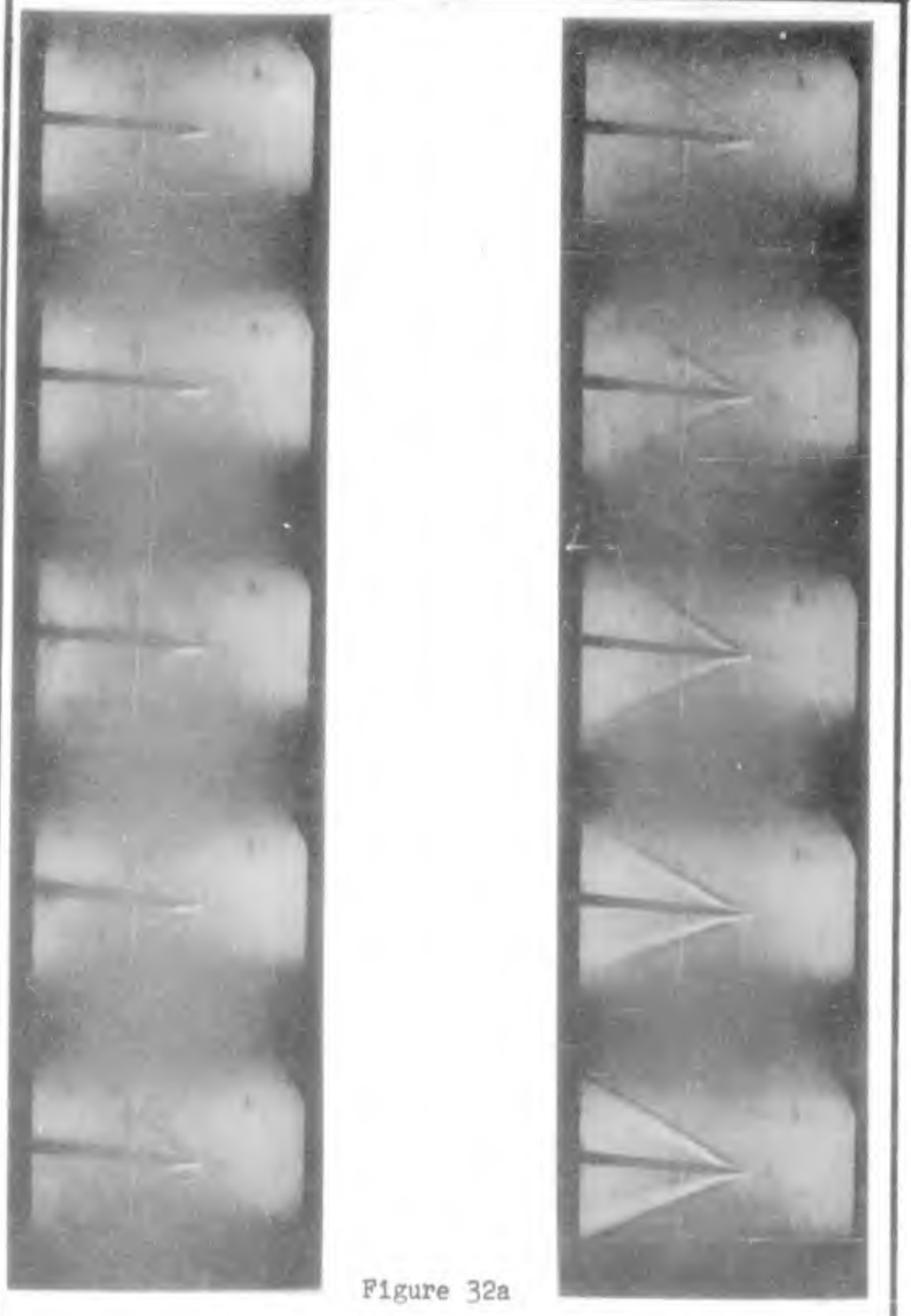

Figure 32a

Run C-6, Frames 1-10
(Frames 11-95 same as 10)
(5000 frames per second)

Figure 32b

Run C-6, Frames 96-105

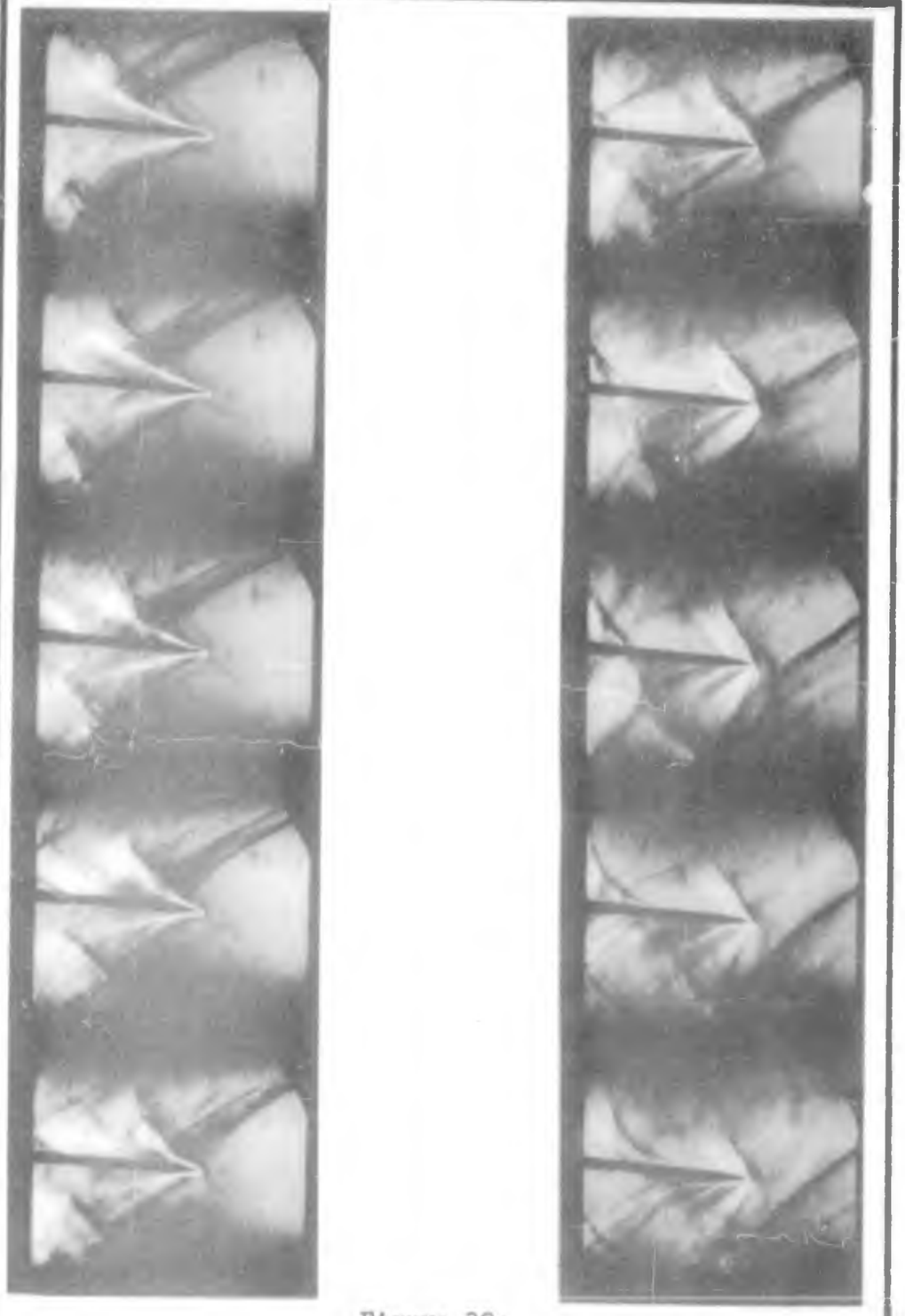

Figure 32c

Run C-6, Frames 106-115

Figure 32d

Run C-6, Frames 116-125

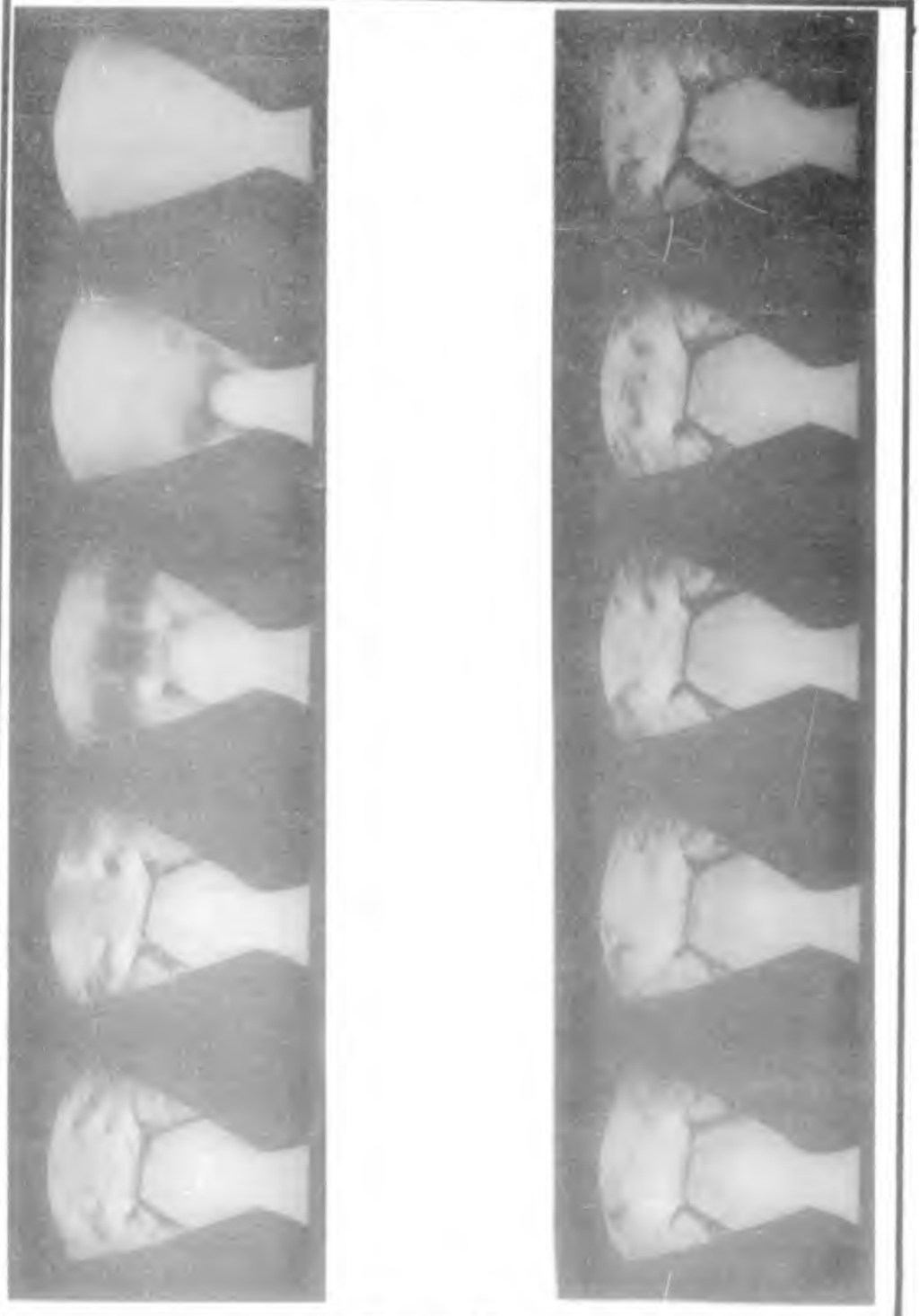

Figure 33

Run D-1, Frames 1-10
(5000 frames per second)

Figure 34

Run D-2, Frames 1-10
(5070 frames per second)

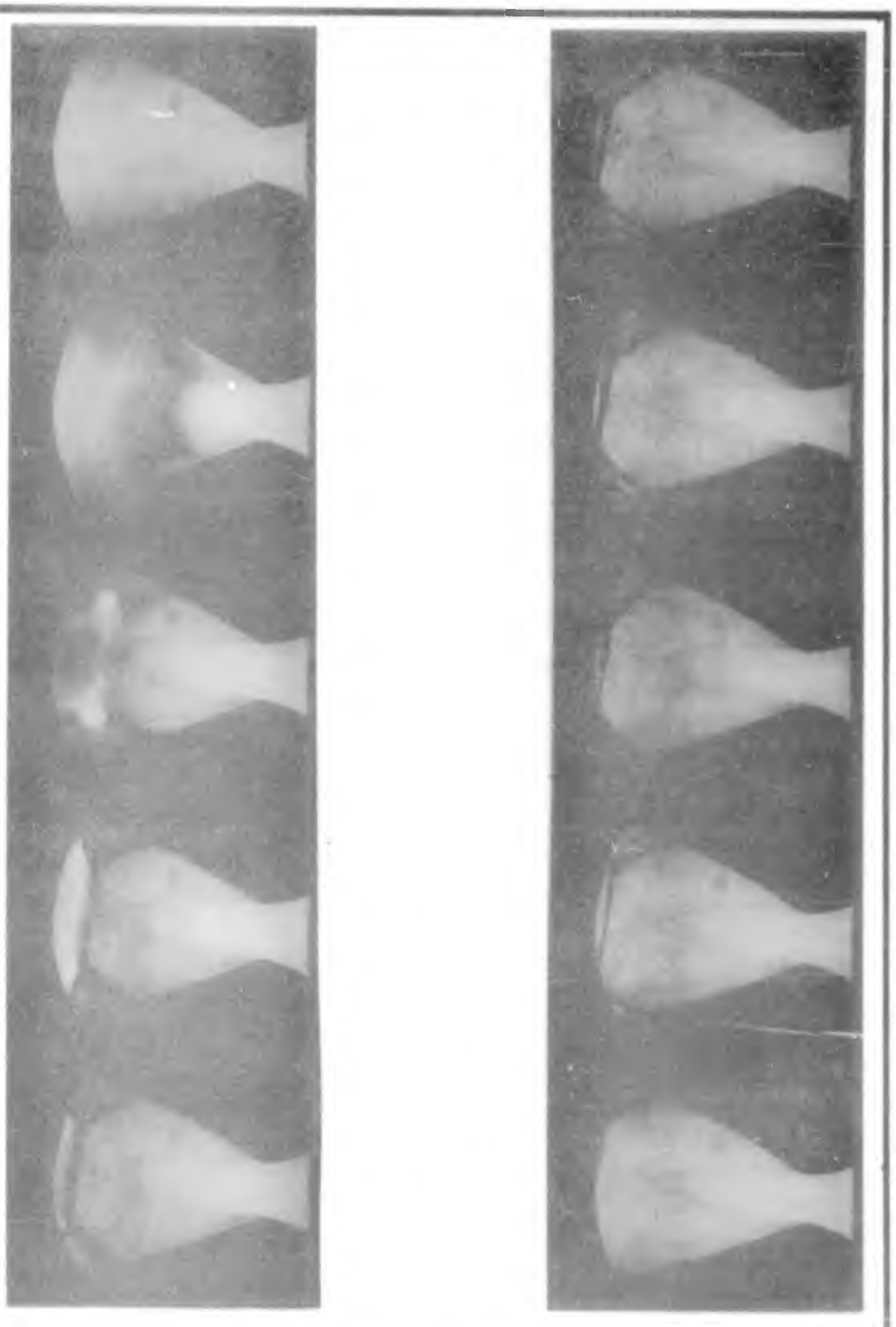

Figure 35

Run D-3, Frames 1-10
(5000 frames per second)

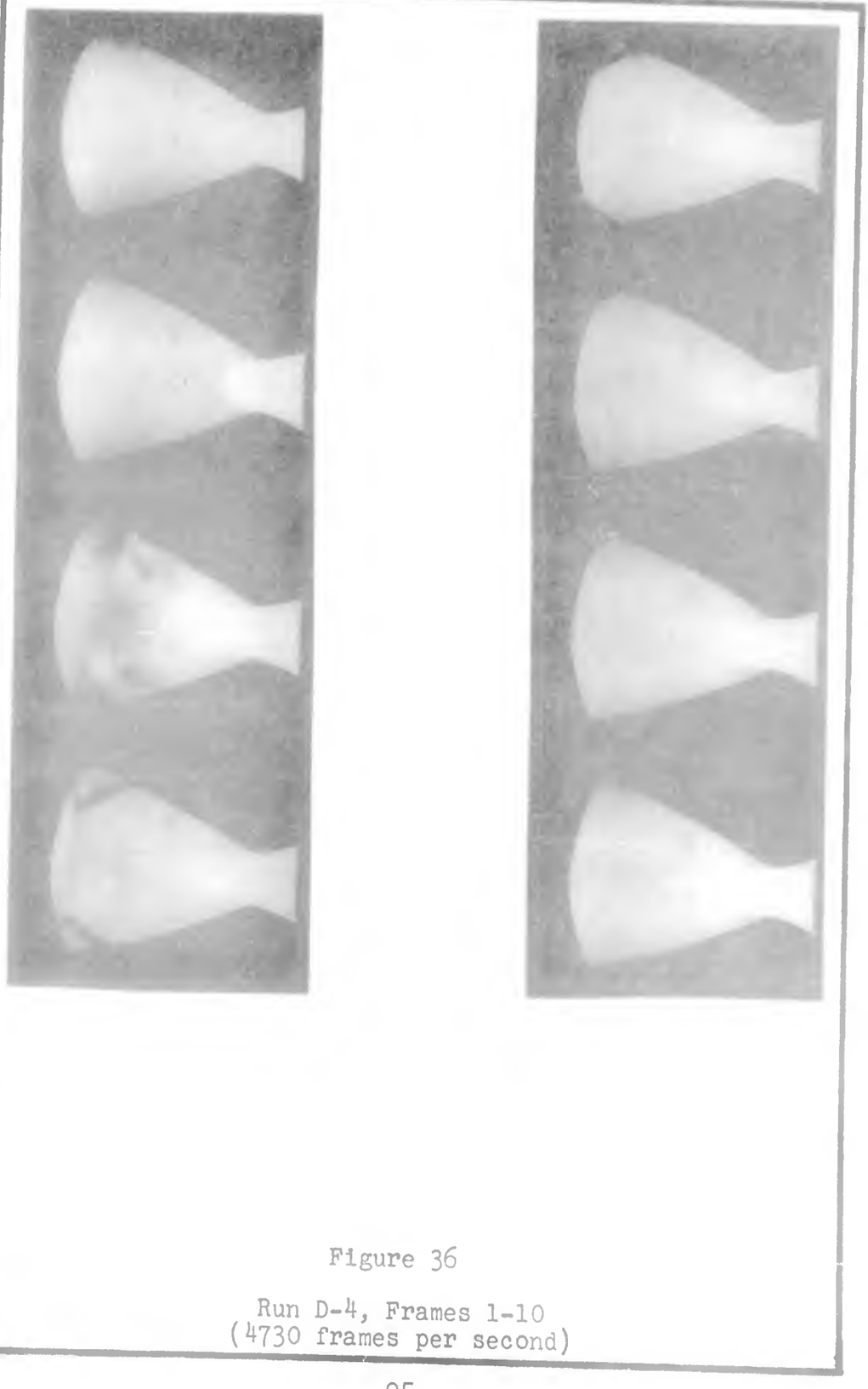

Figure 36

Run D-4, Frames 1-10
(4730 frames per second)

Figure 37

Run D-5, Frames 1-5
(4850 frames per second)

Figure 38a

Run E-1, Frames 1-10
(5000 frames per second)

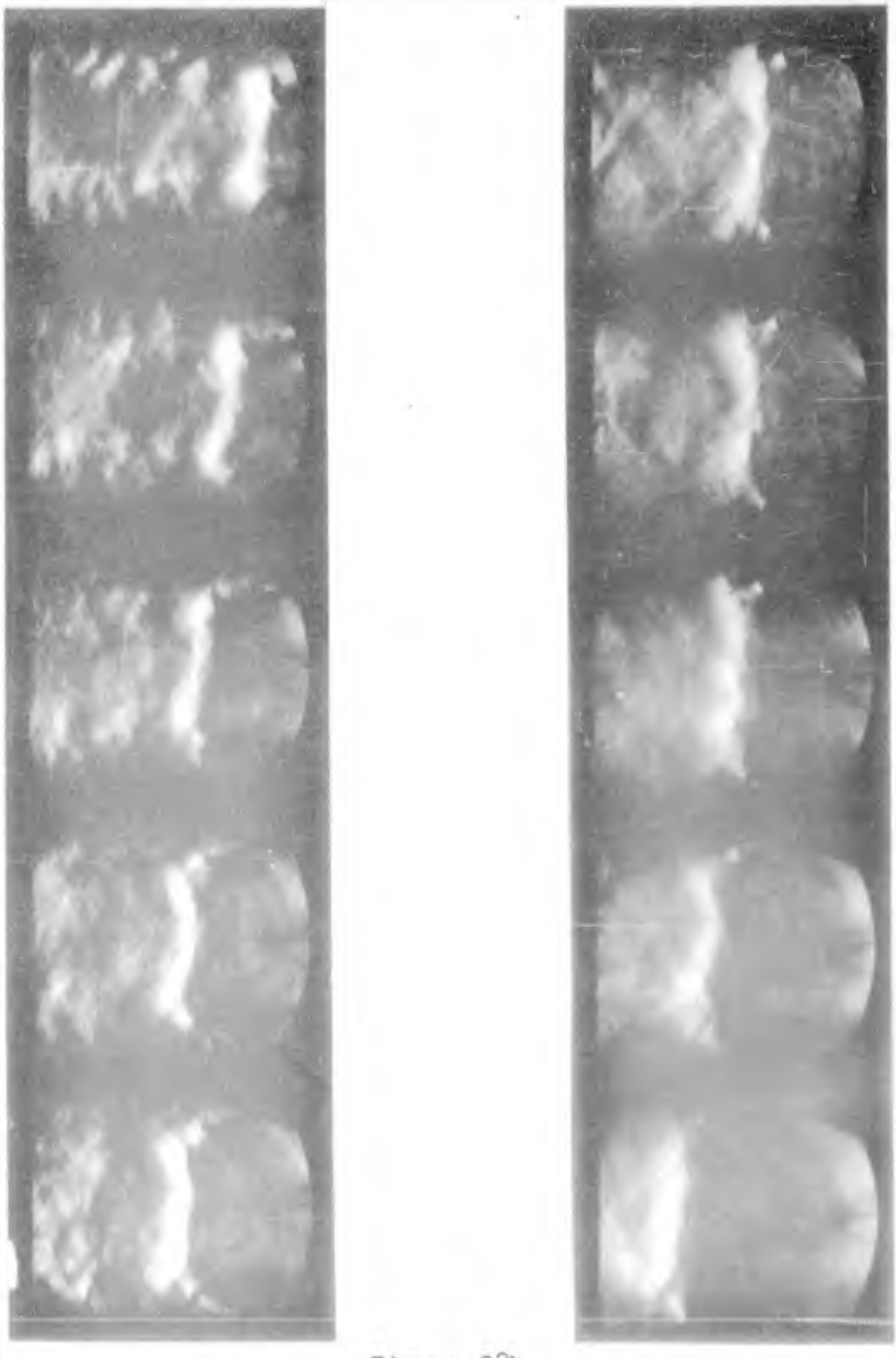

Figure 38b

Run E-1, Frames 10-15 and 26-30
(Frames 16-25 same as 15)

Figure 38c

Run E-1, Frames 31-35 and 41-45
(Frames 36-40 same as 35)

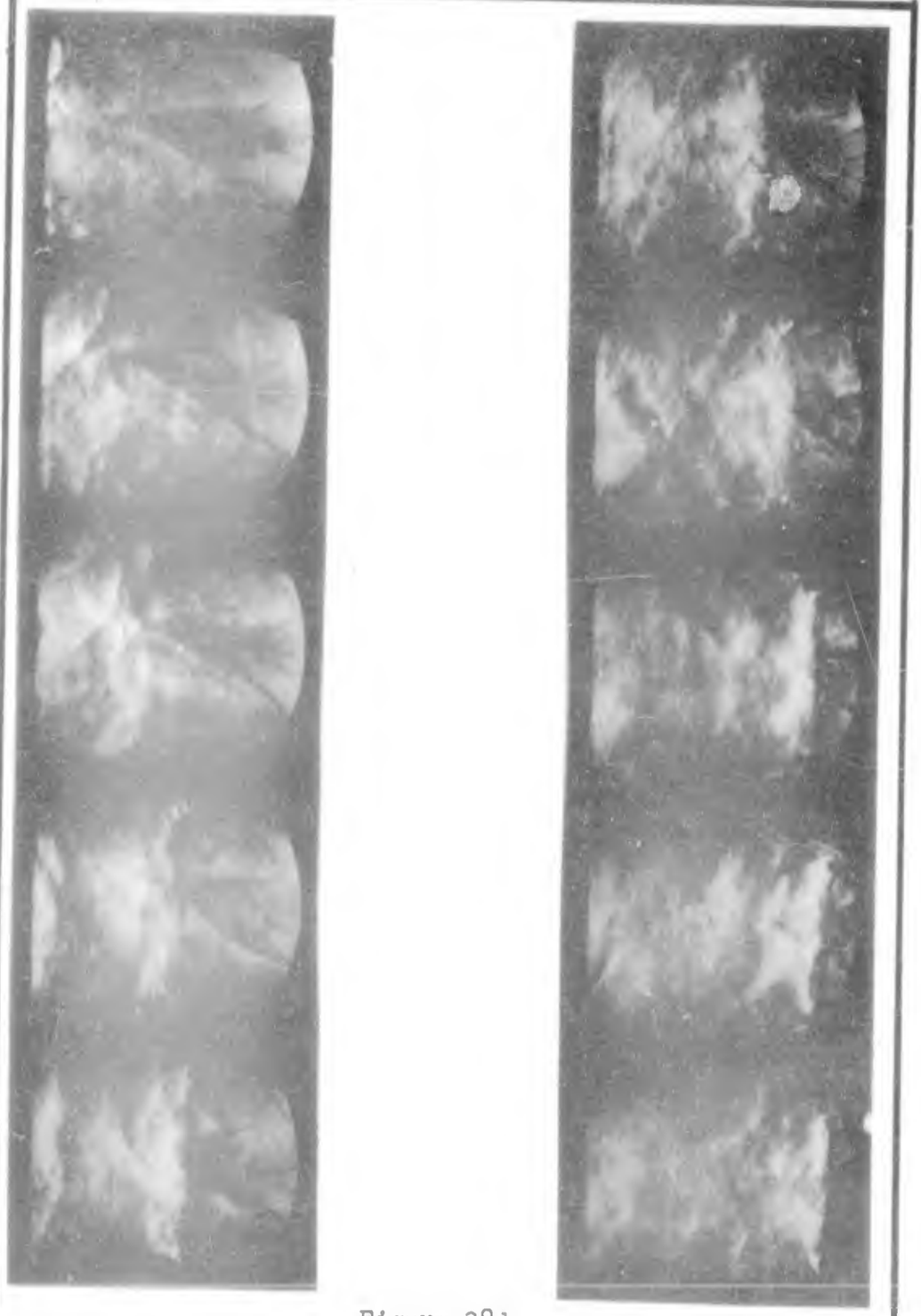

Figure 38d

Run E-1, Frames 46-55

Figure 38e

Run E-1, Frames 55-60

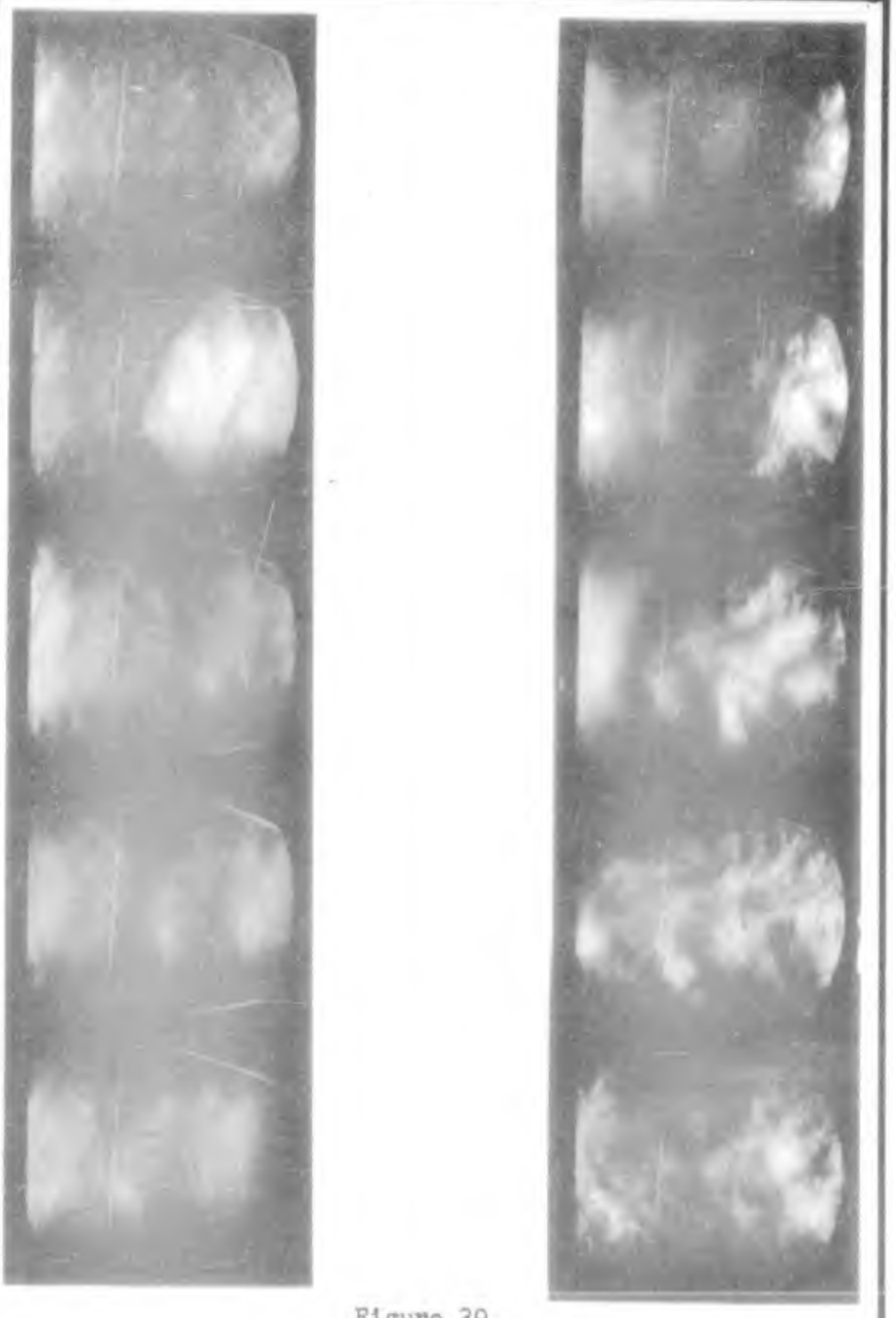

Figure 39

Run E-1, Reflected Shock Sequence

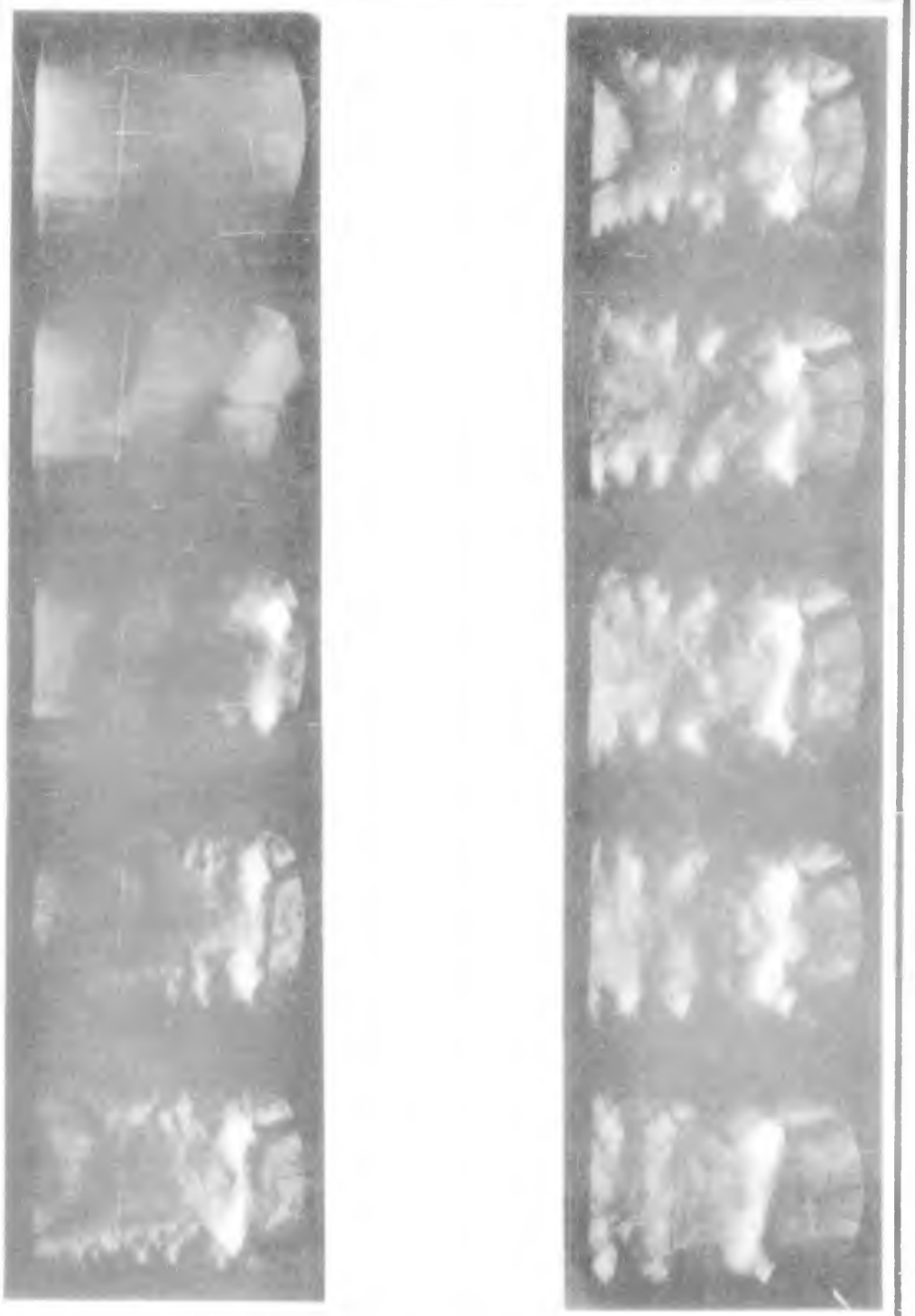

Figure 40a

Run E-2, Frames 1-10
(4850 frames per second)

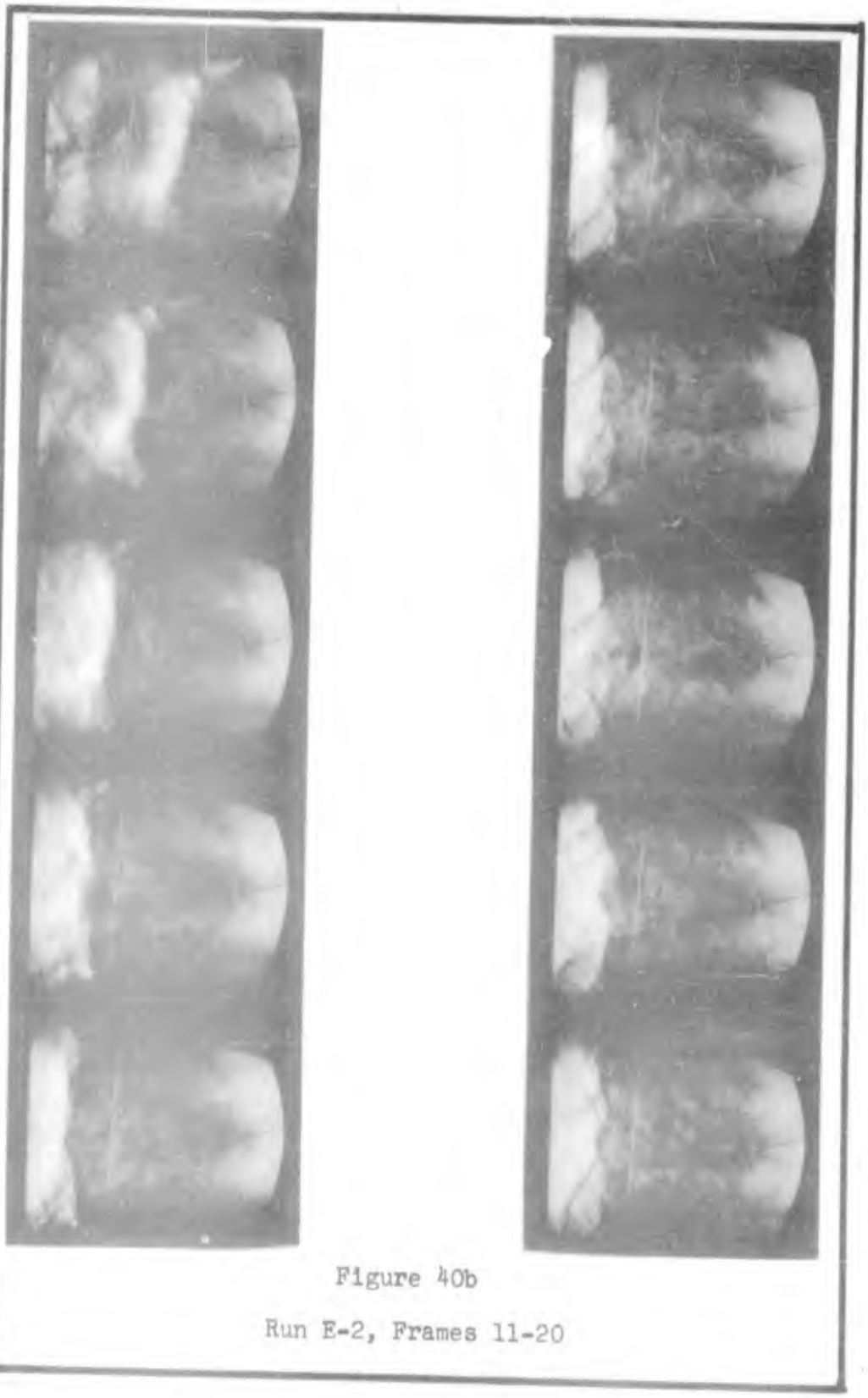

Figure 40b

Run E-2, Frames 11-20

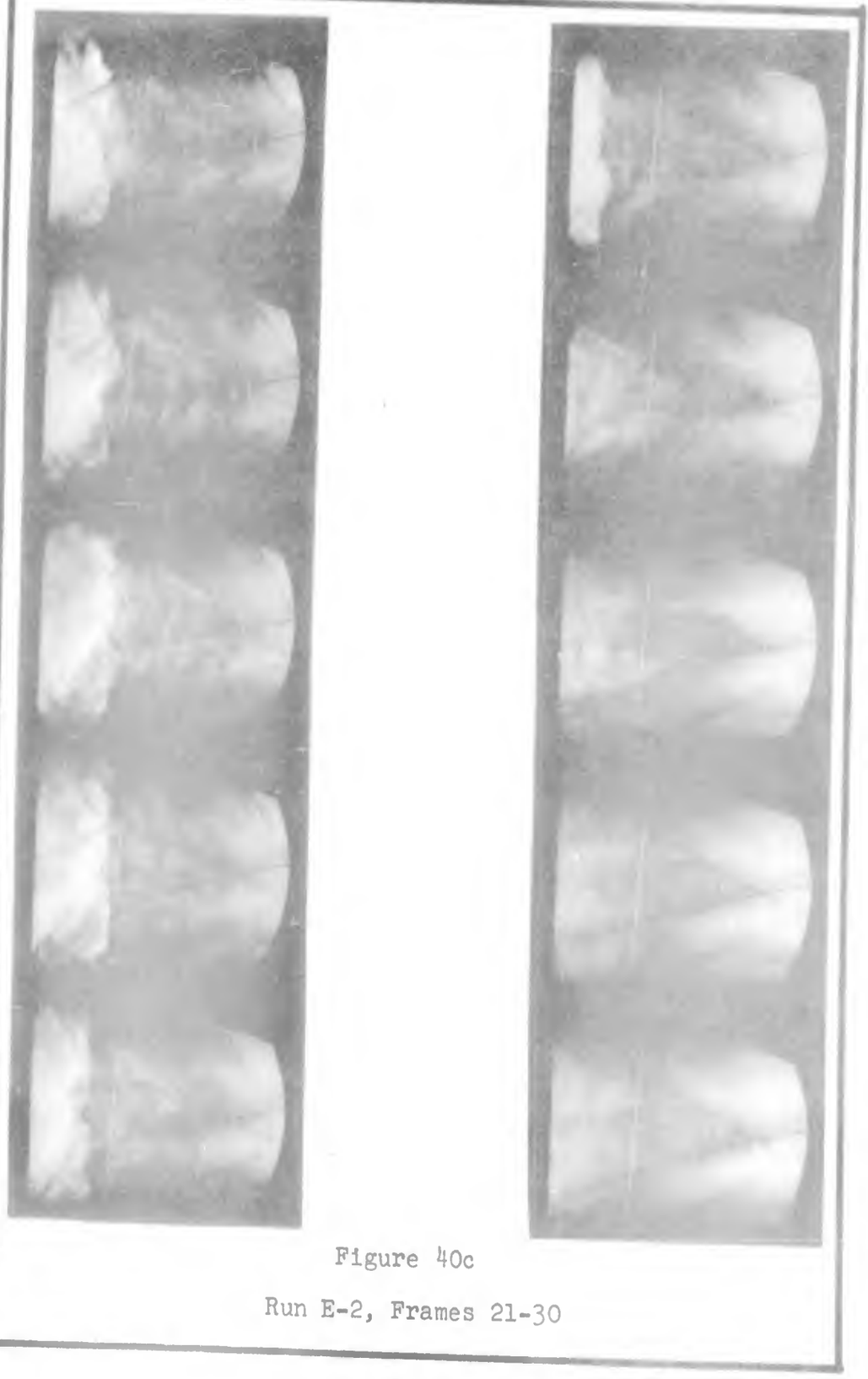

Figure 40c

Run E-2, Frames 21-30

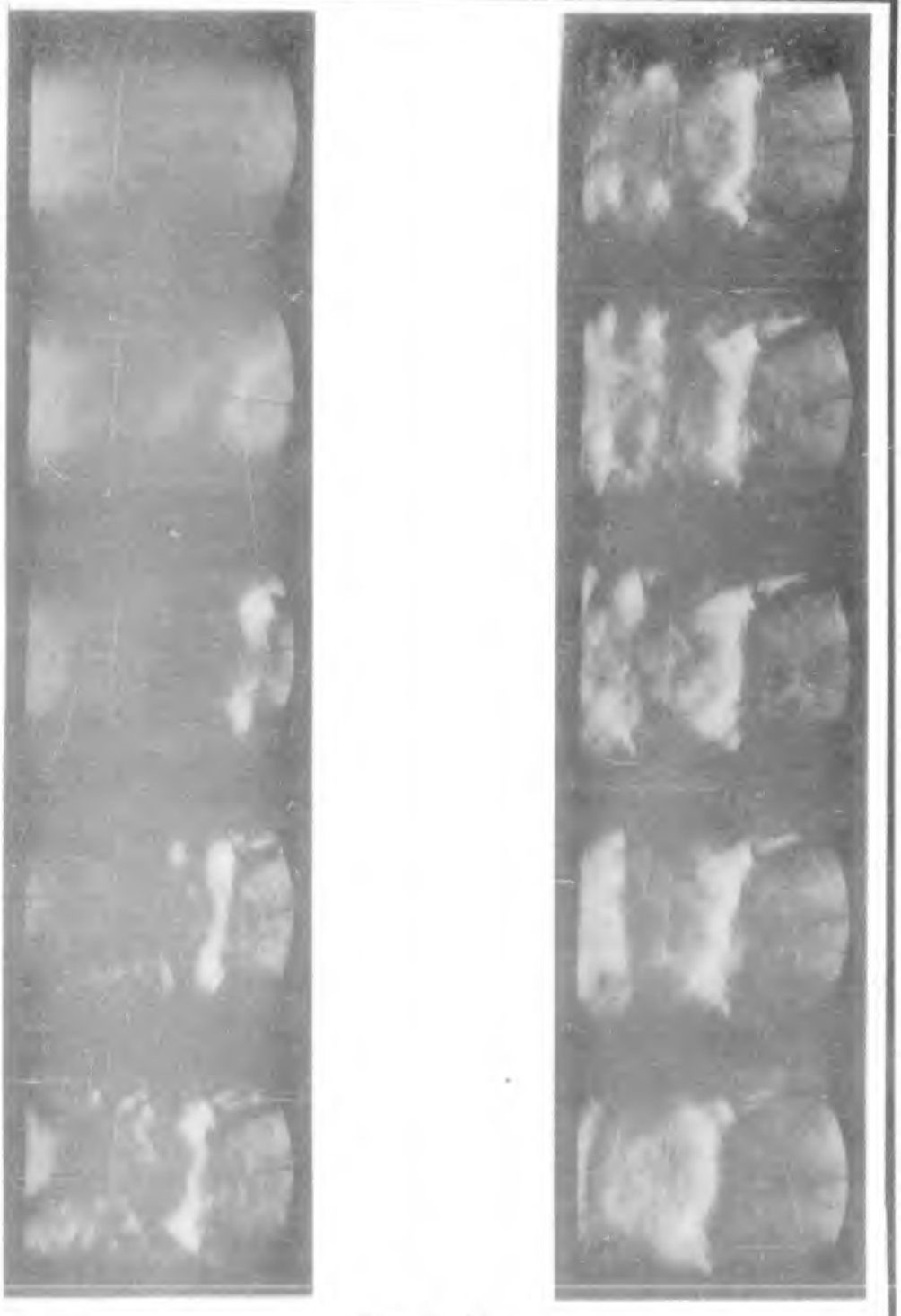

Figure 41a

Run E-3, Frames 1-10
(4800 frames per second)

Figure 41b

Run E-3, Frames 11-15

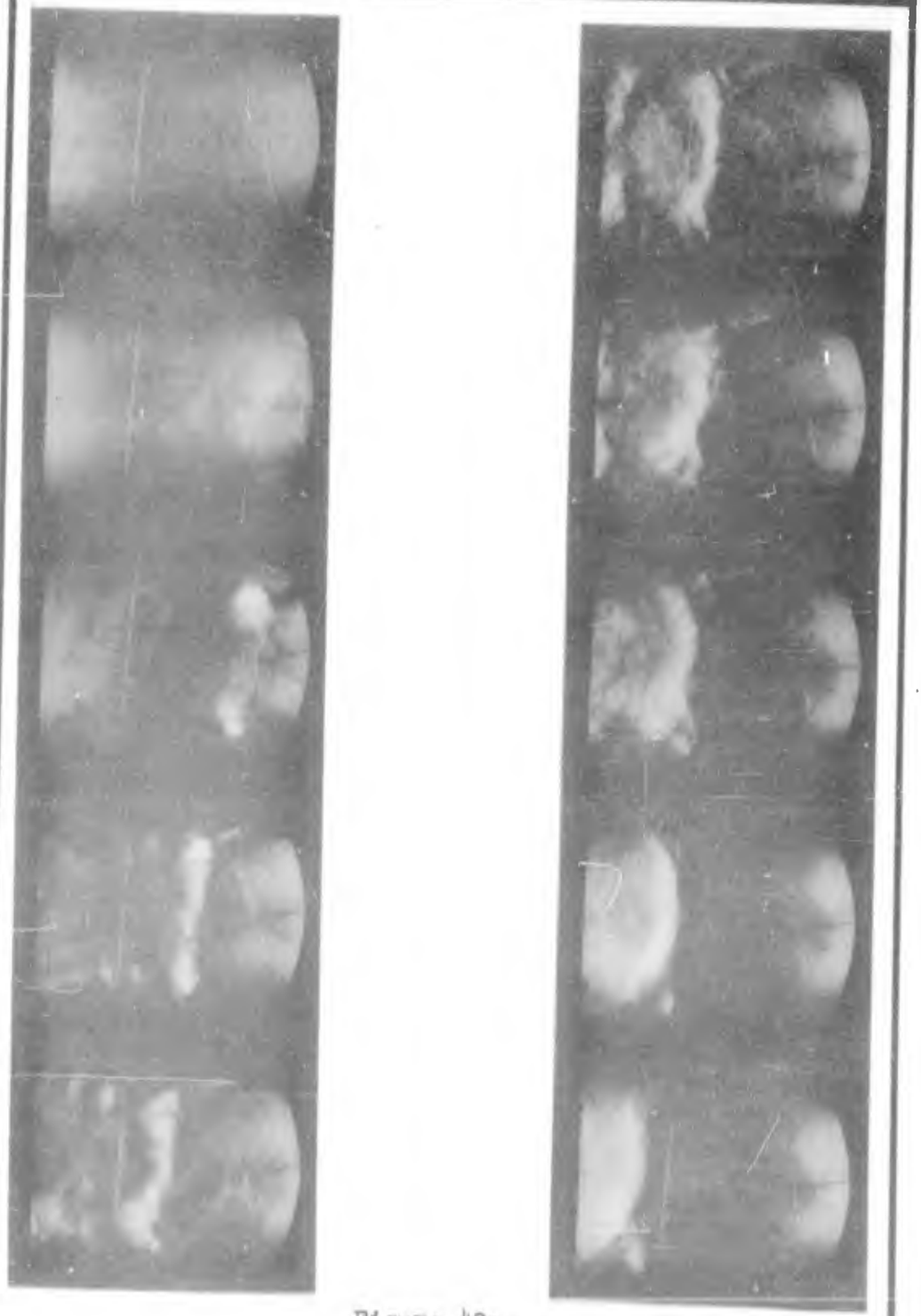

Figure 42a

Run E-4, Frames 1-10
(5000 frames per second)

Figure 42b

Run E-4, Frames 11-15

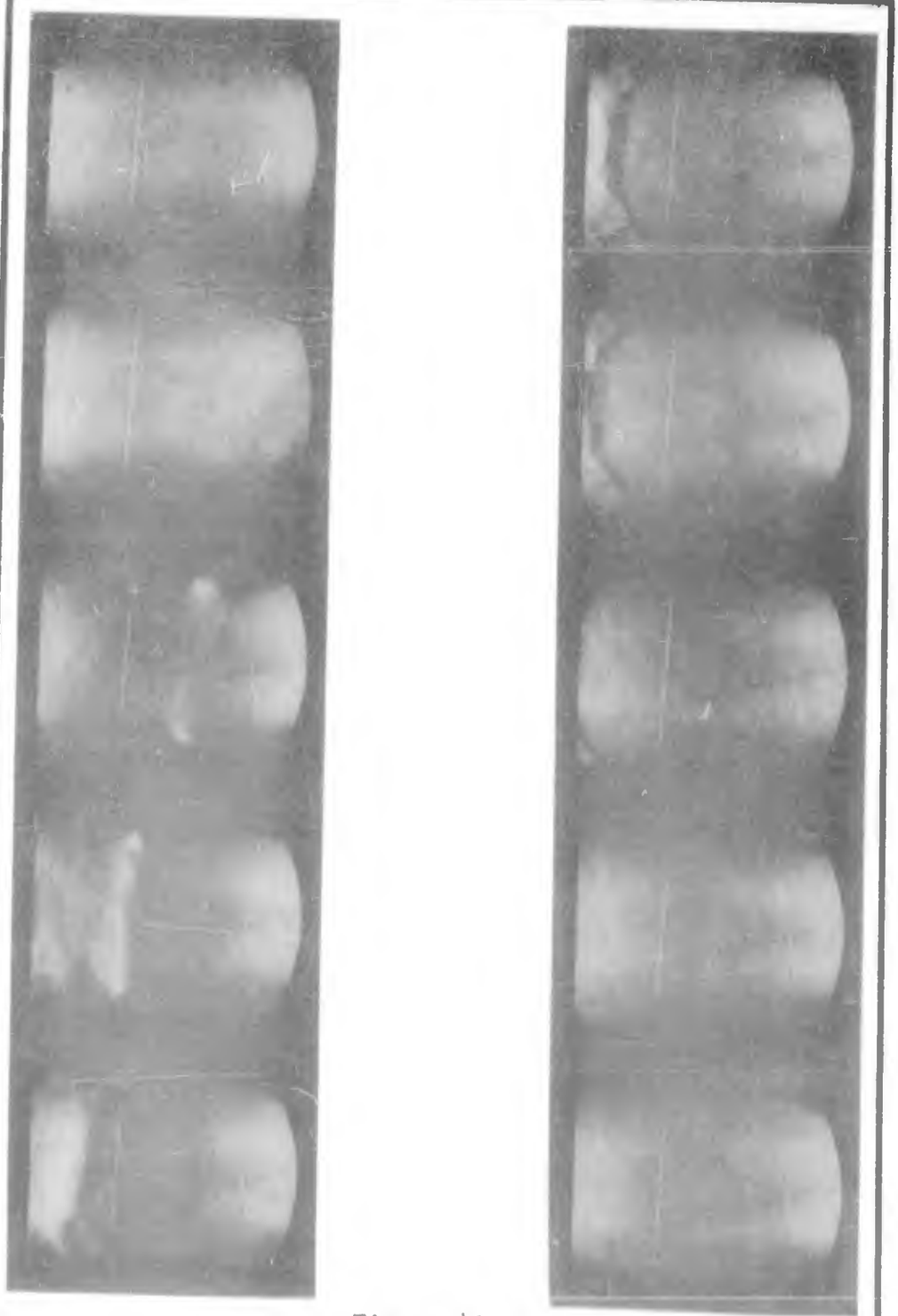

Figure 43

Run E-5, Frames 1-10
(4770 frames per second)

VIII. Conclusions and Recommendations

Conclusions

This study has proven the feasibility of using a convergent-divergent nozzle to improve the performance of the Mechanical Engineering Laboratory shock tube.

The results of the tests indicate:

1. The convergent-divergent nozzle increased the test Mach number from approximately 1.4 for 1.4 milliseconds to 2.6 - 2.8 for up to 18.4 milliseconds.

2. The test section Mach number is independent of incident shock strength and is a function of nozzle design only.

3. The available test time increases with increasing incident shock strength.

4. The usable test flow duration increases with increasing incident shock strength.

5. The test time losses decrease with increasing incident shock strength.

Recommendations

It is recommended that a follow-on study be conducted utilizing a new test section with larger viewing windows. This test section should accommodate a variety of nozzles and a secondary diaphragm for the study of maximum attainable Mach numbers and secondary diaphragm effects.

Bibliography

1. Cameron, R.M. A Study of Shock Waves Moving Over a Perforated Wall. Unpublished Thesis. Wright-Patterson Air Force Base, Ohio: Institute of Technology (AU), August 1960.

2. Davis, H.P., and W.A. French. Design and Construction of a Shock Tube. Unpublished Thesis. Wright-Patterson Air Force Base, Ohio: Institute of Technology (AU), August 1955.

3. Egan, D.S., Jr., and R.A. Foster. Gas Dynamics Research with the Air Force Institute of Technology Shock Tube. Unpublished Thesis. Wright-Patterson Air Force Base, Ohio: Institute of Technology (AU), August 1956.

4. Glass, I.I. Theory and Performance of Simple Shock Tubes. UTIA Review No. 12, Part I. University of Toronto, Canada: Institute of Aerophysics, May 1958.

5. Glass, I.I., W. Martin, and G.N. Patterson. A Theoretical and Experimental Study of the Shock Tube. UTIA Report No. 2. University of Toronto, Canada: Institute of Aerophysics, November 1953.

6. Glick, H.S., A. Hertzberg, and W.E. Smith. Flow Phenomena in Starting a Hypersonic Shock Tunnel. CAL Report No. AD-789-A-3 (AEDC-TN-55-16). Buffalo, New York: Cornell Aeronautical Laboratory, March 1955.

7. Hall, J.G. Production of Strong Shock Waves; Shock Tube Applications, Design and Instrumentation. UTIA Review No. 12, Part II. University of Toronto, Canada: Institute of Aerophysics, May 1958.

8. Hertzberg, A. Shock Tubes for Hypersonic Flow. CAL Report No. AF-702-A-1. Buffalo, New York: Cornell Aeronautical Laboratory, May 1951.

9. Hertzberg, A. The Shock Tunnel and Its Applications to Hypersonic Flight. CAL Report No. AD-1052-A-5 (AFOSR-TN-57-268, AD-126567). Buffalo, New York: Cornell Aeronautical Laboratory, June 1957.

10. Hertzberg, A., et al. Modifications of the Shock Tube for the Generation of Hypersonic Flow. CAL Report No. AD-789-A-2 (AEDC-TN-55-15). Buffalo, New York: Cornell Aeronautical Laboratory, March 1955.

11. Mauterer, O. A Study of Shock Waves Moving Over a Transversely Slotted Wall. Unpublished Thesis. Wright-Patterson Air Force Base, Ohio: Institute of Technology (AU), August 1961.

12. Shames, H. and F.L. Seashore. Design Data for Graphical Construction of Two-Dimensional Sharp-Edge-Throat Supersonic Nozzles. NACA RM No. E8J12. Washington: National Advisory Committee for Aeronautics, December 1948.

13. Shapiro, A.H. The Dynamics and Thermodynamics of Incompressible Fluid Flow. Vol. I. N.Y.: The Ronald Press Co., 1953.

14. Shapiro, A.H. The Dynamics and Thermodynamics of Compressible Fluid Flow. Vol. II. N.Y.: The Ronald Press Co., 1954.

15. Squire, W., A. Hertzberg, and W.E. Smith. Real Gas Effects in a Hypersonic Shock Tunnel. CAL Report No. AD-789-A-I (AEDC-TN-55-14). Buffalo, New York: Cornell Aeronautical Laboratory, March 1955.

Appendix A

Modified Diaphragm Rupturing Device

A device was needed that would rupture the diaphragm at a predetermined time in conjunction with camera operation. It was necessary to control the rupture of the diaphragm with the Wollensak "Goose" Control Unit. The above requirements were fulfilled by inserting a thin wire between the sheets of Mylar film in the diaphragm and then shorting a battery across the wire to heat it rapidly.

The device, as assembled and used, is shown in Figure 44. A piece of 0.0125-inch diameter Nichrome wire, approximately 3 inches long, was soldered to two pieces of 0.003-inch thick steel tape, leaving about 2-1/2 inches of wire between the pieces of tape. After soldering, the wire was bent as shown. This bend keeps the wire from breaking when the diaphragm expands as the high-pressure chamber is pressurized. The assembly was taped to a single sheet of Mylar which was then inserted between the other sheets that serve as the diaphragm.

The diaphragm was inserted in the shock tube with the ends of the steel tape extending beyond the sides of the tube. A 24-volt battery was connected through a switch to the exposed ends of the steel tape. When the switch was closed, the wire heated very rapidly, melted through the Mylar, and caused the diaphragm to rupture.

Tests indicated that the diaphragm ruptured consistently, within 50 milliseconds after the circuit was closed. With a constant applied voltage, the time to rupture is a function of the number of sheets of Mylar in the diaphragm, the pressure ratio across the diaphragm, and the location of the wire in relation to the sheets of Mylar; i.e., downstream side, middle, or upstream side. By controlling these variables, this device was used for this project with excellent results.

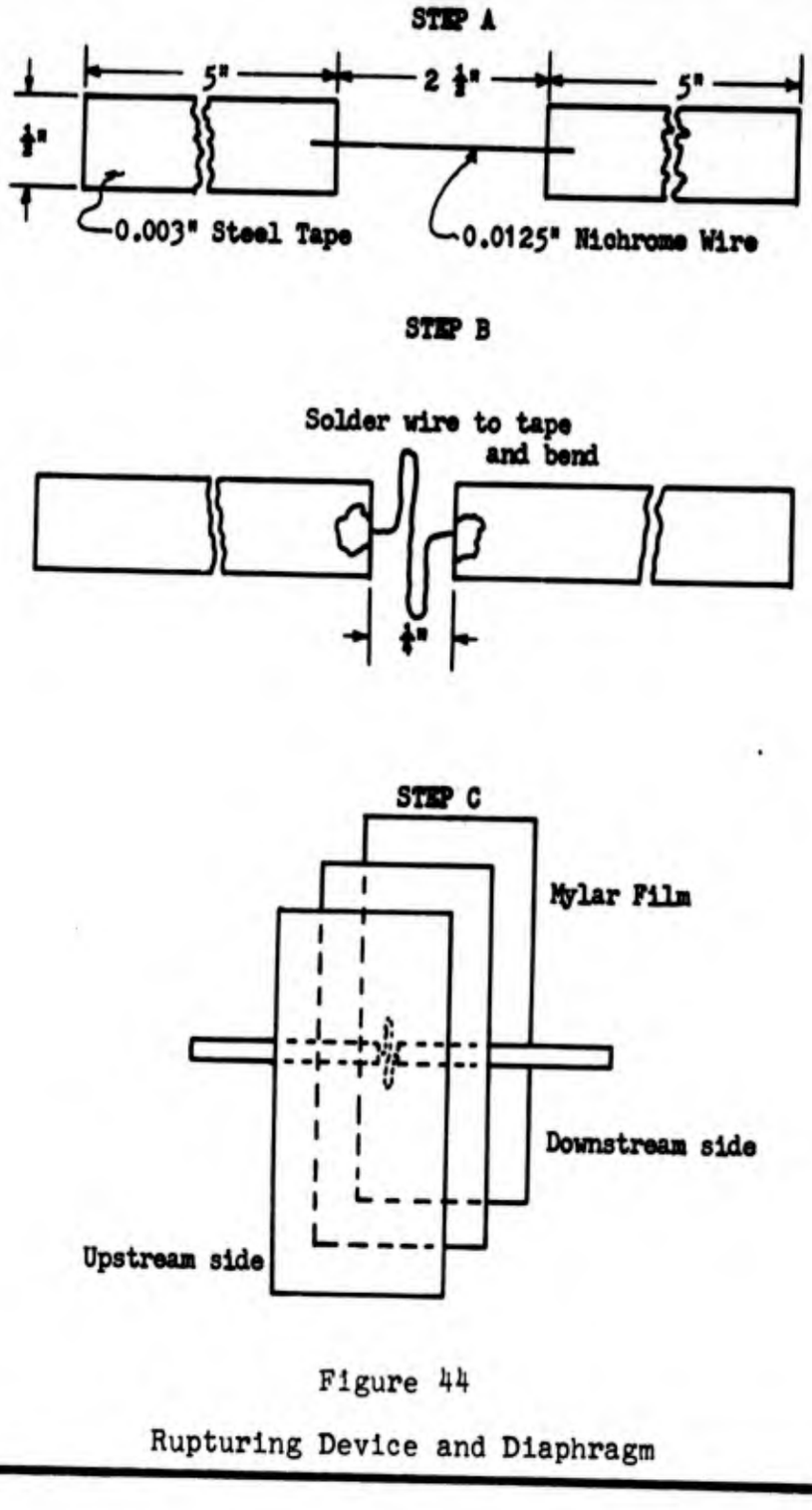

Figure 44

Rupturing Device and Diaphragm

Appendix B

Determination of Incident Shock Strength

The strength of a shock wave is defined as the ratio of the pressure behind the shock to the pressure ahead of it; i.e., P_{21} . This ratio may be calculated if the absolute velocity of the shock and the temperature of the fluid into which the shock moves are known.

$$P_{21} = 1 + \frac{2K}{K+1}\left[\left(\frac{W_s}{c_1}\right)^2 - 1\right] \tag{1}$$

$$c_1 = 49.1\sqrt{T_1} \tag{2}$$

$\frac{W_s}{c_1}$ is defined as M_s , the Mach number of the incident shock wave. Assuming k equals 1.4 , equation (1) reduces to

$$P_{21} = \frac{7M_s^2 - 1}{6} \tag{3}$$

Since the fluid into which the incident shock wave moves is at rest, the velocity of the shock wave with respect to the shock tube is the absolute velocity. This velocity is determined as follows.

Figure 45 shows the electronic configuration used to measure the shock velocity; Figures 46a and 46b are the Polaroid pictures of the oscilloscope traces for the Series E runs.

The trace is started as the shock wave passes transducer 1. Transducer 3, located 3.33 feet downstream, gives the trace an upward deflection as the shock wave passes. The time for the shock to travel between transducers 1 and 3 is represented by the length, from start to deflection, of the trace on the oscilloscope picture. This trace length is measured in centimeters and multiplied by the horizontal oscilloscope trace setting to give the time. The shock velocity is the distance traveled, in this case 3.33 feet, divided by the time.

As the shock wave advances another 0.67 feet, it passes over transducer 4 which then deflects the trace downward. This third portion of the trace represents the time that it takes the incident shock wave to travel to the nozzle face and the reflected shock wave to travel back upstream to transducer 4. As the reflected shock, traveling upstream, passes transducer 4, the trace is again deflected downward.

The fourth portion of the trace represents the time that it takes the reflected shock wave to move upstream from transducer 4 to transducer 3. The reflected shock must travel against the flow generated by the incident shock and it appears that for subsonic or near sonic flows, runs 1 - 5, the reflected shock travels at approximately the same relative velocity. When the flow is supersonic, run 6, the reflected shock apparently does not reach transducer 3 before it dissipates.

An error analysis performed on the calculated incident shock wave data indicated the following.

Measurement error may cause a maximum deviation of 1.5% in the value of trace length. The measurement error plus a possible 3% error in the oscilloscope trace setting led to a maximum possible error of 4.5% in the value of time. There was no appreciable error in either the value of distance between transducers or the speed of sound, therefore the value of shock velocity and Mach number are accurate to within 4.5%

The value of P_{21} , as calculated with equation (2), may have a maximum error of 9.0% .

The maximum percent error in each case applies to the nominal values as given in this study.

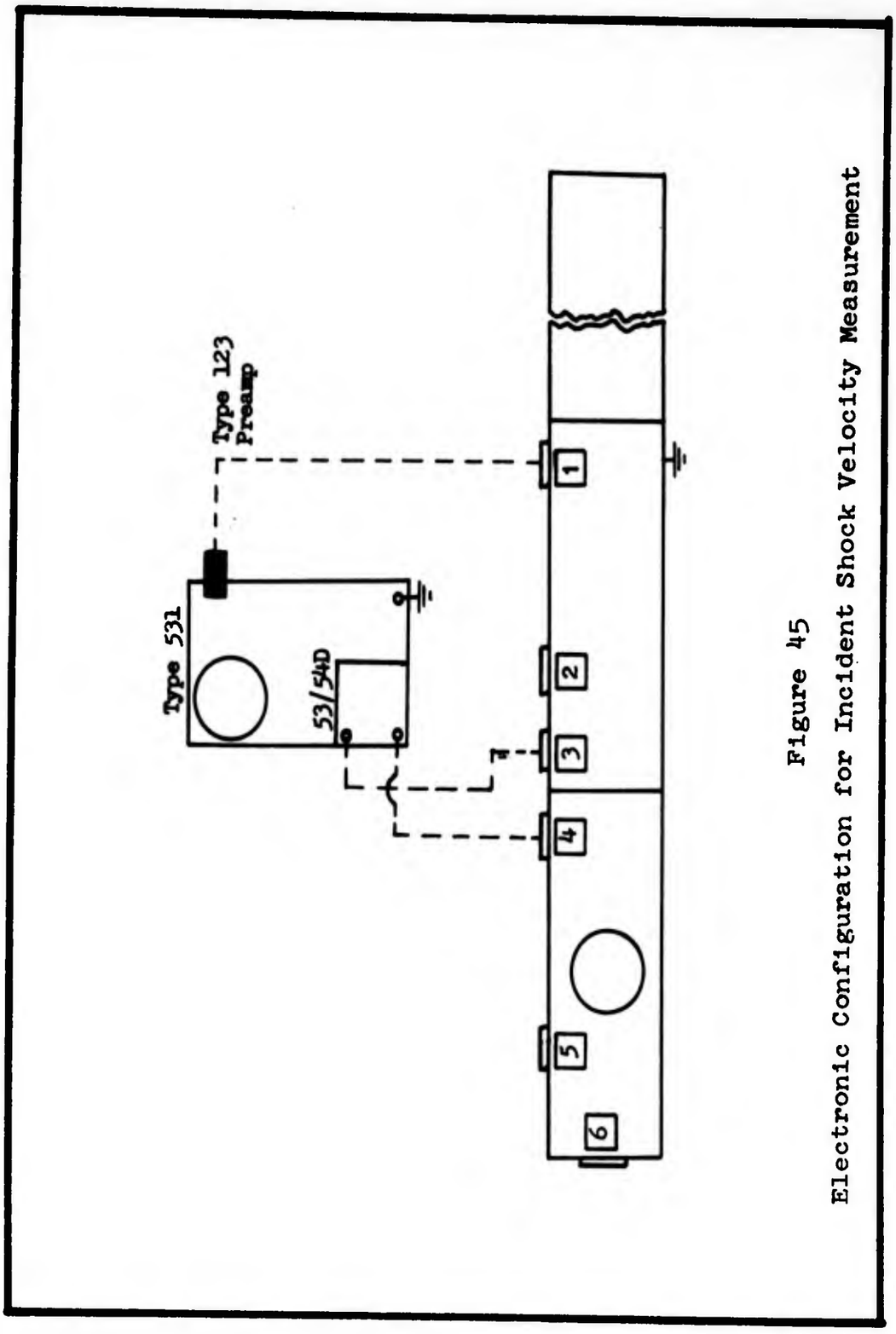

Figure 45
Electronic Configuration for Incident Shock Velocity Measurement

Run No: E-1
H : 0.5 msec/cm
V : 0.2 v/cm
Length: 4.00 cm
t : 2.00 msec
W_s : 1670 fps
M_s : 1.45

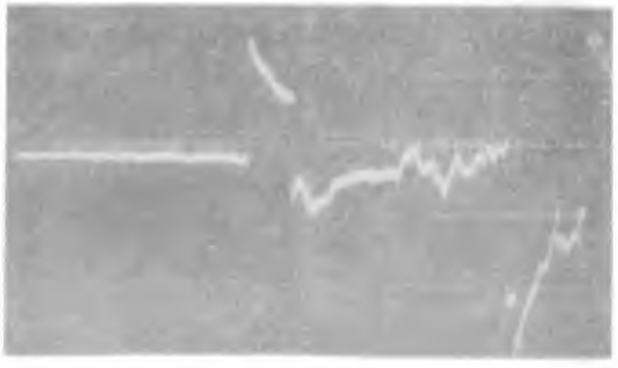

Run No: E-2
H : 0.5 msec/cm
V : 0.2 v/cm
Length: 3.65 cm
t : 1.83 msec
W_s : 1820 fps
M_s : 1.59

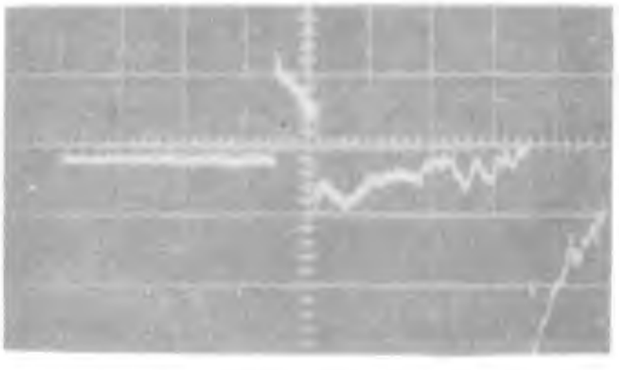

Run No: E-3
H : 0.5 msec/cm
V : 0.2 v/cm
Length: 3.32 cm
t : 1.66 msec
W_s : 2010 fps
M_s : 1.74

H - Horizontal trace setting
V - Vertical deflection scale

Figure 46a

Oscilloscope Trace Pictures and Relative Data
(Series E, Runs 1-3)

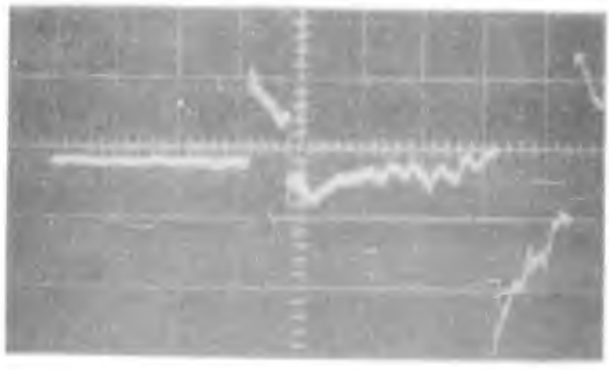

Run No: E-4
H : 0.5 msec/cm
V : 0.2 v/cm
Length: 3.09 cm
t : 1.54 msec
W_s : 2160 fps
M_s : 1.88

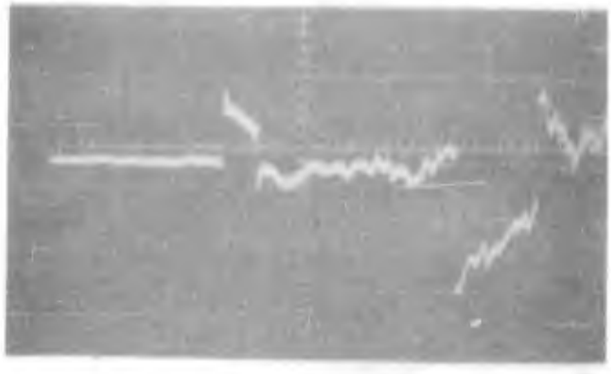

Run No: E-5
H : 0.5 msec/cm
V : 0.2 v/cm
Length: 2.72 cm
t : 1.36 msec
W_s : 2450 fps
M_s : 2.13

Run No: E-6
H : 0.5 msec/cm
V : 0.1 v/cm
Length: 1.87 cm
t : 0.936 msec
W_s : 3560 fps
M_s : 3.10

H - Horizontal trace setting
V - Vertical deflection scale

Figure 46b

Oscilloscope Trace Pictures and Relative Data
(Series E, Runs 4-6)

Appendix C

Determination of Nozzle Test Section Mach Number

When a wedge is inserted into a supersonic stream, an oblique shock wave is formed at the leading edge of the wedge. This oblique shock is visible in Figures 27a through 32d.

Assuming the stream fluid is a perfect gas with a constant specific heat and molecular weight, the shock wave semi-angle is related only to the flow Mach number and the wedge half-angle. With a known wedge half-angle, ω', a measured value of the shock wave semi-angle, α', and assuming k equals 1.4 , the value of the flow Mach number may be determined by reference to Table 56 of the "Gas Tables" (Keenan and Kaye).

The wedge used in this study had a half-angle of 9° . The shock wave semi-angle was measured from an enlarged still projection of the movie film of the Series C test runs. A 1-foot radius protractor was used to determine the angle between the center-line of the wedge and that portion of the shock wave between the wedge point and the intersection with the expansion wave off the top and bottom of the wedge. This angle was measured for both top and bottom halves of the shock wave and for several different pictures of each run. The measured angle was determined to be 29° with a fluctuation of 1° during each run. This indicates that the test section Mach number varied between 2.6 and 2.8 during each run.

Appendix D

Determination of Fluid Properties in Region 6

General

In order to determine the fluid properties in the test section, the properties in region 5 must be calculated. The following analysis assumes that the incident shock is completely reflected and applies steady-state relationships to a "quasi-steady" situation.

If the nozzle throat area is small compared to the area which contains region 5, the velocity in region 5 may be neglected and the static properties may be assumed to be equal to the stagnation properties. In this study, this assumption is not entirely valid because the throat area is 12.5% of the upstream area.

With the stagnation value of properties in region 5 known, test section properties may be calculated by assuming isentropic flow through the nozzle.

Equations

The equations used in this section were developed and presented by Glass (Ref 4). Air is assumed as the working fluid in both the chamber and the channel. The information calculated with these equations is presented in the form of ratios in Table IV and Figures 47, 48, and 49.

Constants: $\gamma_1 = \gamma_4 = 1.4$

$$\alpha_1 = \alpha_4 = \frac{\gamma+1}{\gamma-1} = 6$$

$$\beta_1 = \beta_4 = \frac{\gamma-1}{2\gamma} = \frac{1}{7}$$

$$E_{14} = \frac{c_v T_1}{c_v T_4} = 1$$

(Ref 4:78, eq 12) $$P_{14} = \frac{1}{P_{21}}\left[1 - (P_{21}-1)\sqrt{\frac{\beta_4 E_{14}}{\alpha_1 P_{21}+1}}\right]^{\frac{1}{\beta_4}}$$

$$= P_{21}\left[1 - (P_{21}-1)\sqrt{\frac{1}{42 P_{21}+1}}\right]^{7} \quad (4)$$

$$P_{41} = \frac{1}{P_{14}} \quad (5)$$

(Ref 4:94, eq 10) $$M_s = \left[\beta_1(1+\alpha_1 P_{21})\right]^{\frac{1}{2}}$$

$$= \left(\frac{1+6P_{21}}{7}\right)^{\frac{1}{2}} \quad (6)$$

(Ref 4:80, eq 16) $$T_{21} = \frac{1+\alpha_1 P_{21}}{\alpha_1 + P_{21}}$$

$$= \frac{1+6P_{21}}{6+P_{21}} \quad (7)$$

(Ref 4:55, eq 25) $$T_{21} = \frac{P_{21}}{T'_{21}} \quad (8)$$

(Ref 4:93, eq 6) $$P_{52} = \frac{\alpha_1 + 2 - P_{12}}{1 + \alpha_1 P_{12}}$$

$$= \frac{8 - P_{12}}{1 + 6P_{12}} \qquad (9)$$

$$P_{51} = P_{52} P_{21} \qquad (10)$$

(Ref 4:93, eq 8) $$\Gamma_{52} = \frac{1 + \alpha_1 P_{52}}{\alpha_1 + P_{52}}$$

$$= \frac{1 + 6P_{52}}{6 + P_{52}} \qquad (11)$$

$$\Gamma_{51} = \Gamma_{52} \Gamma_{21} \qquad (12)$$

(Ref 4:94, eq 9) $$T_{52} = \frac{P_{52}(\alpha_1 + P_{52})}{1 + \alpha_1 P_{52}}$$

$$= \frac{P_{52}(6 + P_{52})}{1 + 6P_{52}} \qquad (13)$$

$$T_{51} = T_{52} T_{21} \qquad (14)$$

Procedure

Given the incident shock strength, P_{21} , or the diaphragm pressure ratio, P_{41} ; the pressure ratio P_{51} , the density ratio Γ_{51} , and the temperature ratio T_{51} may be found in Table IV or the appropriate figure. These ratios represent the ratio of the static value of the properties in region 5 to the initial static value of the properties in the channel. They do not represent the ratio across the nozzle after flow is established, because the pressure in the nozzle test section is no longer equal to p_1 .

The property ratios across the reflected shock are given by P_{52} , Γ_{52} , and T_{52} .

The following procedure is used for determining p_6, the nozzle test section pressure. The density and temperature in the test section could be determined in the same manner.

With the known value of P_{21}, determine P_{51} from Table IV or Figure 47. Multiply this value of P_{51} by p_1 to get p_5. Assume that p_5 is equal to p_{05}, the stagnation pressure in region 5. Now obtain the isentropic pressure ratio $\frac{p_6}{p_{06}}$, at the value of the test section Mach number, M_6. Then p_6 is found by multiplying $\frac{p_6}{p_{06}}$ by p_{05}.

Example: Run C-5

Given: $p_1 = 5.00$ in Hg a

$T_1 = 547^\circ$ R

$P_{21} = 4.68 \simeq 4.7$

$M_6 \simeq 2.7$

From Table IV:

$P_{51} = 15.987$

Then: $p_{06} = p_{05} = p_5 = P_{51}(p_1) = (15.987)(5.00)$

$= 79.935$ in Hg a

@ $M_6 = 2.7$, $\frac{p_6}{p_{06}} = 0.04295$

Therefore:

$$p_6 = \frac{p_6}{p_{06}} (p_{05}) = (0.04295)(79.935) = 3.43 \text{ in Hg a}$$

Table IVa

Static Property Ratios

P_{21}	P_{41}	M_s	T_{21}	Γ_{21}	P_{52}	T_{52}	Γ_{52}	P_{51}	T_{51}	Γ_{51}
1.0	1.000	1.000	1.000	1.000	1.000	1.000	1.000	1.000	1.000	1.000
1.2	1.448	1.081	1.054	1.139	1.195	1.052	1.136	1.434	1.109	1.294
1.4	1.995	1.158	1.102	1.270	1.379	1.097	1.257	1.931	1.209	1.596
1.6	2.672	1.229	1.147	1.395	1.553	1.137	1.366	2.485	1.304	1.906
1.8	3.42	1.298	1.190	1.513	1.717	1.172	1.465	3.091	1.418	2.217
2.0	4.35	1.362	1.231	1.625	1.875	1.205	1.556	3.750	1.483	2.529
2.2	5.42	1.425	1.270	1.732	2.026	1.236	1.639	4.457	1.570	2.839
2.4	6.62	1.482	1.309	1.833	2.165	1.264	1.713	5.196	1.655	3.140
2.6	8.00	1.540	1.347	1.930	2.305	1.291	1.786	5.993	1.739	3.447
2.8	9.60	1.590	1.384	2.023	2.433	1.315	1.850	6.812	1.820	3.743
3.0	11.32	1.649	1.421	2.110	2.556	1.339	1.909	7.668	1.903	4.028
3.2	13.4	1.699	1.458	2.195	2.677	1.361	1.966	8.566	1.984	4.315
3.4	15.8	1.751	1.493	2.275	2.788	1.382	2.017	9.479	2.063	4.589
3.6	18.2	1.798	1.525	2.353	2.894	1.402	2.065	10.418	2.138	4.859
3.8	21.1	1.843	1.566	2.425	3.001	1.421	2.112	11.404	2.225	5.122
4.0	24.3	1.890	1.600	2.500	3.100	1.439	2.154	12.400	2.302	5.385
4.2	27.6	1.933	1.635	2.570	3.197	1.457	2.194	13.427	2.382	5.639
4.4	31.6	1.980	1.670	2.635	3.291	1.474	2.233	14.480	2.462	5.884
4.6	35.9	2.023	1.703	2.699	3.381	1.490	2.269	15.553	2.537	6.124
4.8	41.1	2.064	1.738	2.760	3.466	1.505	2.303	16.637	2.616	6.356
5.0	45.5	2.102	1.775	2.818	3.545	1.519	2.333	17.725	2.696	6.574
5.2	51.5	2.145	1.810	2.877	3.628	1.534	2.365	18.866	2.777	6.804
5.4	58.2	2.185	1.845	2.929	3.704	1.548	2.393	20.002	2.856	7.009
5.6	64.4	2.222	1.875	2.980	3.776	1.560	2.420	21.146	2.925	7.212
5.8	72.5	2.261	1.910	3.032	3.846	1.573	2.445	22.307	3.004	7.413

Table IVb

Static Property Values

P_{21}	P_{41}	M_s	T_{21}	Γ_{21}	P_{52}	T_{52}	Γ_{52}	P_{51}	T_{51}	Γ_{51}
6.0	81.2	2.293	1.947	3.081	3.917	1.585	2.471	23.502	3.086	7.613
6.2	91.1	2.332	1.980	3.130	3.985	1.597	2.495	24.707	3.162	7.809
6.4	100.0	2.370	2.012	3.179	4.049	1.609	2.517	25.914	3.237	8.002
6.6	111.6	2.405	2.050	3.215	4.110	1.619	2.538	27.126	3.319	8.160
6.8	123.8	2.440	2.082	3.260	4.173	1.630	2.560	28.376	3.394	8.346
7.0	134.5	2.475	2.115	3.306	4.229	1.640	2.578	29.603	3.469	8.523
7.5	181.6	2.563	2.201	3.407	4.375	1.666	2.627	32.813	3.667	8.950
8.0	222.2	2.645	2.285	3.500	4.500	1.688	2.667	36.000	3.857	9.335
8.5	291.2	2.724	2.370	3.586	4.615	1.707	2.703	39.228	4.046	9.693
9.0	353.0	2.800	2.452	3.662	4.732	1.728	2.739	42.588	4.237	10.030
9.5	457.9	2.877	2.539	3.742	4.844	1.747	2.722	46.018	4.436	10.373
10.0	552	2.952	2.620	3.810	4.938	1.763	2.800	49.380	4.619	10.668
10.5	705	3.023	2.707	3.879	5.031	1.780	2.827	52.826	4.818	10.966
11.0	847	3.094	2.790	3.940	5.118	1.795	2.852	56.298	5.008	11.237
11.5	1067	3.162	2.875	4.000	5.199	1.809	2.875	59.789	5.201	11.500
12.0	1290	3.229	2.948	4.050	5.278	1.822	2.897	63.336	5.371	11.733
12.5	1852	3.294	3.043	4.108	5.351	1.835	2.917	66.888	5.584	11.983
13.0	1940	3.359	3.125	4.160	5.422	1.847	2.936	70.486	5.772	12.214
13.5	2670	3.421	3.210	4.205	5.487	1.858	2.953	74.075	5.964	12.417
14.0	2913	3.485	3.290	4.250	5.551	1.869	2.970	77.714	6.149	12.623
14.5	3668	3.545	3.378	4.293	5.609	1.879	2.985	81.331	6.347	12.815
15.0	4280	3.606	3.462	4.330	5.667	1.889	3.000	85.005	6.540	12.990

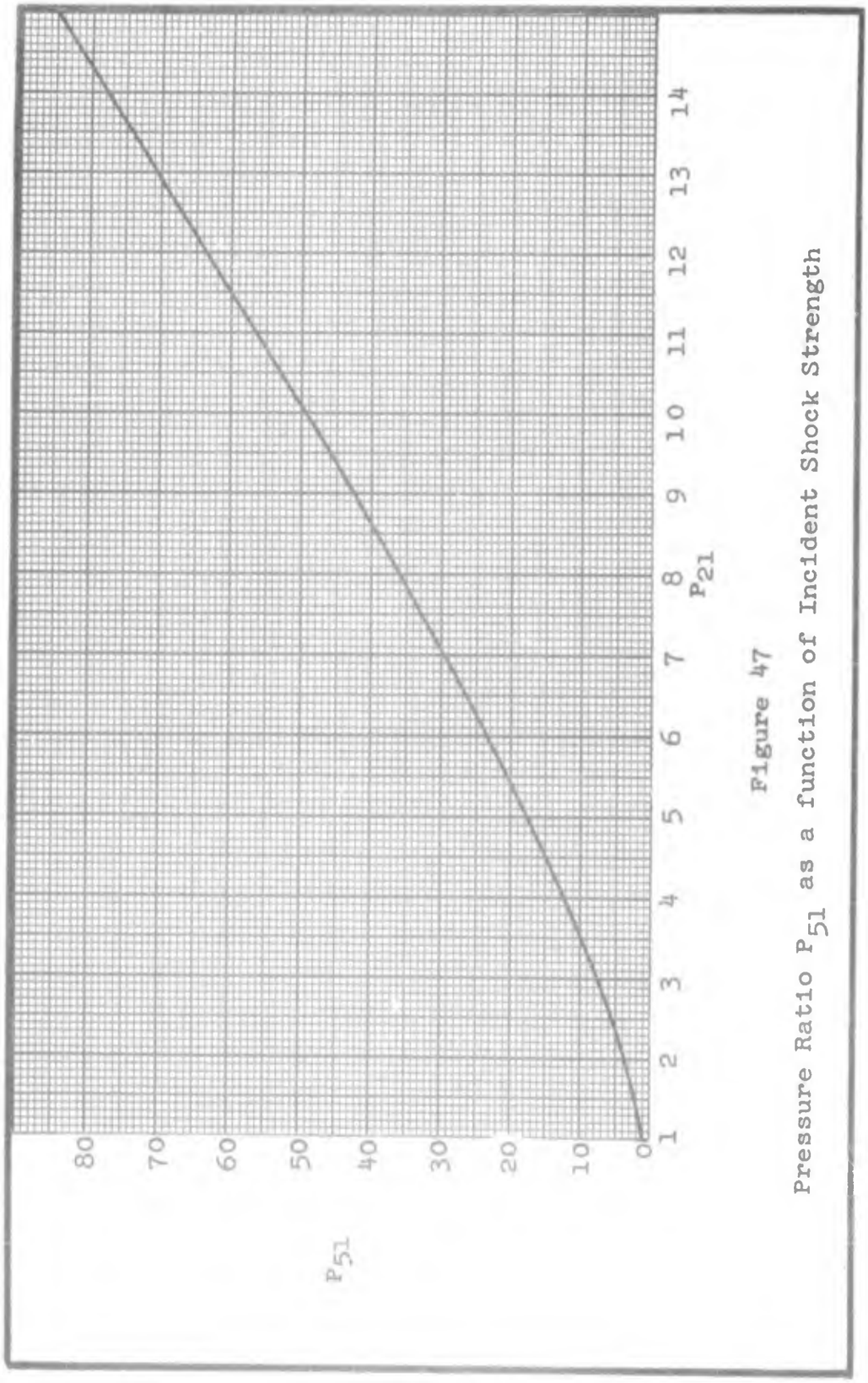

Figure 47

Pressure Ratio P_{51} as a function of Incident Shock Strength

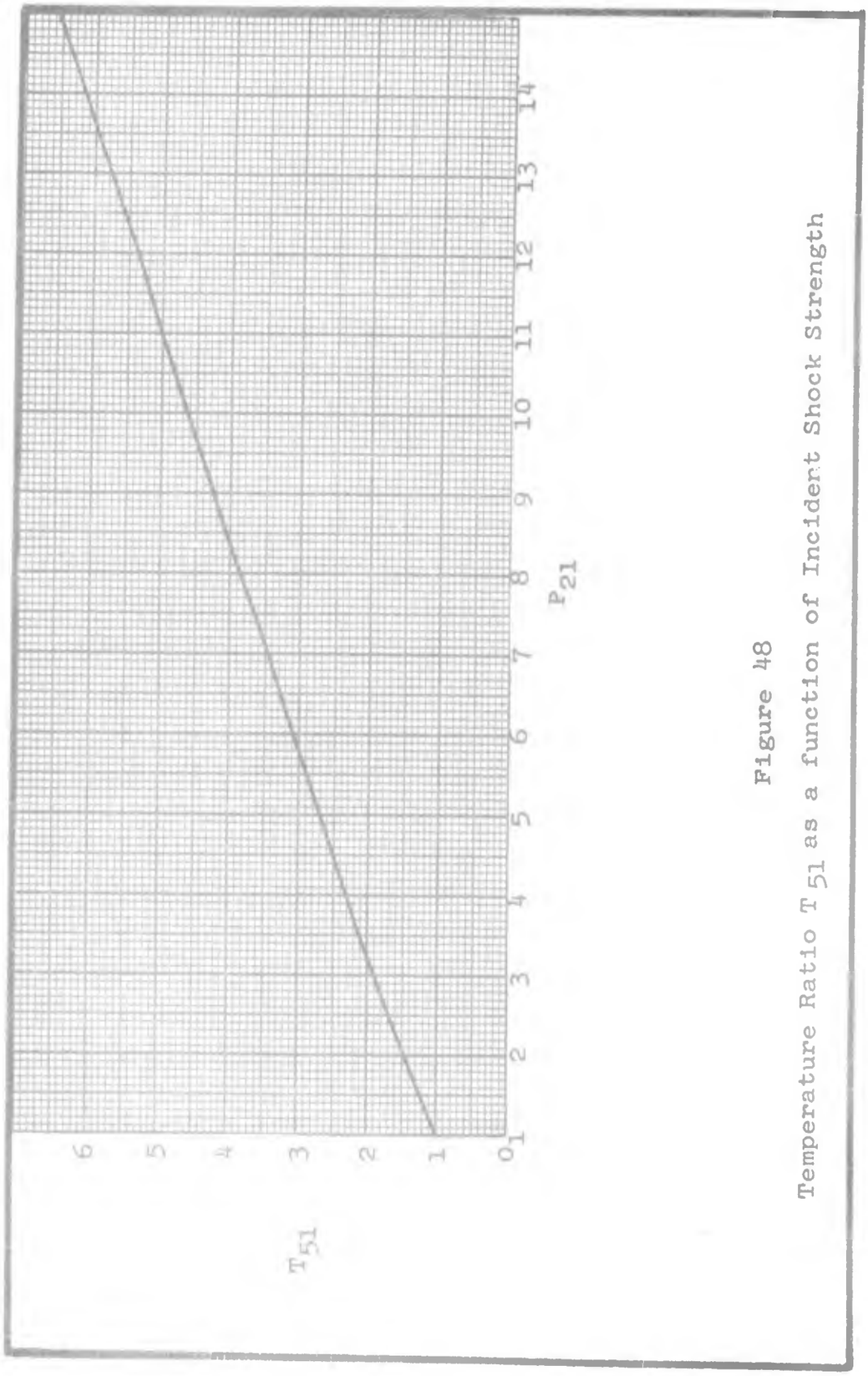

Figure 48

Temperature Ratio T_{51} as a function of Incident Shock Strength

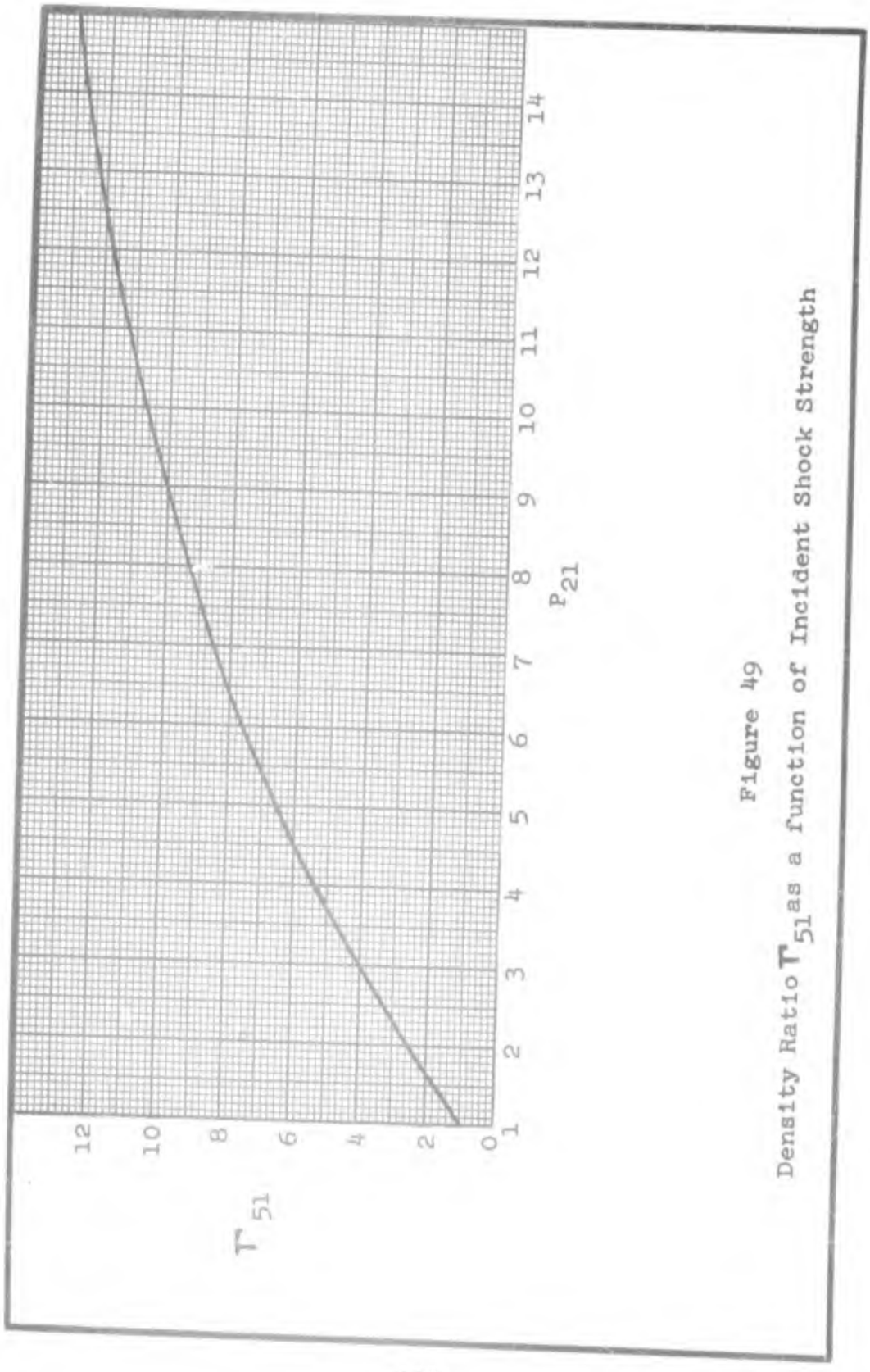

Figure 49

Density Ratio τ_{51} as a function of Incident Shock Strength

Appendix E

Quantitative Measurement with Endevco Model 2501-500 Pressure Transducers

The Endevco transducer is an accurate, highly refined instrument, but its limitations must be recognized. Some difficulty was encountered early in this study because these limitations were not completely understood. It is hoped that this section will point out those limitations particularly applicable to the use of Endevco transducers in the Mechanical Engineering Laboratory shock tube.

Two instruction manuals supplied by Endevco Corporation were used as references for this section.

The older Model 2501-500 transducer is nominally rated at 30 peak-volts at a pressure step of 500 psi. The newer model is nominally rated at 50 peak-millivolts per peak psi pressure step. This sensitivity is variable by changing the external capacitance in the circuit with the transducer.

The amplitude linearity deviation is given as plus or minus 2% of full scale output, measured from the best straight line through zero. The dynamic linearity is given as accurate to better than plus or minus 1% up to 100 volts output.

The transducer generates a voltage proportional to a pressure step; i.e., $(p_2 - p_1)$. For applications in the shock tube, the shock strength is of interest; i.e., P_{21} .

Now consider a plot of P_{21} as the abscissa and $(p_2 - p_1)$ or $p_1(P_{21} - 1)$ as the ordinate, with the initial channel pressure, p_1 , as a parameter (Fig 50). The function $p_1(P_{21} - 1)$ is the actual input to the transducer or, assuming 100% accuracy, its output.

Using maximum chamber pressure, the channel pressure must be lowered in order to generate a stronger incident shock; i.e., higher value of P_{21} . Therefore, it is obvious from Figure 50, that a slight error in evaluating $(p_2 - p_1)$ causes only a small error in the value of P_{21} if p_1 is 30 inches of mercury pressure. However, this same small error in $(p_2 - p_1)$ causes a sizeable error in the value of P_{21} if p_1 is only 1 inch of mercury.

It should be apparent then, that the transducers are of very little value for determining directly the strength of strong shock waves because they are only encountered at low channel pressures.

This limitation causes no problem when the transducers are used as shock wave indicators; i.e., to start the oscilloscope trace and to indicate shock wave passage at a certain point in the shock tube.

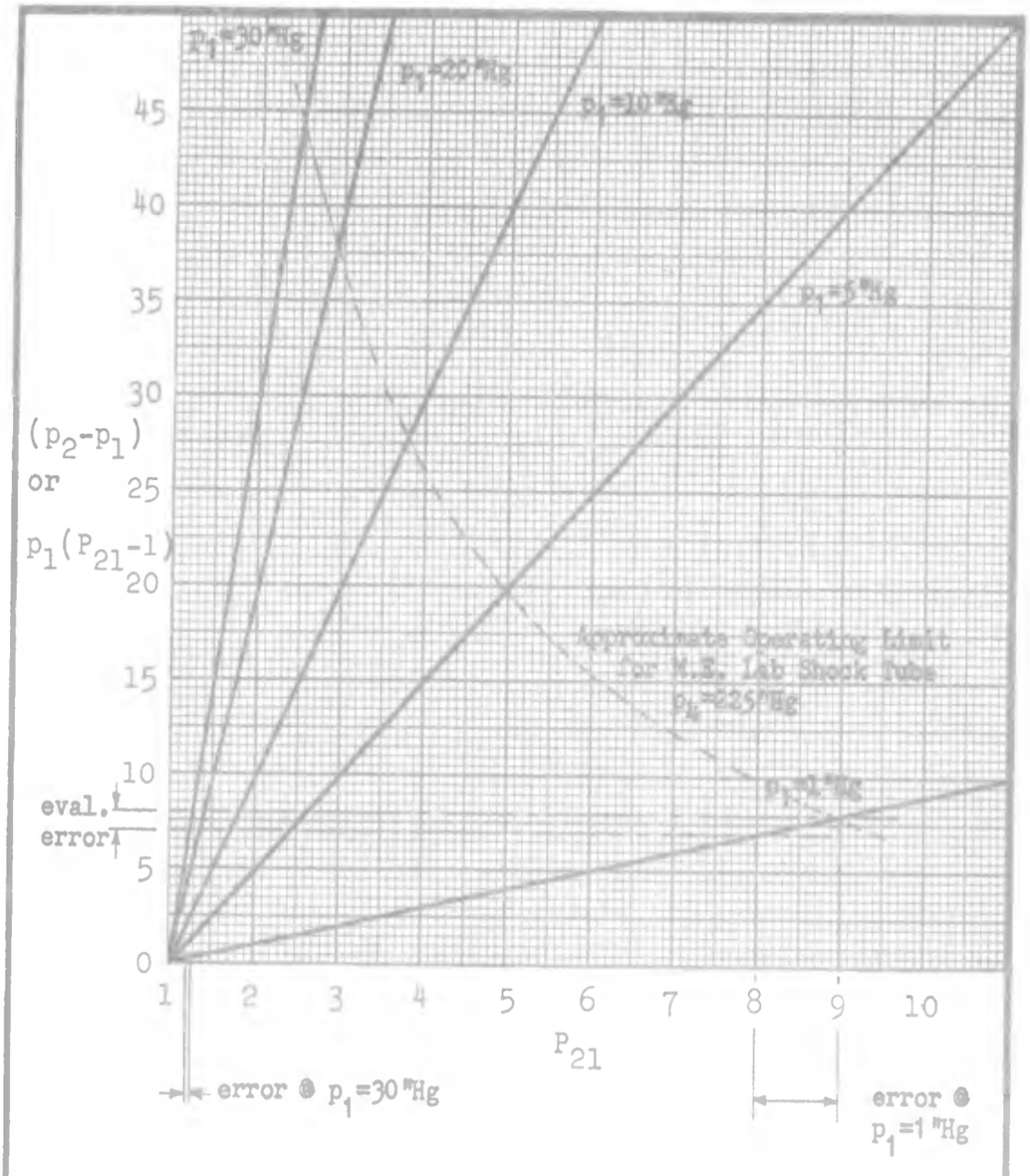

Figure 50

Transducer Output

as a function of Incident Shock Strength

with Initial Channel Pressure as a Parameter

Vita

Carroll Clifford Rands was born to Hilda [redacted] Rands and Virgil Leroy Rands in [redacted]. He graduated from high school in Tomah, Wisconsin and received a B. S. degree in Mechanical Engineering from the University of Wisconsin in June, 1955. He was employed as a design engineer with Lockheed Aircraft Corporation until entry into the Air Force in February, 1956. After the completion of pilot and instructor training, he was assigned to Greenville Air Force Base, Mississippi until enrollment in the Air Force Institute of Technology. Duties while at Greenville included Flight Instructor, Military Training Officer, and School Secretary. His proudest possessions are his wife, Shirley, and his two sons, Mark and Gregory.

Permanent Address: [redacted]

This thesis was typed by the author.

UNCLASSIFIED

UNCLASSIFIED